STUDY AND EVALUATION OF IMPULSE MASS SPECTROMETERS FOR ION ANALYSIS IN THE D AND E REGIONS OF THE IONOSPHERE

Final Report

covering the period

June 1, 1965 to December 31, 1979

NASA Grant No. NGL 39-009-032

Work carried out in:

The Department of Physics
and
The Ionosphere Research Laboratory
The Pennsylvania State University

Principal Investigator

Bruce R. Kendall
305 Davey Laboratory
University Park, PA 16802

STUDY AND EVALUATION OF IMPULSE MASS SPECTROMETERS FOR ION ANALYSIS IN THE D AND E REGIONS OF THE IONOSPHERE

Final Report

covering the period

June 1, 1965 to December 31, 1979

NASA Grant No. NGL 39-009-032

Work carried out in:

The Department of Physics
and
The Ionosphere Research Laboratory
The Pennsylvania State University

Principal Investigator

Bruce R. Kendall
305 Davey Laboratory
University Park, PA 16802

ABSTRACT

Theoretical and numerical analyses were made of planar, cylindrical and spherical-electrode time-of-flight mass spectrometers in order to optimize their operating conditions. A numerical analysis of potential barrier gating in time-of-flight spectrometers was also made. The results were used in the design of several small mass spectrometers. These were constructed and tested in a laboratory space simulator.

Detailed experimental studies of a miniature cylindrical-electrode time-of-flight mass spectrometer and of a miniature hemispherical-electrode time-of-flight mass spectrometer were made. The extremely high sensitivity of these instruments and their ability to operate at D-region pressures with an open source make them ideal instruments for D-region ion composition measurements.

Two flight experiments based on cylindrical-electrode time-of-flight mass spectrometers were prepared for launch on Boosted Arcas sounding rockets. Vehicle and telemetry failures limited the scientific data collection to a short period near 76 km on the second flight. The results suggested the presence of a substantial number of charged particles having masses above 275 a.m.u.

Two further flight experiments of the same general type were prepared for launch on Nike-Apache and Nike-Cajun sounding rockets. The first of these again indicated the presence of substantial numbers of charged particles with masses above 500

a.m.u. up to altitudes around 92 km. Above 92 km, the mass spectrum showed the conventional features of NO^+, N_2^+, and layers of Fe^+ ions. The final payload, which was to have been recovered by air-snatch, was lost when the second stage rocket failed to fire.

It is possible that the very heavy charged particles are part of a continuum of particles ranging up to sizes normally associated with dust. They might be water vapor clusters, possibly around a metallic or other ionic core, or submicroscopic dust particles covered with a layer of adsorbed water.

An appendix details work on a mass filter of the Eiber-Loeb type which appears well suited to the study of heavy charged particles in the lower ionosphere.

TABLE OF CONTENTS

CHAPTER I

INTRODUCTION

1.1 The Ionosphere

The study of the weakly ionized plasma enveloping the entire earth and extending from about 50 km to about 1000 km in altitude was stimulated by two primary reasons. The first was to discover its effects on radio waves, while the second was to discover its effects on the geomagnetic field. Although there were earlier proposals relating to the existence of this plasma, the first significant papers were written by Kennelly (1902) and Heaviside (1902). These researchers explained the success of Marconi's radio experiment (in 1901) by postulating the existence of a conducting layer at a high altitude. The use of the name "ionosphere" for the ionized plasma surrounding the earth was proposed by Watson-Watt (1929) and has become the commonly used term.

The beginnings of the modern theory of the ionosphere were with the works of Hulbert (1928) and Chapman (1931a, b). Since the description by Chapman (1931a, b) of an ionospheric layer, the division of the ionosphere has commonly been into layers. However, the boundaries between these layers have usually been regions of large electron density gradients. These layers are known as the D, E and F-regions (and sometimes the C-region). The D-region is roughly the region below 90 km. The region from about 90 km to between 140 km and 180 km is known as the E-region. The F-region

(usually divided into the F_1 and F_2-regions) extends from 140-180 km to about 300 km. Above 300 km is usually referred to as the topside. The C-region is sometimes used to describe the region from 50 km to 60 km.

With the definite proof of the existence of the ionosphere obtained in the early portion of this century, theorists have attempted to construct ionospheric models. These attempts continue to the present day. The data needed as inputs, for modeling, include temperatures (ionic, neutral and electron), the pressure, the chemical composition (neutral and ionic), reaction rates and solar radiation information. This thesis will discuss the use of time-of-flight mass spectrometers for the measurement of the positive ion composition of the D-region and E-region of the ionosphere.

1.2 Mass Spectrometry in the Ionosphere

The mass spectrometer has become an established and sensitive tool for use in the quantitative analysis of complex mixtures of gases. It is natural, therefore, to apply mass spectrometry to the measurement of neutral and ionic species in the earth's atmosphere. Of special interest, in this thesis, is the study of the ionic species of the earth's atmosphere. The first measurements of ionospheric composition were made using the radio frequency mass spectrometer developed by Bennett (1950). These early measurements were made in the E and F-regions of the ionosphere by Townsend (1952), Johnson and Meadows (1955) and Johnson and Heppner (1955). Although the quantitative results of these measurements are in doubt, they did indicate that the principal ions present in the altitude range of 100 km to 200 km were O^+ (16), NO^+ (30) and O_2^+ (32).

Since these measurements, numerous experimenters, using a variety of mass spectrometers, have entered this field. These experimenters include Boyd and Morris (1955), Boyd (1959, 1960), Boyd et al., (1974), Sayers (1959), Hoffman (1967, 1969, 1970), Hoffman et al., (1973), Istomin (1962), Istomin and Pokhunkov (1963), Bowen et al., (1964), Taylor et al., (1965, 1968), Raitt et al., (1965, 1973), Taylor and Brinton (1961), Young et al., (1967), Goldberg and Aikin (1973), Aikin and Goldberg (1973), Smith et al., (1967), Zhlood'ko et al., (1974), Brinton et al., (1973), Arnold et al., (1969), Goldberg (1975) and Krankowsky et al., (1972c).

A subject of great interest, since the middle 1960's, has been the ionic composition of the D-region. The discovery of hydrated ions of the form $H_3O^+ \cdot (H_2O)_n$ by Narcisi and Bailey (1965) stimulated a great amount of debate. However, the presence of these ions is generally accepted today. The type of ions in the D-region have a great affect on VLF radio wave propagation and knowledge of these ions is crucial for reliable communication using VLF radio wave propagation. Experimental measurements in this region are made extremely difficult by the high ambient pressure and the small ion concentrations. The higher pressures mean a smaller mean free path than the dimensions of the instruments used for measurements. The small ion concentrations result in small ion currents, 10^{-10} amps or less, and introduce problems of current detection. The workers in this field have, for the most part, used quadrupole mass filters which sample through an orifice, typically 1 mm in diameter,

and are differentially pumped by cryopumps or ion pumps. This method allows the use of electron multiplier detectors for ion current detection. Some of the researchers who are working in, or have worked in, D-region ion composition measurements are Narcisi and Bailey (1965), Goldberg and Blumle (1970), Narcisi (1966, 1967, 1969, 1970, 1973), Narcisi et al., (1967, 1969a, b, 1971, 1972a, b, c), Narcisi and Roth (1970), Goldberg and Aikin (1971), Arnold et al., (1969, 1971, 1974), Krankowsky et al., (1972a, b), Johannessen and Krankowsky (1972, 1974), Johannessen et al., (1972) and Arnold and Krankowsky (1974). All these researchers used the quadrupole mass filter introduced by Paul and Raether (1955). More recently a pumped magnetic sector mass spectrometer was flown by Zbinden et al., (1975) and measured D and E-region positive ion composition.

Negative ions in the D-region have also been subject to study by a number of experimenters. These include Johnson and Heppner (1956), Narcisi (1969, 1973), Arnold et al., (1971), Narcisi et al., (1971, 1972a, b) and Krankowsky et al., (1972a).

1.3 Time-of-Flight Mass Spectrometry

The instruments which are the subject of this thesis are time-of-flight mass spectrometers. The original studies of time-of-flight mass spectrometers were carried out more or less simultaneously by Stephens (1946) and Cameron and Eggers (1948). Further investigations were done by Keller (1949), Takekoshi et al., (1951), Glenn (1952), Wolff and Stephens (1953), Ionov and Mamyrin (1953) and Katzenstein and Friedland (1955).

In 1955, Wiley and McLaren introduced the two-field time-of-flight mass spectrometer. This instrument used two acceleration regions in the ion source. This produced significantly improved resolving power compared to earlier time-of-flight mass spectrometers. The mass spectrometer of Wiley and McLaren (1955) and the earlier time-of-flight mass spectrometers used planar electrodes.

Sayers (1959) and MacKenzie (1964) developed time-of-flight mass spectrometers which used a cylindrical geometry. These instruments were designed for use in ion composition measurements in the E-region of the ionosphere. They did not use the two-field source of Wiley and McLaren (1955) and with a flight path length of 12 cm, had a resolving power of only 3. A successful sounding rocket flight showed the presence of NO^+ (30) and O_2^+ (32). Work was also done on a cylindrical-geometry time-of-flight mass spectrometer by Lincoln (1957). He used a modified vacuum tube with an ion flight path of 5.6 cm and observed a resolving power of about 1.

Diem (1967) reported a time-of-flight mass spectrometer combining the cylindrical geometry of MacKenzie (1964) and the two-field acceleration source of Wiley and McLaren (1955). This instrument had a drift region length of about 4 cm and had a resolving power of 5. These early results were extended by Zabielski (1970), Zabielski, Diem and Kendall (1970), Stein (1974) and Kendall and Reiter (1975). In 1970, Zabielski described a time-of-flight mass spectrometer using a spherical geometry and the two-field source of

Wiley and McLaren (1955). The theory of this instrument was subsequently described, in more detail, by Zabielski, Stein and Kendall (1972/1973) and Stein (1974). Experimental studies of this instrument were reported by Reiter and Kendall (1974). The laboratory version of this instrument had an ion drift length of about 4 cm and a resolving power of 13.

The compactness and very light weight of these miniature analyzers made them ideally suited to sounding rocket applications. Their ability to function without internal pumping and their large active area made for simplicity. The elimination of some of the errors associated with the ion sampling and ion current measurement processes further increased the value of this analyzer as an alternative type of mass spectrometer for ion composition measurements in the lower ionosphere.

CHAPTER II

TWO-FIELD TIME-OF-FLIGHT MASS SPECTROMETER THEORY AND NUMERICAL STUDIES

2.1 Introduction

This chapter will develop the mathematical basis for study of the operating conditions of two-field time-of-flight mass spectrometers with planar, cylindrical and spherical geometries This will be done by first introducing the definitions and the necessary background in order to understand the terms and the previous work on two-field time-of-flight mass spectrometers. This will be followed by a detailed analysis of the time-of-flight for the three geometries.

2.2 Definitions

Time-of-flight mass spectrometers can usually be classified as constant energy or constant momentum devices. Constant energy time-of-flight mass spectrometers give the same energy to ions with different mass-to-charge ratios. Constant momentum time-of-flight mass spectrometers give the same momentum to ions with different mass-to-charge ratios. The spectrometers considered in this thesis are all constant energy devices.

In constant energy time-of-flight mass spectrometers, the resolving power is given by $R = t/2\Delta t$ where t is the ion flight

time and Δt is the spread in the time-of-flight of the ions of a given mass. In this thesis, Δt will always signify the full width at half height of any mass peak under study. The resolving power is often equated with resolution in recent studies of mass spectrometers. This is not really correct and this thesis will only use the definition of resolving power given above.

Two important focusing principles, which will be referred to often in this chapter and in the rest of this thesis, are space focusing and velocity focusing. The definitions of space focusing and velocity focusing applied to time-of-flight mass spectrometry are different from the definitions of these terms which are applied to the rest of the mass spectrometry. In this thesis, space focusing occurs if ions of a given mass-to-charge ratio, produced at the same time at different places in the source region with the same velocity, are focused so that they reach the collector at nearly the same time. Velocity focusing occurs, again in this thesis, if ions of a given mass-to-charge ratio, produced at the same time and same place with slightly different velocities, are focused so that they reach the collector at nearly the same time. If perfect velocity focusing and perfect space focusing occur simultaneously, the result is perfect double time focusing.

In order to properly analyze and understand the operation of two-field time-of-flight mass spectrometers with planar, cylindrical and spherical geometries, it will be necessary to derive analytical expressions for the time-of-flight for each geometry. The theory for the planar geometry two-field time-of-

flight mass spectrometer was first worked out by Wiley and McLaren (1955). This work was extended by Stein (1974). A series solution for the cylindrical geometry was derived by Diem (1967) and extended by Zabielski (1970) and Zabielski, Diem and Kendall (1970). A series solution for the spherical geometry was derived by Zabielski (1970) and extended by Zabielski, Stein and Kendall (1972/1973). Closed form solutions for both the cylindrical and spherical geometries were derived by Stein (1974). The expressions presented in this thesis for the time-of-flight for all three geometries will follow those of Stein very closely.

2.3 Linear Constant Energy Time-of-Flight Equation

Consider an ion of mass m, charge q, starting at a point x_i, and with initial velocity v_i. When this ion is placed in an electrostatic field E(x), corresponding to a potential V(x), the equation of motion can be written as

$$\frac{1}{2} m v_i^2 + q V(x_i) = \frac{1}{2} m v^2 + q V(x) \qquad (2.1)$$

In this expression, v is the ion velocity at any point x, and $V(x_i)$ is the potential at the ion's starting point. The time-of-flight equation follows from equation (2.1) by substituting $\frac{dx}{dt} = v$ and integrating both sides of the equation after rearranging terms. This gives

$$t = \pm \left(\frac{m}{2q}\right)^{1/2} \int_{x_i}^{x} \frac{dx'}{\left[\frac{m v_i^2}{2q} + V(x_i) - V(x')\right]^{1/2}} \qquad (2.2)$$

where x is the final position of the ion and the sign is to be chosen to insure an increasing t. The denominator under the integral is always positive so the (+) sign is chosen if $dx' > 0$ and the (-) sign if $dx' < 0$. Equation (2.2) defines the time-of-flight of an ion moving in a straight line.

Reflection points in an ion's path, for an ion with initial velocity in the opposite direction of the electrostatic field, can be calculated from equation (2.1). Since $v = 0$ at the reflection point

$$V(x_m) = V(x_i) + \frac{mv_i^2}{2q} \qquad (2.3)$$

and if the expression for V(x) is known, a solution for x_m can be calculated.

2.4 Two-Field Time-of-Flight Mass Spectrometers; Definitions

The theory of time-of-flight mass spectrometers presented in this chapter deals with idealized mass spectrometers. This ideal two-field time-of-flight mass spectrometer (referred to hereafter as TOFMS) has four electrodes which are planar, (see Figure (2.1)), concentric cylinders (see Figure (2.2)), or concentric spheres (see Figure (2.3)). The outer or left-hand electrode, designated electrode 1, with applied voltage V_1, and radius r_1, is either solid or a grid. The next two electrodes, labeled electrodes 2 and 3, have voltages V_2 and V_3 and radii r_2 and r_3 and need to be essentially transparent to ions. The right-hand or inner electrode, the collector,

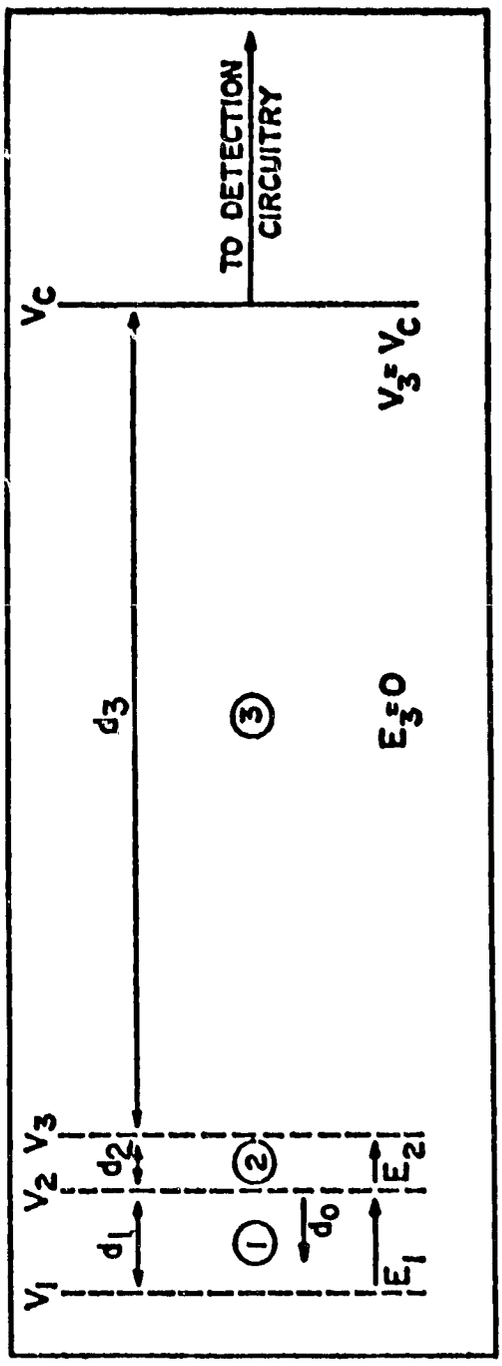

Figure 2.1 Side View of Linear Time-of-Flight Mass Spectrometer of Wiley and McLaren (1955). (Reference: Zabielski (1970)).

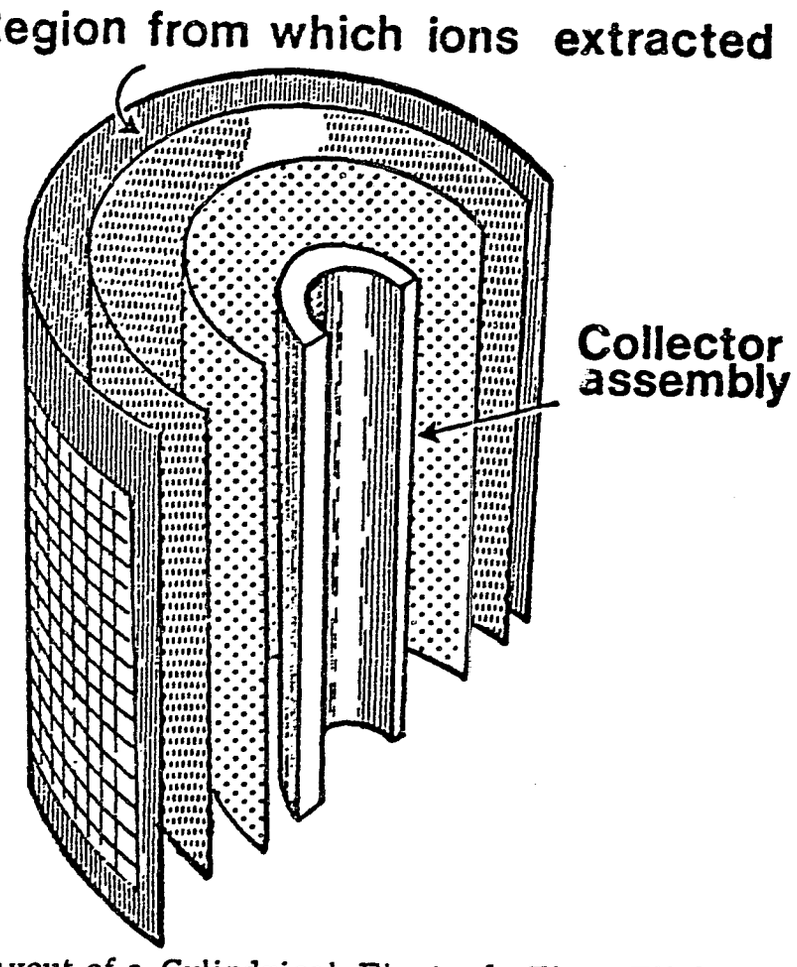

Figure 2.2 Practical Layout of a Cylindrical-Electrode Time-Flight Mass Spectrometer Electrode Structure. (Reference: Zabielski, Diem and Kendall (1970)).

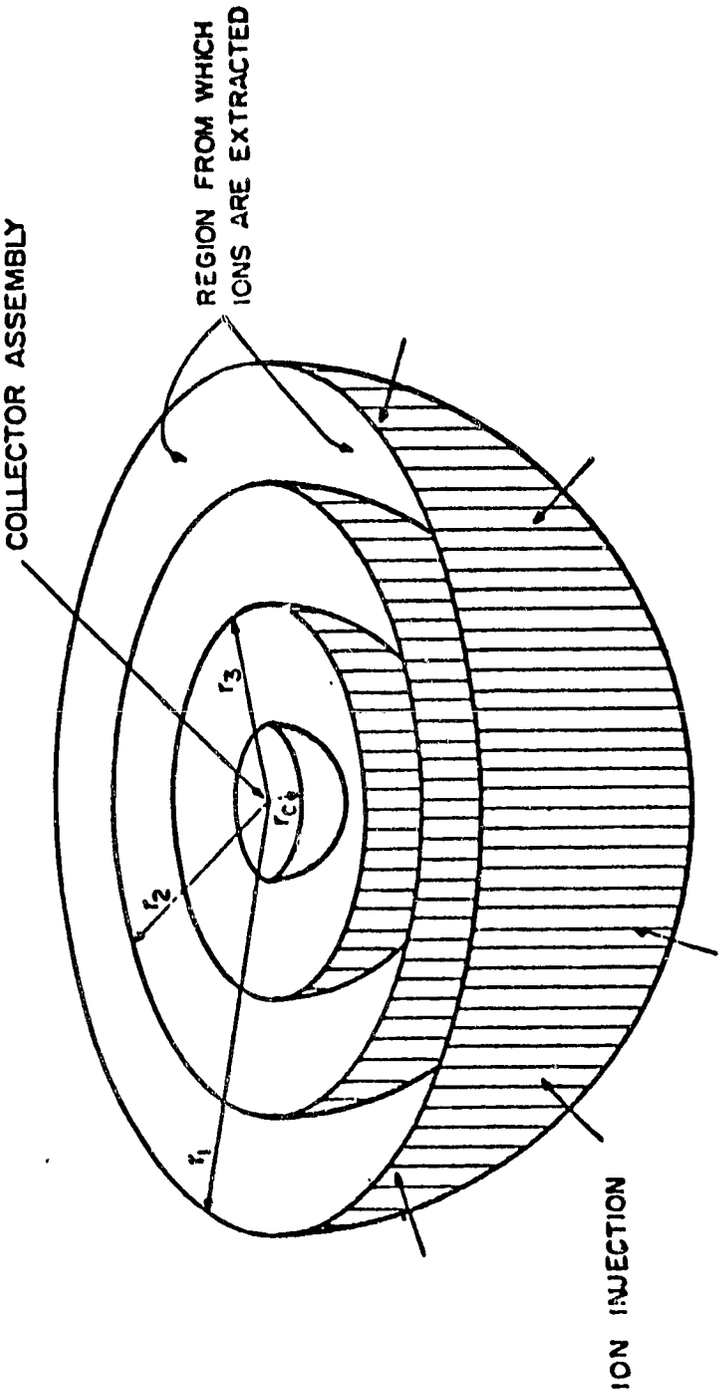

Figure 2.3 Practical Layout of a Spherical-Electrode Time-of-Flight Mass Spectrometer Electrode Structure. (Reference: Zabielski, Stein and Kendall (1972/1973)).

has voltage V_c and radius r_c. These four electrodes bound three regions (designated 1, 2 and 3) and are defined as the source, acceleration and drift regions. The widths of these regions are d_1, d_2 and d_3.

Ions are formed or drawn into the source region when it is field-free ($V_1 = V_2$). The electric field in the source region, E, is then turned on. For positive ions in the TOFMS considered in this thesis, this is usually done by pulsing V_1 more positive (so that $V_1 > V_2$) until all the ions have left the source region. The ion initial position is x_i or r_i and the initial ion velocity is v_i.

In the planar geometry the time-of-flight is independent of initial velocities parallel to the grids. However, in the cylindrical and spherical geometries, non-radial initial ion velocities will affect the time-of-flight. In order to slightly simplify the theory, and because the non-radial velocities will be small in most applications, only radial initial velocities will be considered.

The ions arrive at grid 2 in time t_1, unless the ions have an initial velocity away from the collector large enough so that the ions pass through or strike grid 1, and are lost. When the ions enter the acceleration region, they are influenced by a new electric field E_2 (where $V_2 > V_3$ for positive ions). The time for the ions to traverse the acceleration region is t_2. The ions then pass through grid 3 and enter the field-free drift region. The time for the ions to pass through the drift region is t_3. The total time-of-flight can now be written as

$$t = t_1 + t_2 + t_3 \qquad (2.4)$$

A more general expression for the total time-of-flight should include the turn around time for ions initially travelling away from the collector. If the turn around time is defined as t_t, then we can redefine the time-of-flight for the source region as

$$t_1 = t_1' + \frac{1}{2} t_t \pm \frac{1}{2} t_t \qquad (2.5)$$

where t_1' is now the time-of-flight in the source region for ion with initial velocity toward the collector. This now redefines the total time-of-flight as

$$t = t_1' + \frac{1}{2} t_t \pm \frac{1}{2} t_t + t_2 + t_3 \qquad (2.6)$$

where the (+) sign represents an initial velocity away from the collector and the (-) sign represents an initial velocity toward the collector.

2.5 Planar Two-Field TOFMS

The electric field E between planar electrodes is a constant (assuming no time variation of the potentials on the electrodes). Therefore, the potential is $V(x) = C_1 x + C_2$, where C_1 and C_2 are defined by the boundary conditions. For two planes, j and k, separated by a distance d, and set at potentials V_j and V_k, the potential between the planes is

$$V(x) = \frac{(V_j - V_k)}{d} x + V_k \qquad (2.7)$$

(see Figure (2.4)). The time-of-flight can now be calculated for any initial position x_i, between j and k planes, to any final position x, for any initial velocity v_i, from the time-of-flight equation (equation (2.2)).

For an initial velocity toward the collector, the time-of-flight is

$$t = \pm \left(\frac{m}{2q}\right)^{1/2} \int_{x_i}^{x} \frac{dx'}{\left[\frac{mv_i^2}{2q} + \frac{(V_j - V_k)}{d}(x_i - x')\right]^{1/2}} \tag{2.8}$$

Since $x < x_i$, dx' will be less than 0 and the (-) sign should be used so that $t > 0$. Solving the integral in equation (2.8) gives

$$t = -\left(\frac{m}{2q}\right)^{1/2} \left(\frac{-2d}{(V_j - V_k)}\right) \left[\frac{mv_i^2}{2q} + \frac{(V_j - V_k)}{d}(x_i - x')\right]^{1/2} \Bigg|_{x_i}^{x} \tag{2.9}$$

Evaluating this expression at the limits reduces it to

$$t = \left(\frac{m}{2q}\right)^{1/2} \left(\frac{2d}{(V_j - V_k)}\right) \left[\left\{\frac{(V_j - V_k)}{d}(x_i - x) + \frac{mv_i^2}{2q}\right\}^{1/2} - \left\{\frac{mv_i^2}{2q}\right\}^{1/2}\right] \tag{2.10}$$

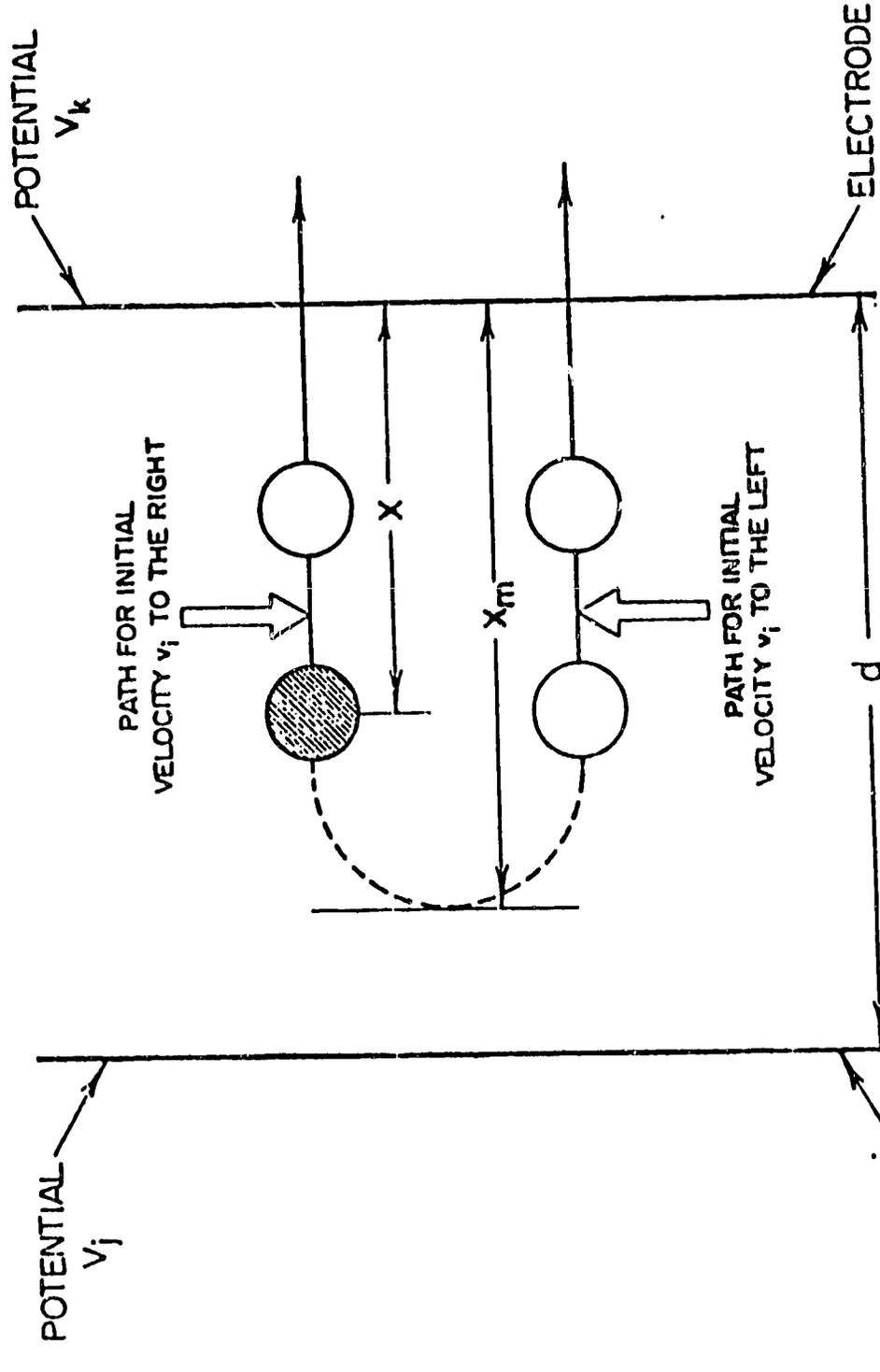

Figure 2.4 Generalized Region Bounded by Planar Electrodes j and k. For Clarity the Cases of Ions Initially Directed to the Left and Right are Indicated with a Separation of Ion Paths. (Reference: Stein (1974)).

The turn around time for an ion with an initial velocity away from the collector must be included. Substituting the appropriate potentials into equation (2.3) produces

$$\frac{(V_j - V_k)}{d} x_m + V_k = \frac{mv_i^2}{2q} + \frac{(V_j - V_k)}{d} x_i + V_k \qquad (2.11)$$

which reduces to

$$x_m = x_i + \left(\frac{mv_i^2}{2q}\right) \frac{d}{(V_j - V_k)} \qquad (2.12)$$

Notice that if $x_m > x_j$, the ion is lost. The turn around time will be just twice the time for the ion to travel from x_m to x_i. Substituting for x_m into equation (2.10) and multiplying by 2 gives the turn around time as

$$t_t = 2\left(\frac{m}{2q}\right)^{1/2} \left(\frac{2d}{(V_j - V_k)}\right) \left(\frac{mv_i^2}{2q}\right)^{1/2} \qquad (2.13)$$

The time-of-flight can now be calculated for all three regions in the planar TOFMS. In the source region we substitute $d = d_1$, $v_i = v_o$, $x_i - x = d_0$ and $\frac{(V_j - V_k)}{d} = \frac{(V_1 - V_2)}{d_1}$ into equations (2.10) and (2.13).

Then using equation (2.5), the time-of-flight for the source region is

$$t_1 = \left(\frac{m}{2q}\right)^{1/2} \left(\frac{2d_1}{(V_1 - V_2)}\right) \left[\left\{ \frac{(V_1 - V_2)}{d_1} d_o + \frac{mv_o^2}{2q} \right\}^{1/2} \pm \left\{ \frac{mv_o^2}{2q} \right\}^{1/2} \right] \tag{2.14}$$

In the acceleration region $(x_i - x) = d = d_2$, $(V_j - V_k)/d = (V_2 - V_3)/d_2$ and

$$v_i^2 = v_o^2 + \frac{2q}{m} (V_i - V_2) \tag{2.15}$$

Substituting $V_i = (V_1 - V_2)\frac{d_o}{d_1} + V_2$ into equation (2.15) gives

$$v_i^2 = v_o^2 + \frac{2q}{m} \frac{d_o}{d_1} (V_1 - V_2) = \gamma^2 \tag{2.16}$$

When equation (2.16) and the other parameters for the acceleration region are substituted into equation (2.10), the time-of-flight for the acceleration region is given by

$$t_2 = \left(\frac{m}{2q}\right)^{1/2} \left(\frac{2d_2}{(V_2 - V_3)}\right) \left[\left\{ V_2 - V_3 + \frac{m\gamma^2}{2q} \right\}^{1/2} - \left\{ \frac{m\gamma^2}{2q} \right\}^{1/2} \right] \tag{2.17}$$

As the ions traverse the drift region, their velocities will be constant and the equation of motion is

$$qV_3 + \frac{1}{2} mv_d^2 = qV_i + \frac{1}{2} mv_o^2 \tag{2.18}$$

Solving for the drift region velocity gives

$$v_d = \left(\frac{2q}{m}\right)^{1/2} \left\{V_i - V_3 + \frac{mv_o^2}{2q}\right\}^{1/2} \qquad (2.19)$$

where V_i is the potential at the ion starting position. Since v_d is constant through the field-free drift region, the time-of-flight is given by d_3/v_d or

$$t_3 = \left(\frac{m}{2q}\right)^{1/2} \frac{d_3}{\left\{V_i - V_3 + \frac{mv_o^2}{2q}\right\}^{1/2}} \qquad (2.20)$$

Because the drift region is field-free, the same expression for t_3, with the appropriate expression for V_i, can be used for all three geometries to be discussed here. Substituting the proper expression for V_i into equation (2.20) gives

$$t_3 = \left(\frac{m}{2q}\right)^{1/2} \frac{d_3}{\left\{(V_1 - V_2)\frac{d_o}{d_1} + V_2 - V_3 + \frac{mv_o^2}{2q}\right\}^{1/2}} \qquad (2.21)$$

Combining the expressions for the time-of-flight in the three regions gives the total time-of-flight for a planar two-field TOFMS

$$t = \left(\frac{m}{2q}\right)^{1/2}\left\{\left\{\frac{2d_1}{(V_1 - V_2)}\right\}\left[\left\{\frac{(V_1 - V_2)}{d_1} d_o + \frac{mv_o^2}{2q}\right\}^{1/2} \pm \left\{\frac{mv_o^2}{2q}\right\}^{1/2}\right]\right.$$

$$+ \frac{2d_2}{(V_2 - V_3)}\left[\left\{V_2 - V_3 + \frac{m\gamma^2}{2q}\right\}^{1/2} - \left\{\frac{m\gamma^2}{2q}\right\}^{1/2}\right]$$

$$\left. + \frac{d_3}{\left\{(V_1 - V_2)\frac{d_o}{d_1} + V_2 - V_3 + \frac{mv_o^2}{2q}\right\}^{1/2}}\right\} \qquad (2.22)$$

The (+) sign is for an initial velocity away from the collector, while the (-) sign is for an initial velocity toward the collector.

Equation (2.22) reduces to the expressions for the time-of-flight calculated by Wiley and McLaren (1955) and given by their equations (2a), (2b) and (2c). It is necessary to substitute $d_0 = s_0$, $d_1 = s$, $d_2 = d$, $d_3 = D$, $U_0 = \frac{mv_o^2}{2}$, $\frac{(V_1 - V_2)}{d_1} = E_s$, $\frac{(V_2 - V_3)}{d_2} = E_d$ and $U = U_0 + qsE_s + qdE_d$ into equation (2.22) and rearrange the terms. It is also necessary to change the units kg, m, V and sec into amu, cm, eV and μsec, respectively, in order to produce the multiplicative factor of 1.02 used in Wiley and McLaren (1955). Equation (2.22) also reduces to the result presented in equation (1) in Pavlenko et al., (1968) if the erroneous symbol s is corrected to s_0 in Pavlenko's equation (1).

2.6 Cylindrical Two-Field TOFMS

Between two concentric cylinders, the electric field E(r) is proportional to $\frac{1}{r}$. Therefore, the potential is $V(r) = C_1 \ln r + C_2$, where C_1 and C_2 are determined by the boundary conditions. For two concentric cylinders, labelled j and k, with potentials V_j and V_k and radii r_j and r_k, the potential between cylinders is given by

$$V(r) = \frac{(V_j - V_k)}{\ln (r_j/r_k)} \ln (r/r_j) + V_j \qquad (2.23)$$

(see Figure (2.5)).

For an initial velocity toward the collector (inward in the spectrometer considered here) the time-of-flight equation for the cylindrical-geometry mass spectrometer can be derived by substituting the potential given by equation (2.23) into the time-of-flight equation (2.2) and using r instead of x. This gives

$$t = \pm \left(\frac{m}{2q}\right)^{1/2} \int_{r_i}^{r} \frac{dr'}{\left\{\frac{mv_i^2}{2q} + \frac{(V_j - V_k)}{\ln(r_j/r_k)} \ln(r_i/r')\right\}^{1/2}} \qquad (2.24)$$

Since $r < r_0$, dr' will be less than 0 and the (-) sign is chosen so that $t > 0$. If we define

$$C_{jk} = \left\{\frac{mv_i^2}{2q}\right\} \frac{\ln (r_j/r_k)}{(V_j - V_k)} \qquad (2.25)$$

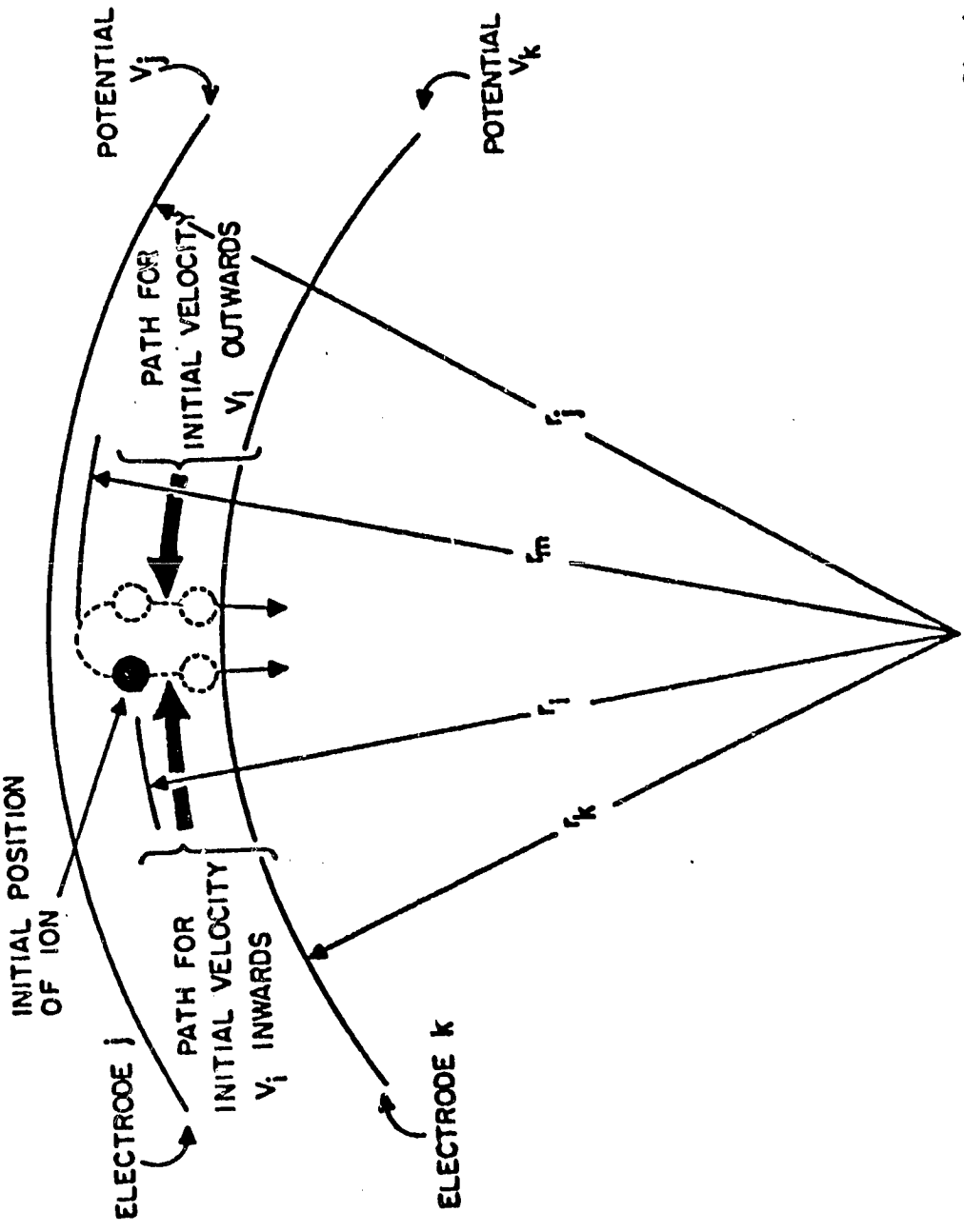

Figure 2.5 Generalized Region Bounded by Cylindrical Electrodes j and k. For Clarity, the Cases of Inward Directed and Outward Directed Initial Velocities are Indicated with Slightly Separate Ion Paths. (Reference: Zabielski, Stein and Kendall (1972/1973)).

and

$$P = \left\{\ln (r_i/r') + C_{jk}\right\}^{1/2} \tag{2.26}$$

then

$$r' = r_i\, e^{-(P^2 - C_{jk})} \tag{2.27}$$

and

$$dr' = -2r_i P\, e^{-(P^2 - C_{jk})}\, dP \tag{2.28}$$

Substituting equations (2.25), (2.26), (2.27) and (2.28) into (2.24) and rearranging terms produces

$$t = -\left(\frac{m}{2q}\right)^{1/2} \int_{C_{jk}^{1/2}}^{\{\ln (r_i/r) + C_{jk}\}^{1/2}} \frac{-2r_i\, P\, e^{-(P^2 - C_{jk})}\, dP}{P\left\{\frac{(V_j - V_k)}{\ln(r_j/r_k)}\right\}^{1/2}} \tag{2.29}$$

Taking the constants out of the integral reduces equation (2.29) to

$$t = \left(\frac{m}{2q}\right)^{1/2} 2r_i \left\{\frac{\ln (r_j/r_k)}{(V_j - V_k)}\right\}^{1/2} e^{C_{jk}} \int_{C_{jk}^{1/2}}^{\{\ln(r_i/r)+C_{jk}\}^{1/2}} e^{-P^2} dP \tag{2.30}$$

We can write

$$\int_B^A e^{-P^2}\,dP = \int_o^A e^{-P^2}\,dP - \int_o^B e^{-P^2}\,dP = \frac{\sqrt{\pi}}{2}(\text{erf}\,A - \text{erf}\,B) \tag{2.31}$$

where

$$\text{erf}\,A = \frac{2}{\sqrt{\pi}} \int_o^A e^{-y^2}\,dy \tag{2.31a}$$

Equation (2.30) can now be written as

$$t = \left(\frac{m}{2q}\right)^{1/2} r_i \left\{\frac{\pi \ln(r_j/r_k)}{(V_j - V_k)}\right\}^{1/2} e^{C_{jk}} \left\{\text{erf}\left[\,(\ln(r_i/r) + C_{jk})^{1/2}\right] - \text{erf}\,\left[\,C_{jk}^{1/2}\,\right]\right\} \tag{2.32}$$

The time-of-flight for each region of the mass spectrometer can now be derived. For an initial ion velocity toward the collector in the source region we substitute $r_i = r_o$, $V_j = V_1$, $V_k = V_2$, $r_j = r_1$, $v_i = v_o$ and $r_k = r_2$ into equation (2.32) giving

$$t_1' = \left(\frac{m}{2q}\right)^{1/2} r_o \left\{\frac{\pi \ln(r_1/r_2)}{(V_1 - V_2)}\right\}^{1/2} e^{C_{12}} \left\{\text{erf}\left[\,(\ln(r_o/r) + C_{12})^{1/2}\right] - \text{erf}\,\left[\,C_{12}^{1/2}\right]\right\} \tag{2.33}$$

where

$$C_{12} = \frac{mv_o^2}{2q} \frac{\ln (r_1/r_2)}{(V_1 - V_2)} \tag{2.34}$$

When the ion has an initial outward velocity, the turn around time can be calculated after calculating the turn around radius, r_m. Substituting the appropriate potentials into equation (2.3) gives

$$\frac{(V_j - V_k)}{\ln (r_j/r_k)} \ln (r_m/r_j) + V_j = \frac{mv_i^2}{2q} + \frac{(V_j - V_k)}{\ln(r_j/r_k)} \ln(r_i/r_j) + V_j \tag{2.35}$$

This yields

$$r_m = r_i e^{C_{jk}} \tag{2.36}$$

Note that if $r_m > r_j$ the ion is lost. From equation (2.32) we can solve for the time for an ion to travel from r_m to the initial position r_i by substituting $r = r_i$, $r_i = r_m$ and $v_i = 0$. The turn around time will be exactly twice this time or

$$t_t = \left(\frac{m}{2q} \right)^{1/2} 2r_m \left\{ \frac{\pi \ln(r_j/r_k)}{(V_j - V_k)} \right\}^{1/2} \text{erf} \left[\{\ln(r_m/r_i)\}^{1/2} \right] \tag{2.37}$$

Now substituting for r_m from equation (2.36) gives

$$t_t = \left(\frac{m}{2q} \right)^{1/2} 2r_i \left\{ \frac{\pi \ln (r_j/r_k)}{(V_j - V_k)} \right\}^{1/2} e^{C_{jk}} \text{erf} \left[C_{jk}^{1/2} \right] \tag{2.38}$$

Making the same substitutions used in the derivation of equation (2.33) produces

$$t_t = \left(\frac{m}{2q}\right)^{1/2} 2r_o \left\{\frac{\pi \ln(r_1/r_2)}{(V_1 - V_2)}\right\}^{1/2} e^{C_{12}} \operatorname{erf}\left[C_{12}^{1/2}\right] \tag{2.39}$$

Combining equations (2.33) and (2.39) into equation (2.5) gives an expression for the time-of-flight in the source region

$$t_1 = \left(\frac{m}{2q}\right)^{1/2} r_o \left\{\frac{\pi \ln(r_1/r_2)}{(V_1 - V_2)}\right\}^{1/2} e^{C_{12}} \left\{\operatorname{erf}\left[(\ln(r_o/r_2) + C_{12})^{1/2}\right] \pm \operatorname{erf}\left[C_{12}^{1/2}\right]\right\} \tag{2.40}$$

In the acceleration region region we substitute $r_j = r_i = r_2$, $r = r_k = r_3$, $V_j = V_2$ and $V_k = V_3$ into equation (2.32) along with the initial velocity. The initial velocity for the acceleration region can be calculated from equation (2.1) by making the appropriate substitutions. This gives

$$\frac{1}{2} m v_o^2 + \frac{q(V_1 - V_2)}{\ln(r_1/r_2)} \ln(r_o/r_1) + qV_1 = \frac{1}{2} m v_i^2 + qV_2 \tag{2.41}$$

where v_i is the velocity in question. Solving for v_i^2 gives

$$v_i^2 = \frac{2q}{m} \frac{(V_1 - V_2) \ln(r_o/r_2)}{\ln(r_1/r_2)} + v_o^2 = \beta^2 \tag{2.42}$$

Now the time-of-flight for the acceleration region is given by

$$t_2 = \left(\frac{m}{2q}\right)^{1/2} r_2 \left\{\frac{\pi \ln(r_2/r_3)}{(V_2 - V_3)}\right\}^{1/2} e^{C_{23}} \left\{\operatorname{erf}\left[(\ln(r_2/r_3) + C_{23})^{1/2}\right] - \operatorname{erf}\left[C_{23}^{1/2}\right]\right\} \tag{2.43}$$

where

$$C_{23} = \left(\frac{m\beta^2}{2q}\right) \frac{\ln(r_2/r_3)}{(V_2 - V_3)} \tag{2.44}$$

In the drift region we substitute $d_3 = r_3 - r_c$ into equation (2.20). This gives the time-of-flight for region 3 as

$$t_3 = \left(\frac{m}{2q}\right)^{1/2} \frac{r_3 - r_c}{\left\{V_i - V_3 + \frac{mv_o^2}{2q}\right\}^{1/2}} \tag{2.45}$$

Now combining equations (2.40), (2.43) and (2.45) gives the total time-of-flight for a cylindrical two-field TOFMS as

$$t = \left(\frac{m}{2q}\right)^{1/2} \left\{r_o \left\{\frac{\pi \ln(r_1/r_2)}{(V_1 - V_2)}\right\}^{1/2} e^{C_{12}} \left\{\operatorname{erf}\left[(\ln(r_o/r_2) + C_{12})^{1/2}\right] \pm \operatorname{erf}\left[C_{12}^{1/2}\right]\right\} + r_2 \left\{\frac{\pi \ln(r_2/r_3)}{(V_2 - V_3)}\right\}^{1/2} e^{C_{23}} \left\{\operatorname{erf}\left[(\ln(r_2/r_3) + C_{23})^{1/2}\right] - \operatorname{erf}\left[C_{23}^{1/2}\right]\right\}$$

$$+ \frac{r_3 - r_c}{\left\{V_i - V_3 + \frac{mv_o^2}{2q}\right\}^{1/2}} \Bigg\} \qquad (2.46)$$

The (+) sign corresponds to an initial ion velocity away from the collector while the (-) sign corresponds to an initial ion velocity toward the collector.

Expanding the error function terms of equation (2.46) in Maclaurin series and making the substitutions $r_0 = r_s$, $v_0 = v_s$, $C_{12} = A_{12}$, $V_i = V_s$ and $C_{23} = A_{23}$ produces an expression for the time-of-flight in a cylindrical TOFMS which is identical to the expression obtained by combining equations (11), (12), (15) and (16) in Zabielski, Diem and Kendall (1970), according to equation (2.6) in this thesis. Equation (2.46) is also identical to equation (2.5.26) in Stein (1974) if the substitutions $r_0 = r_s$, $v_0 = v_s$, $C_{12} = A_{12}$, $C_{23} = A_{23}$ and $V_i = V_s$ are made.

2.7 Spherical Two-Field TOFMS

When two concentric spheres, labelled j and k, with radii r_j and r_k, are set at potentials V_j and V_k, the potential between the spheres is $V(r) = C_1/r + C_2$ where C_1 and C_2 are defined by the boundary conditions. Solving for C_1 and C_2 yields

$$V(r) = \frac{-k_{jk}}{r} + \frac{(r_j V_j - r_k V_k)}{(r_j - r_k)} \qquad (2.47)$$

with

$$k_{jk} = \frac{r_j r_k (V_j - V_k)}{(r_j - r_k)} \qquad (2.48)$$

This potential produces an electric field E(r) proportional to $\frac{1}{r^2}$ (see Figure (2.6)).

The time-of-flight can now be calculated for any initial position r_i, between the j and k spheres, to any final position $r(r < r_i)$ for an inward velocity. Substituting equation (2.47) into equation (2.2) and using the variable r instead of x produces

$$t = \pm \left(\frac{m}{2q}\right)^{1/2} \int_{r_i}^{r} \frac{dr'}{\left\{\frac{mv_i^2}{2q} + k_{jk}\left(\frac{1}{r'} - \frac{1}{r_i}\right)\right\}^{1/2}} \tag{2.49}$$

Since $r < r_i$, dr' will be less than 0 and the (-) sign is chosen to give an increasing t. Multiply the numerator and denominator of equation (2.49) by $r'^{1/2}$. After rearranging terms, this yields

$$t = - \left(\frac{m}{2q}\right)^{1/2} \int_{r_i}^{r} \frac{r'^{1/2}\, dr'}{\left\{k_{jk} + \left[\frac{mv_i^2}{2q} - \frac{k_{jk}}{r_i}\right] r'\right\}^{1/2}} \tag{2.50}$$

Now dividing numerator and denominator by

$$\left[\frac{k_{jk}}{r_i} - \frac{mv_i^2}{2q}\right]^{1/2}$$

and defining

$$\alpha_{jk} = \frac{r_i k_{jk}}{k_{jk} - r_i\left(\frac{mv_i^2}{2q}\right)} \tag{2.51}$$

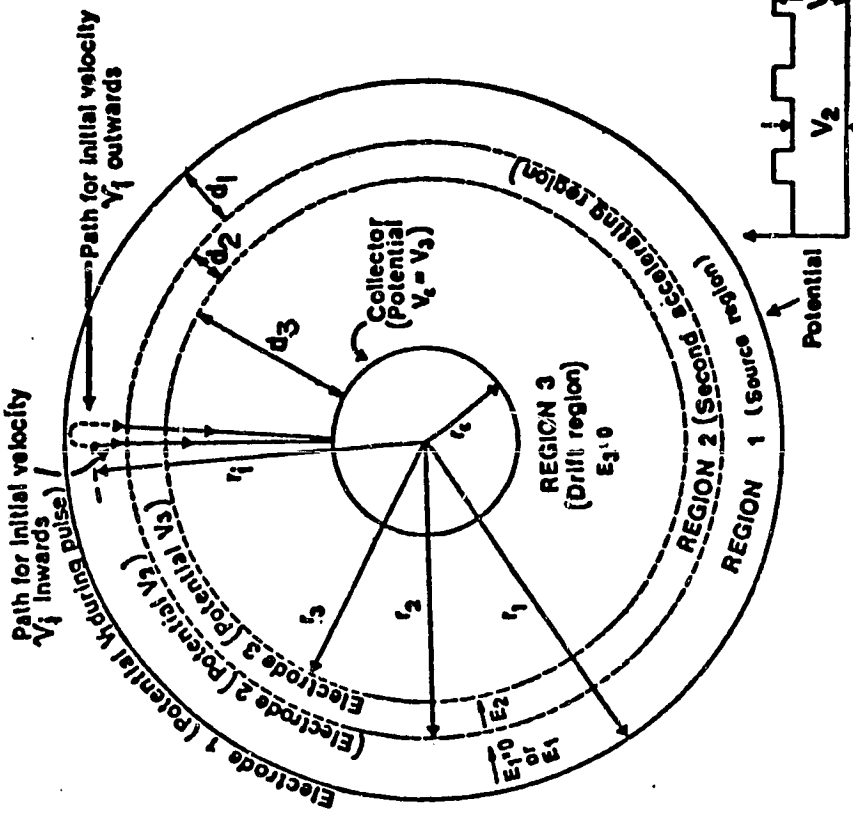

Figure 2.6 Cross Section of Spherical Time-of-Flight Mass Spectrometer with Two Accelerating Regions and a Single Drift Region. Ions are Initially in Region 1, the Source Region. (Reference: Zabielski, Stein and Kendall (1972/1973)).

give t as

$$t = -\left(\frac{m}{2q}\right)^{1/2} \left(\frac{\alpha_{jk}}{k_{jk}}\right)^{1/2} \int_{r_i}^{r} \frac{r'^{1/2}\, dr'}{(\alpha_{jk} - r')^{1/2}} \qquad (2.52)$$

It is now necessary to show that $\alpha_{jk} > 0$ and $\alpha_{jk} - r > 0$ in order to solve the integral in equation (2.52). Let us calculate the maximum radius for an ion with an initial velocity away from the collector. Substituting the proper potentials into equation (2.3) results in

$$\left[\frac{-k_{jk}}{r_m} + \frac{r_j V_j - r_k V_k}{(r_j - r_k)}\right] = \frac{mv_i^2}{2q} + \left[\frac{-k_{jk}}{r_i} + \frac{r_j V_j - r_k V_k}{(r_j - r_k)}\right] \qquad (2.53)$$

Solving for r_m yields $r_m = \alpha_{jk}$ (2.54)

Therefore, $\alpha_{jk} > 0$, and since $r_m \geq r_i$, then $\alpha_{jk} - r > 0$. With the substitution of $r' = x^2$ into equation (2.52) we get

$$t = -\left(\frac{m}{2q}\right)^{1/2} \left(\frac{\alpha_{jk}}{k_{jk}}\right)^{1/2} \int_{r_i^{1/2}}^{r} \frac{2x^2\, dx}{(\alpha_{jk} - x^2)^{1/2}} \qquad (2.55)$$

Since $\alpha_{jk} > 0$ and $\alpha_{jk} - x^2 > 0$, this integral can be evaluated as

$$t = -\left(\frac{m}{2q}\right)^{1/2}\left(\frac{\alpha_{jk}}{k_{jk}}\right)^{1/2}\left\{-x(\alpha_{jk} - x^2)^{1/2} + \alpha_{jk}\sin^{-1}\left\{\frac{x}{\alpha_{jk}^{1/2}}\right\}\right\}\Bigg|_{r_i^{1/2}}^{r^{1/2}} \tag{2.56}$$

where only the principal values for $\sin^{-1}$ are to be used. Evaluating the limits of equation (2.56) yields

$$t = \left(\frac{m}{2q}\right)^{1/2}\left(\frac{\alpha_{jk}}{k_{jk}}\right)^{1/2}\left\{r^{1/2}(\alpha_{jk} - r)^{1/2} - r_i^{1/2}(\alpha_{jk} - r_i)^{1/2} - \alpha_{jk}\left[\sin^{-1}\left\{\left(\frac{r}{\alpha_{jk}}\right)^{1/2}\right\} - \sin^{-1}\left\{\left(\frac{r_i}{\alpha_{jk}}\right)^{1/2}\right\}\right]\right\} \tag{2.57}$$

The time spent in the source region for an ion initially moving toward the collector can be calculated by substituting $v_i = v_0$, $r_i = r_0$, $V_j = V_1$, $V_k = V_2$, $r_j = r_1$ and $r = r_k = r_2$ into equation (2.57). This yields

$$t_1' = \left(\frac{m}{2q}\right)^{1/2}\left(\frac{\alpha_{12}}{k_{12}}\right)^{1/2}\left\{r_2^{1/2}(\alpha_{12} - r_2)^{1/2} - r_o^{1/2}(\alpha_{12} - r_o)^{1/2} - \alpha_{12}\left[\sin^{-1}\left\{\left(\frac{r_2}{\alpha_{12}}\right)^{1/2}\right\} - \sin^{-1}\left\{\left(\frac{r_o}{\alpha_{12}}\right)^{1/2}\right\}\right]\right\} \tag{2.58}$$

The turn around time for ions initially moving away from the collector in the source region can be calculated by substituting $k_{jk} = k_{12}$, $V_j = V_1$, $V_k = V_2$, $r_j = r_1$, $r_k = r_2$, $r_i = r_m = \alpha_{12}$, $r = r_0$, $\alpha_{jk} = \alpha_{12}$ and $v_i = 0$ into equation (2.57) and multiplying by 2. This yields

$$t_t = 2 \left(\frac{m}{2q}\right)^{1/2} \left(\frac{\alpha_{12}}{k_{12}}\right)^{1/2} \left\{ r_o^{1/2} (\alpha_{12} - r_o)^{1/2} - \alpha_{12} \cdot \left[\sin^{-1} \left\{ \left(\frac{r_o}{\alpha_{12}} \right)^{1/2} \right\} - \frac{\pi}{2} \right] \right\} \qquad (2.59)$$

Combining equations (2.58) and (2.59) according to equation (2.5) gives the total time-of-flight in the source region as

$$t_1 = \left(\frac{m}{2q}\right)^{1/2} \left(\frac{\alpha_{12}}{k_{12}}\right)^{1/2} \left\{ r_2^{1/2} (\alpha_{12} - r_2)^{1/2} - \alpha_{12} \cdot \left[\sin^{-1} \left\{ \left(\frac{r_2}{\alpha_{12}} \right)^{1/2} \right\} - \frac{\pi}{2} \right] \pm \left(r_o^{1/2} (\alpha_{12} - r_o)^{1/2} - \alpha_{12} \cdot \left[\sin^{-1} \left\{ \left(\frac{r_o}{\alpha_{12}} \right)^{1/2} \right\} - \frac{\pi}{2} \right] \right) \right\} \qquad (2.60)$$

The initial velocity of an ion as it enters the acceleration region is given by v_i where v_i is defined by

$$\frac{mv_o^2}{2q} + V_i = \frac{mv_i^2}{2q} + V_2 \qquad (2.61)$$

and where

$$V_i = \frac{-k_{12}}{r_o} + \frac{V_1 r_1 - V_2 r_2}{r_1 - r_2} \qquad (2.62)$$

Solving for v_i^2 yields

$$v_i^2 = \frac{2q}{m} (V_i - V_2) + v_o^2 = \Delta^2 \qquad (2.63)$$

In the acceleration region we substitute $r_j = r_i = r_2$, $r_k = r = r_3$, $\alpha_{jk} = \alpha_{23}$, $k_{jk} = k_{23}$, $V_j = V_2$, $V_k = V_3$ and $v_i = \Delta$ into equation (2.57) to calculate the time-of-flight. This yields

$$t_2 = \left(\frac{m}{2q}\right)^{1/2} \left(\frac{\alpha_{23}}{k_{23}}\right)^{1/2} \left\{ r_3^{1/2} (\alpha_{23} - r_3)^{1/2} - r_2^{1/2} (\alpha_{23} - r_2)^{1/2} \right.$$

$$\left. - \alpha_{23} \left[\sin^{-1} \left\{ \left(\frac{r_3}{\alpha_{23}} \right)^{1/2} \right\} - \sin^{-1} \left\{ \left(\frac{r_2}{\alpha_{23}} \right)^{1/2} \right\} \right] \right\} \qquad (2.64)$$

To calculate the time-of-flight for the drift region, we substitute $d_3 = r_3 - r_c$ into equation (2.20) yielding

$$t_3 = \left(\frac{m}{2q}\right)^{1/2} \frac{r_3 - r_c}{\left\{ V_i - V_3 + \frac{mv_o^2}{2q} \right\}^{1/2}} \qquad (2.65)$$

Combining equations (2.60), (2.64) and (2.65) gives the total time-of-flight as

$$t = \left(\frac{m}{2q}\right)^{1/2} \left\{ \left(\frac{\alpha_{12}}{k_{12}}\right)^{1/2} \left[r_2^{1/2} (\alpha_{12} - r_2)^{1/2} - \alpha_{12} \cdot \left\{ \sin^{-1} \left[\left(\frac{r_2}{\alpha_{12}}\right)^{1/2} \right] - \frac{\pi}{2} \right\} \right.\right.$$

$$\pm \left[r_o^{1/2} (\alpha_{12} - r_o)^{1/2} - \alpha_{12} \left\{ \sin^{-1} \left[\left(\frac{r_o}{\alpha_{12}}\right)^{1/2} \right] - \frac{\pi}{2} \right\} \right] \Bigg]$$

$$+ \left(\frac{\alpha_{23}}{k_{23}}\right)^{1/2} \left[r_3^{1/2} (\alpha_{23} - r_3)^{1/2} - r_2^{1/2} (\alpha_{23} - r_2)^{1/2} - \alpha_{23} \cdot \right.$$

$$\left. \left\{ \sin^{-1} \left[\left(\frac{r_3}{\alpha_{23}}\right)^{1/2} \right] - \sin^{-1} \left[\left(\frac{r_2}{\alpha_{23}}\right)^{1/2} \right] \right\} \right]$$

$$\left. + \frac{r_3 - r_c}{\left\{ V_i - V_3 + \frac{mv_o^2}{2q} \right\}^{1/2}} \right\} \qquad (2.66)$$

where

$$k_{12} = \frac{r_1 r_2 (V_2 - V_3)}{r_1 - r_2} \qquad (2.67)$$

$$k_{23} = \frac{r_2 r_3 (V_2 - V_3)}{r_2 - r_3} \qquad (2.68)$$

$$\alpha_{12} = \frac{r_o k_{12}}{k_{12} - r_o\left(\frac{mv_o^2}{2q}\right)} \tag{2.69}$$

and

$$\alpha_{23} = \frac{r_2 k_{23}}{k_{23} - r_2\left(\frac{m\Delta^2}{2q}\right)} \tag{2.70}$$

The (+) sign represents an initial ion velocity away from the collector and the (-) sign represents an initial ion velocity toward the collector.

Equation (2.66) can be shown to be identical with equations (12), (13), (18) and (19) of Zabielski, Stein and Kendall (1972/1973) combined, using equation (2.6) in this thesis. The substitutions of $r_0 = r_s$, $v_0 = v_s$, $\Delta^2 = \phi^2$, $\frac{k_{12}}{\alpha_{12}} = \frac{\gamma_{12}}{r_s}$ and $\frac{k_{23}}{\alpha_{23}} = \frac{\gamma_{23}}{r_2}$ into equation (2.66) are necessary. When the $\sin^{-1}$ terms are expanded into Maclaurin series and $(\alpha_{12} - r_2)^{1/2}$, $(\alpha_{12} - r_0)^{1/2}$, $(\alpha_{23} - r_3)^{1/2}$ and $(\alpha_{23} - r_2)^{1/2}$ are expanded into binomial series, a simple rearrangement of terms will show equation (2.66) is identical with the results of Zabielski, Stein and Kendall (1972/1973).

Equation (2.66) is also identical with equation (2.6.27) in Stein (1974), with the substitutions of $r_0 = r_s$, $v_0 = v_s$, $V_i = V_s$ and $\Delta^2 = \phi^2$ into equation (2.66).

2.8 Numerical Studies; Two-Field TOFMS

The most convenient method of studying the effect of various operating voltages and grid spacings on the ion flight time

characteristics of TOF mass spectrometers is to use computer simulation. Computer programs were developed by myself using the time-of-flight equations derived earlier in this chapter. These programs calculated ion flight time as a function of ion starting position in the source region, ion initial energy (velocity), electrode spacings, operating voltages and ion mass for planar, cylindrical and spherical-electrode TOFMS.

Numerical studies using computer simulation have been reported by Zabielski (1970), Zabielski, Diem and Kendall (1970), Zabielski, Stein and Kendall (1972/1973) and Stein (1974). Zabielski (1970) discussed time-of-flight versus starting position for all three geometries when there was zero initial ion velocity and near to the optimum space focusing operating conditions. The effects of initial velocities, initial energy spreads, operating voltages which produce better velocity focusing characteristics and varying electrode spacings were, for the most part, ignored. Zabielski, Diem and Kendall (1970) and Zabielski, Stein and Kendall (1972/1973) discussed only optimum space focusing operating conditions for zero initial ion velocities for the cylindrical and spherical geometries, respectively. Stein (1974) concentrated on optimum space focusing characteristics with zero ion initial velocities. However, he did study the effects of varying electrode spacings and discussed the effects of initial ion velocities and initial energy spreads on the flight time characteristics.

One striking characteristic of the results presented by the above authors is the lack of significant variation in the time-of-flight

versus starting position curves between the three TOFMS geometries. Obviously, the radius of curvature of the electrodes for the cylindrical and spherical geometries studies was not small enough, in relation to the interelectrode spacings, to produce a significant variation in the source and acceleration region electric fields as compared with a planar geometry.

In order to fill in the gaps left by previous researchers, this section will concentrate on the effects of initial ion velocities, initial energy spreads, velocity focusing characteristics and exaggerating the cylindrical and spherical geometry effects on flight time characteristics.

Figure (2.7) shows the space focusing characteristics of the planar, cylindrical and spherical geometries for near the optimum space focusing voltage ratio (the voltage ratio is defined as $R = (V_1 - V_3)/(V_2 - V_3)$). This Figure is presented for comparison with the Figures which will follow. The time scale of Figure (2.7) is greatly expanded to bring out the characteristics. An excellent discussion of these curves and the resulting peak shapes can be found in Stein (1974). It must be emphasized that no initial velocity spread has been considered in producing the curves in Figure (2.7). The effect of an initial velocity spread on resolving power is significant. For example, the space focusing resolving power for $R = 1.64$ in a spherical-electrode TOFMS, taken from Figure (2.7), is 1450. However, the actual resolving power for this type of instrument in the laboratory is about 10 due to the initial velocity spread.

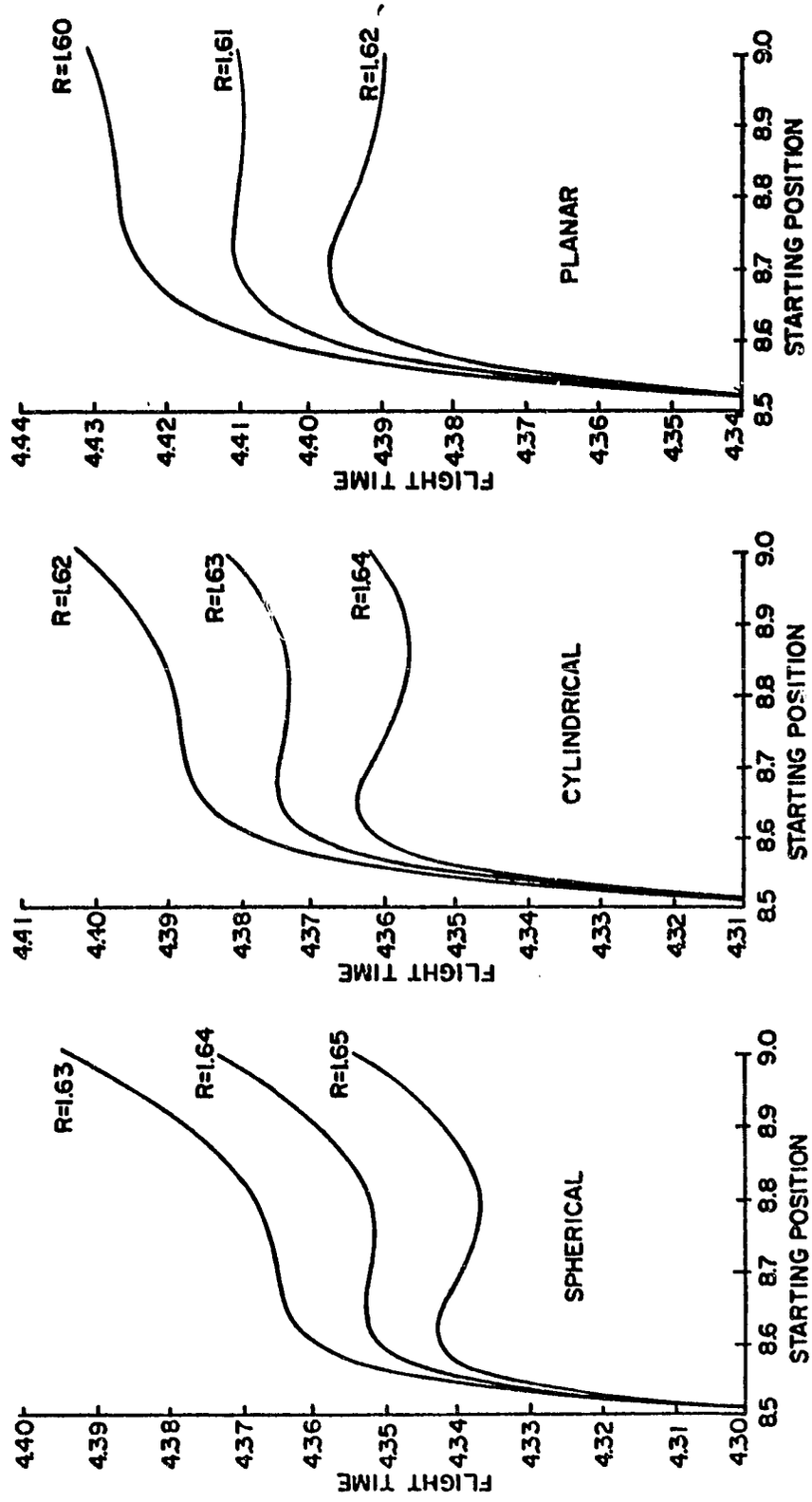

Figure 2.7 Computer Generated Space Focusing Characteristics of Planar, Cylindrical and Spherical Time-of-Flight Mass Spectrometers Having $r_1 = 9.00$, $r_2 = 8.50$, $r_3 = 8.50$ and $r_c = 4.60$ Units. A Normalized Time Scale is Plotted Vertically, Initial Ion Position Horizontally, Initial Velocity Assumed Zero. The Voltage Ratio is Defined by $R = (V_1 - V_3)/(V_2 - V_3)$. (Reference: Zabielski, Stein and Kendall (1972/1973)).

Figure (2.8) illustrates the space focusing curves for high voltage ratios with an initial ion energy of 4 eV in a cylindrical-electrode TOFMS. The bars represent an energy spread of ± 1 eV around the ion initial energy. As the voltage ratio increases, the poorer space focusing characteristic can be easily seen. Also notice the decreasing spread in the flight times due to the initial energy spread. Figure (2.9) illustrates the space focusing characteristics for a spherical-electrode TOFMS for the same conditions as were used in Figure (2.8).

Figure (2.10) represents the changes in the flight time spread for a cylindrical-electrode TOFMS due to a 2 eV initial energy spread as the voltage ratio is increased. This Figure is derived from the time spread bars of Figure (2.8). These curves can be said to represent the velocity focusing characteristics of the cylindrical TOFMS. Perfect velocity focusing would be represented by a straight line at zero time spread. These curves suggest that an extremely high voltage ratio or an extremely long drift region length would be required for perfect velocity focusing. This conclusion confirms the suggestion made by Stein (1974) and by Sanzone (1970). Figure (2.11) represents the velocity focusing characteristics for a spherical TOFMS taken from Figure (2.9).

A comparison of Figure (2.8) to Figure (2.9) and Figure (2.10) to Figure (2.11) illustrates, again, the similarity of the space and velocity focusing characteristics for the cylindrical and spherical geometries. The differences in the curves are minimal for the

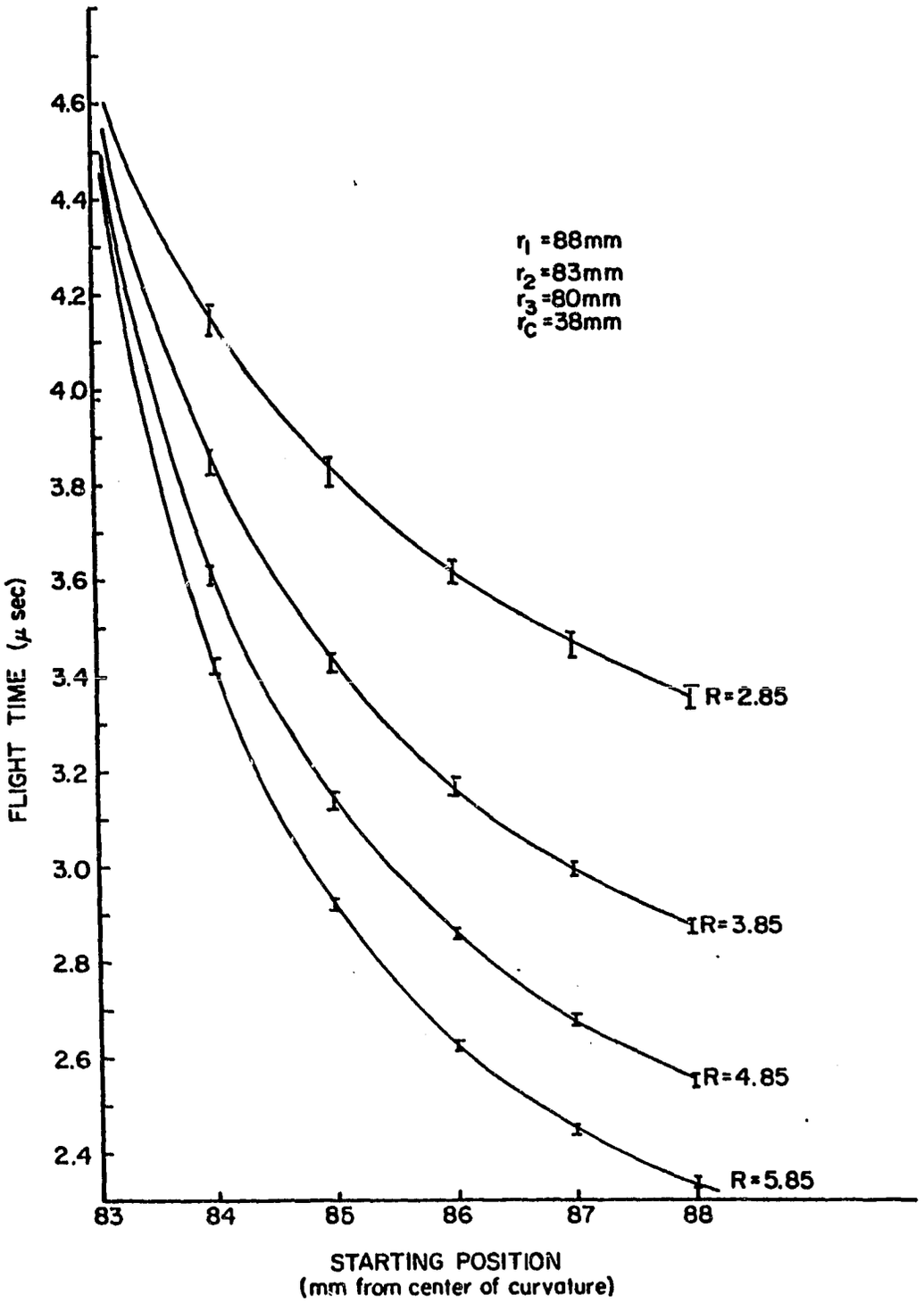

Figure 2.8 Computer Generated Space Focusing Characteristics for a Cylindrical-Electrode TOFMS Having r_1 = 88 mm, r_2 = 83 mm, r_3 = 80 mm, r_c = 38 mm, an Ion Mass of 133 amu, and an Initial Ion Energy of 4 eV (Directed Toward the Collector). The Bars Represent an Initial Energy Spread of ± 1 eV.

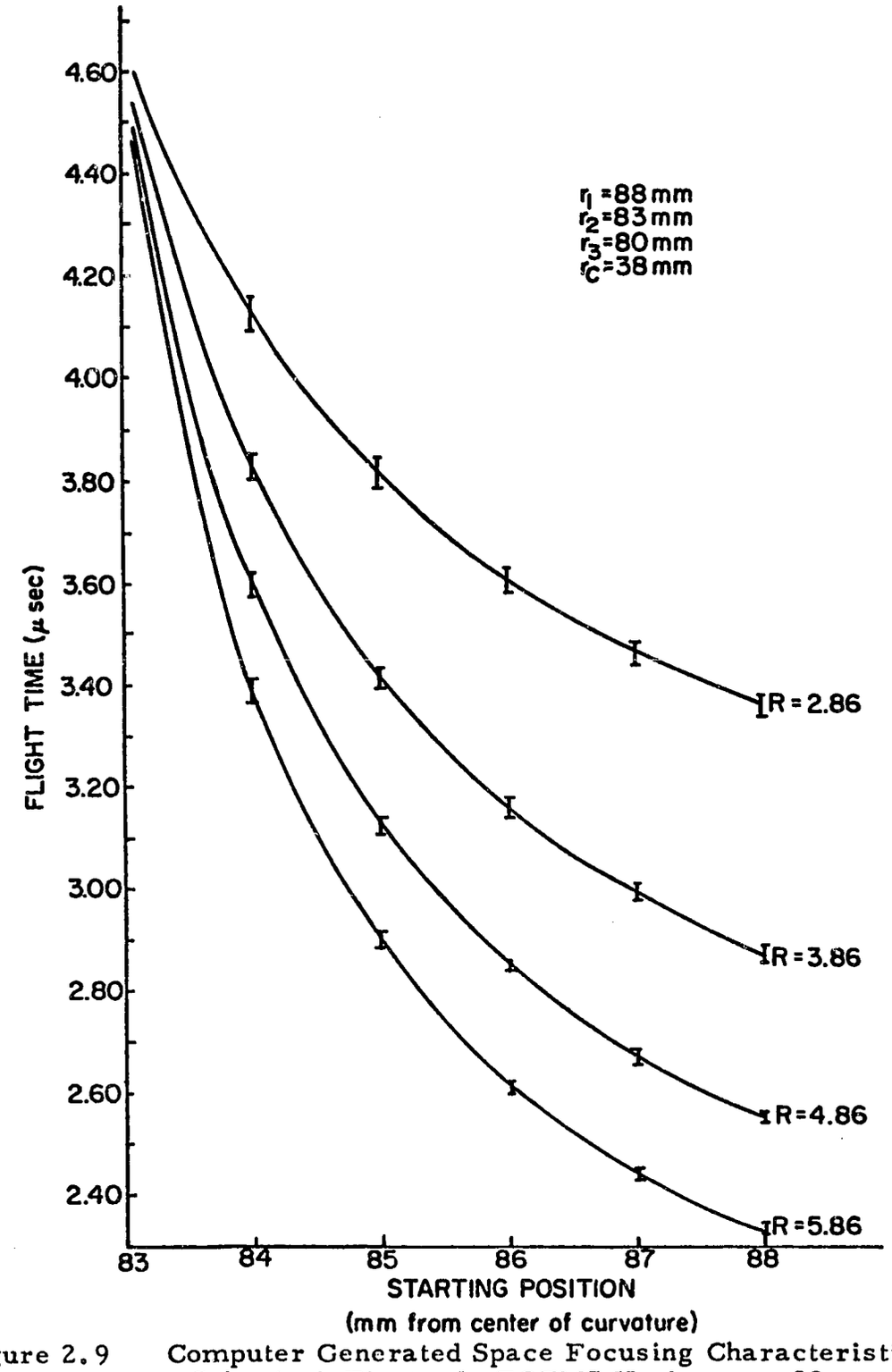

Figure 2.9 Computer Generated Space Focusing Characteristics of a Spherical-Electrode TOFMS Having r_1 = 88 mm, r_2 = 83 mm, r_3 = 80 mm, r_c = 38 mm, an Ion Mass of 133 amu, and an Initial Ion Energy of 4 eV (Directed Toward the Collector). The Bars Represent an Initial Ion Energy Spread of ± 1 eV.

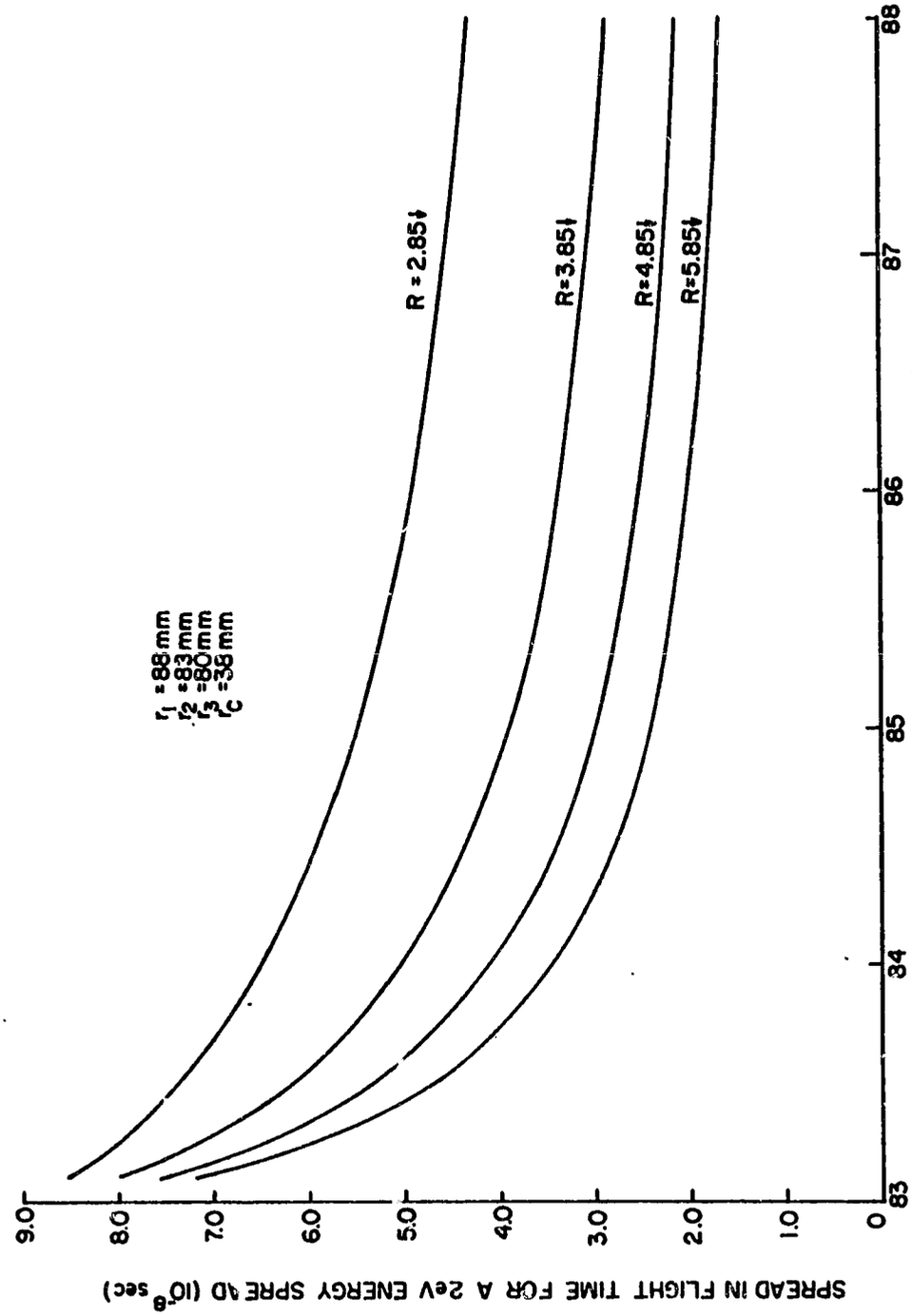

Figure 2.10 Computer Generated Velocity Focusing Characteristics for a Cylindrical-Electrode TOFMS Having r_1 = 88 mm, r_2 = 83 mm, r_3 = 80 mm, r_c = 88 mm, an Ion Mass of 133 amu, and an Initial Ion Energy of 4 eV (Directed Toward the Collector). The Flight Time Spread was Derived from Figure 2.8 for an Initial Ion Energy Spread of ± 1 eV.

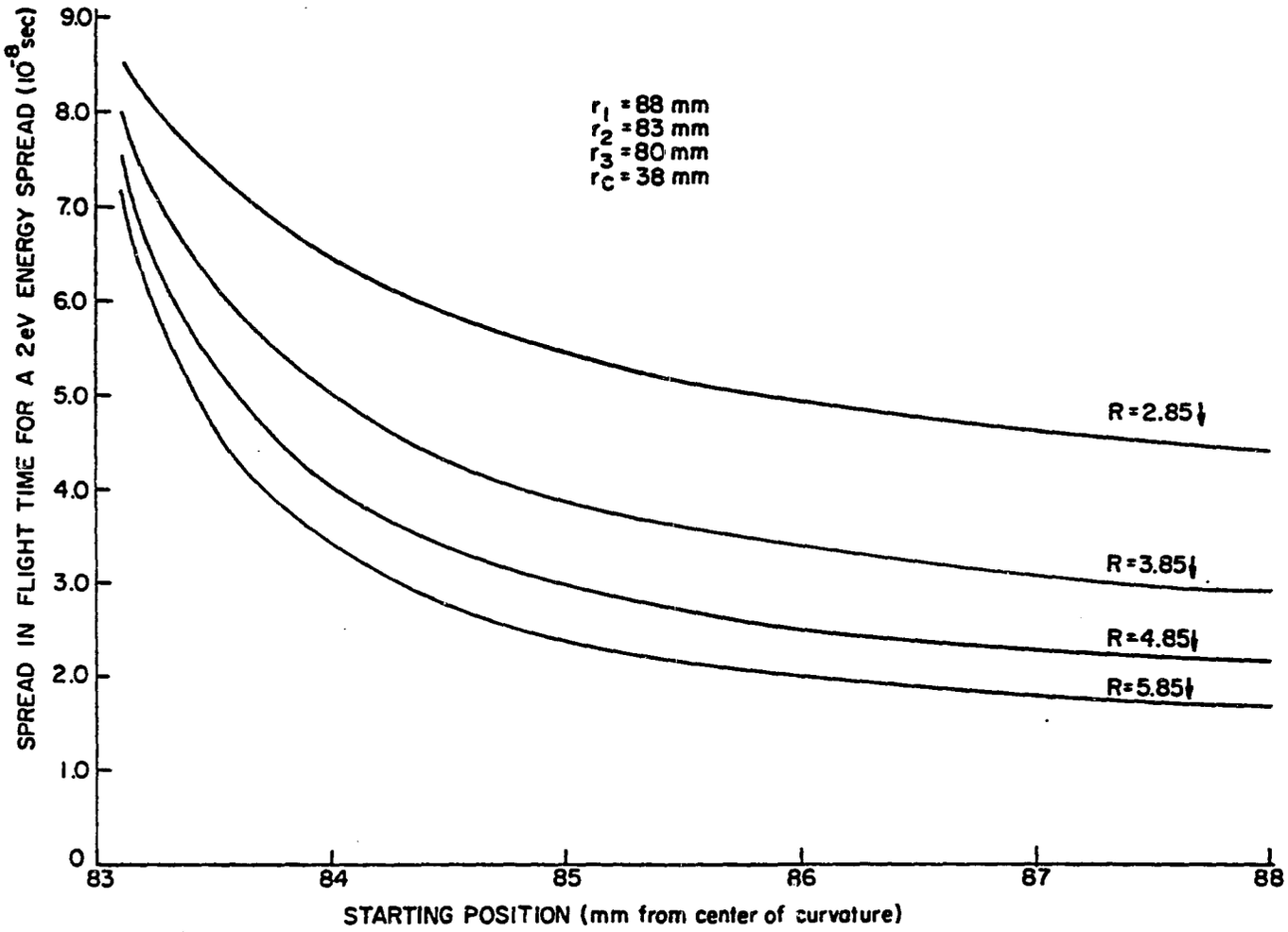

Figure 2.11 Computer Generated Velocity Focusing Characteristics for a Spherical-Electrode TOFMS Having r_1 = 88 mm, r_2 = 83 mm, r_3 = 80 mm, r_c = 38 mm, an Ion Mass of 133 amu, and an Initial Ion Energy of 4 eV (Directed Toward the Collector). The Flight Time Spread was Derived from Figure 2.9 for an Initial Ion Energy Spread of ± 1 eV.

electrode spacings and electrode radii being considered. For simplicity and convenience, I will concentrate on the cylindrical geometry for the remaining Figures in this section.

Figure (2.12) shows the effects of changing the initial ion velocity when a low voltage ratio was used. It also illustrates the time spread (bars) due to a 2 eV initial energy spread for a low voltage ratio. The initial ion velocity was not constant across the source region in the calculation of these curves since V_2 was held constant while V_0 was varied. V_0 was the voltage applied to electrode 1 when the buncher pulse was off. In the usual operation of the two-field TOFMS considered in this thesis $V_0 = V_2$ and the source region is field free, but in these cases, the source region was operated with an electric field when the buncher pulse is off. The ion initial velocity was then dependent on the ion distance from r_2. Varying the ion initial velocity distribution as a function of the position in the source had two important effects. First, changing the ion initial velocity distribution from initial velocities which increased as the ions approach electrode 2 to a distribution in which initial velocities decreased as the ions approach electrode 2 is equivalent to increasing the voltage ratio. Second, the time spread due to the initial energy spread decreases as the initial ion energy is increased. This decrease in the flight time spread occurs because the ion initial energy spread becomes a smaller fraction of the ion initial energy as the initial velocity is increased. This Figure illustrates clearly the reason for reported poor resolving power at near the optimum

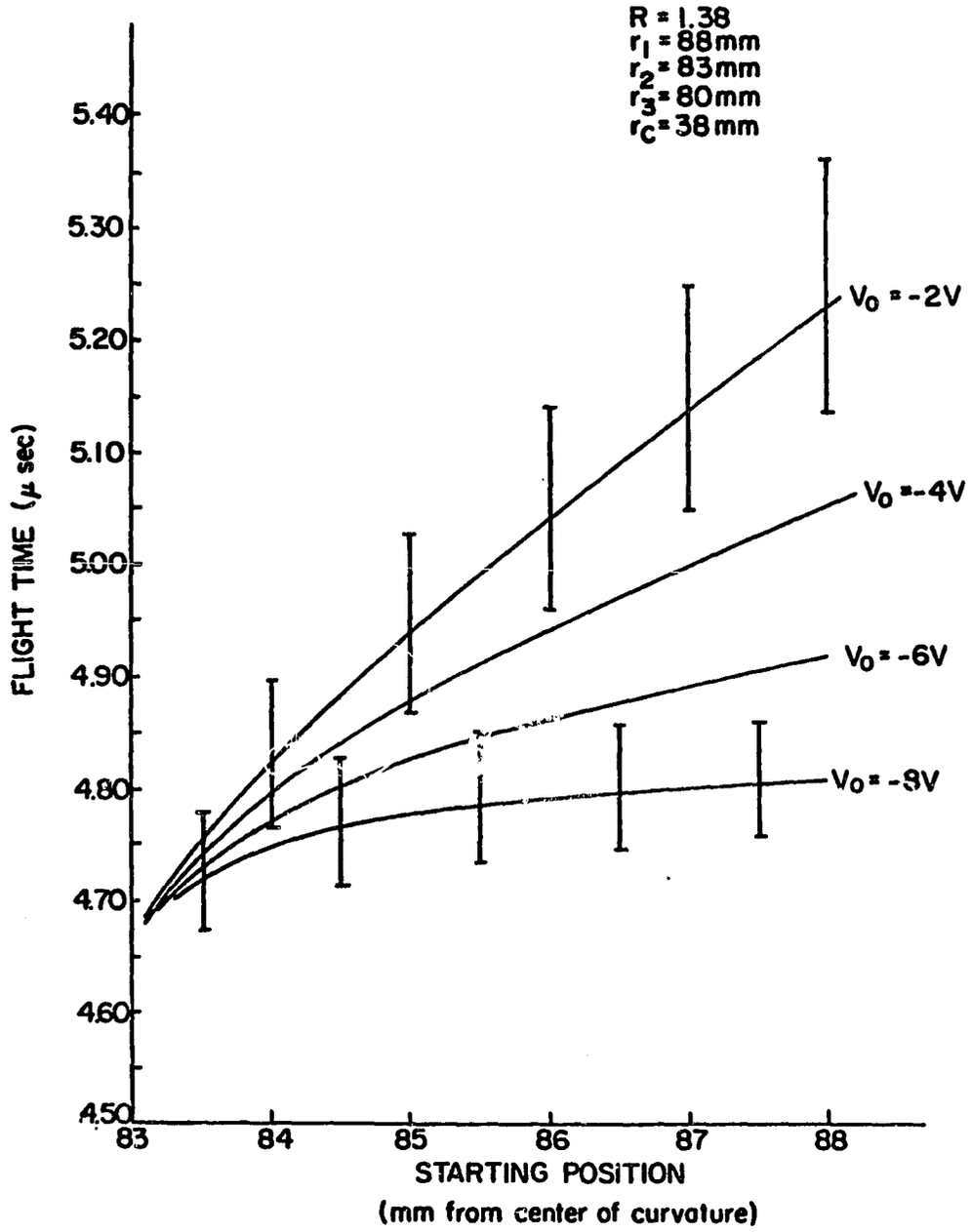

Figure 2.12 Computer Generated Space Focusing Characteristics for a Cylindrical-Electrode TOFMS Having r_1 = 88 mm, r_2 = 83 mm, r_3 = 80 mm, r_c = 38 mm, R = 1.38, and an Ion Mass of 133 amu, While V_0 was Varied. The Bars Represent an Initial Ion Energy Spread of ± 1 eV.

space focusing voltage ratio. The flight time spread, due to an initial ion energy spread (2 eV in this example), is significantly larger than the time spread due to the different ion starting positions (see the curve for $V_0 = -8$ V).

Figure (2.13) shows the effect of varying the collector radius while holding the source and acceleration regions at a constant radius of curvature for R = 1.56. This varies the drift region length. Variation of the drift region length was studied by Stein (1974) to deduce the effect of grid waviness. He looked at only very small variations in the drift region length (less than 1 mm) and concluded that this had very little effect on the shape of the space focusing curves. The effects of larger variations in the drift region length are more pronounced and are very similar to changing the voltage ratio. The curve for $r_c = 38$ mm in Figure (2.13) is very similar to the curve for the cylindrical TOFMS in Figure (2.7). However, when r_c is moved to 58 mm (from the center of curvature), the resulting curve is very similar to the curves in Figure (2.12) for low voltage ratios. The bars in Figure (2.13) again represent the flight time spread due to an initial energy spread of 2 eV (all the remaining Figures in this section will use bars to indicate the flight time spread due to an initial energy spread of 2 eV). The ion initial energy in this Figure and the remaining Figures in this section was 4 eV for all starting positions in the source region. Notice the decrease in the flight time spread in Figure (2.13) due to the initial energy spread as compared with the lower voltage ratio curves in Figure (2.12)

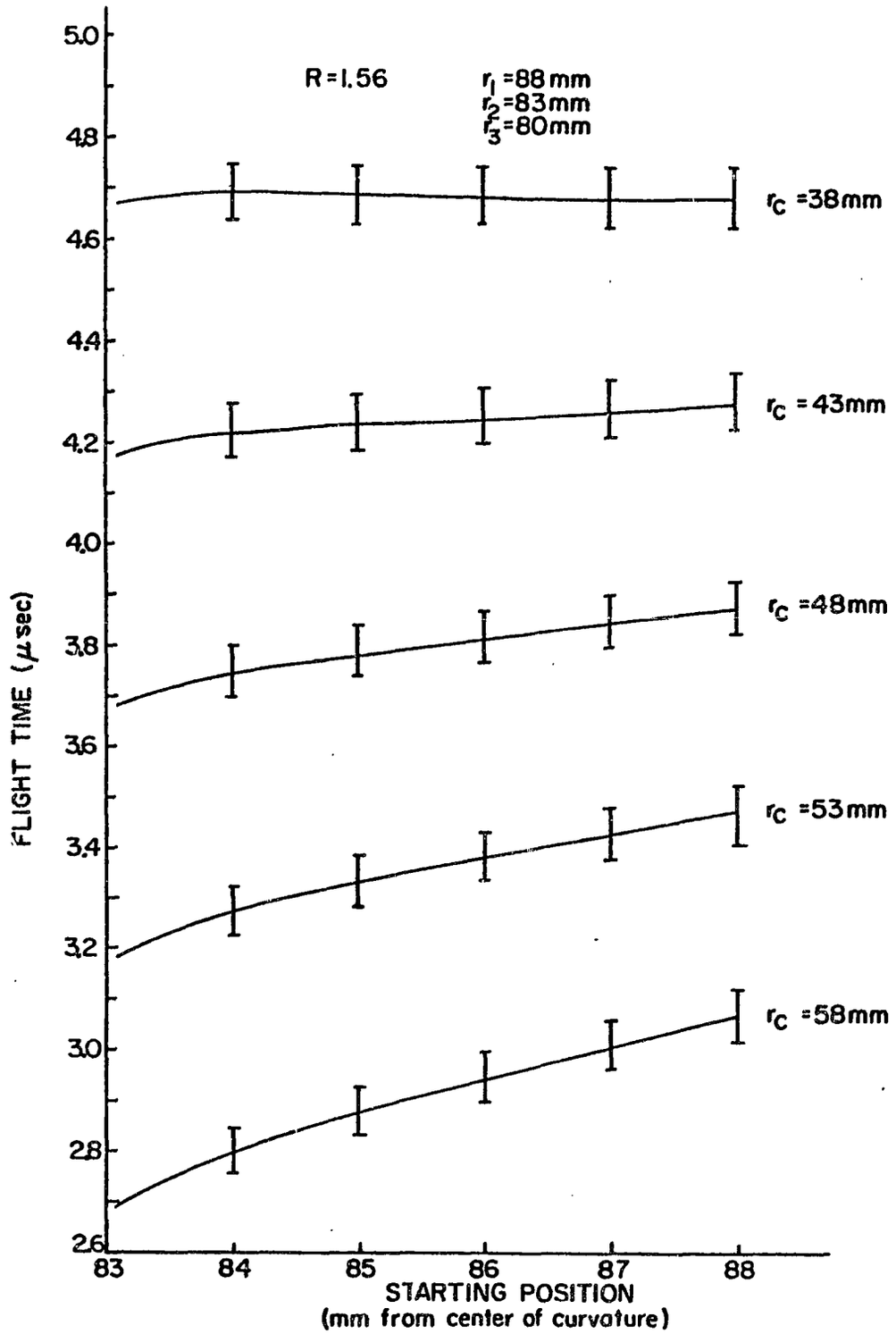

Figure 2.13 Computer Generated Space Focusing Characteristics for a Cylindrical-Electrode TOFMS Having r_1 = 88 mm, r_2 = 83 mm, r_3 = 80 mm, R = 1.56, an Ion Mass of 133 amu, and an Ion Initial Energy of 4 eV (Directed Toward the Collector), While r_c was Varied. The Bars Represent an Initial Ion Energy Spread of ± 1 eV.

Figures (2.14), (2.15) and (2.16) show the flight time curves for voltage ratios of 2.10, 2.56 and 3.06, respectively, while the drift region length is varied as in Figure (2.13). Two important observations can be made from these Figures. The first is the equivalence of decreasing the drift region length to decreasing the voltage ratio, as far as the space focusing characteristics are concerned, without significant variation of the velocity focusing characteristics. The second is the steadily decreasing flight time spread due to the initial energy spread as the voltage ratio increases.

Figures (2.17), (2.18), (2.19) and (2.20) represent the computer derived flight time curves for voltage ratios of 1.5, 2.0, 2.56 and 3.0, respectively, for grid radii which are greatly reduced from those used in Figures (2.13) through (2.16). The source and acceleration region grid spacings are the same as Figures (2.13) through (2.16), but the radii of curvature are greatly reduced. It was thought that these grid radii would emphasize the effect of the cylindrical electrodes on the source and acceleration region electric fields. However, close examination of Figures (2.17) through (2.20) reveals no significant differences from Figures (2.13) through (2.16). Evidently, the electric field between cylindrical electrodes spaced as in Figures (2.13) through (2.20) does not vary significantly from the electric field for similarly spaced planar electrodes. In fact, subsequent calculations showed that a significant variation (greater than 10 per cent) from the electric field between planar electrodes 5 mm apart does not occur until the radii of curvature for similarly

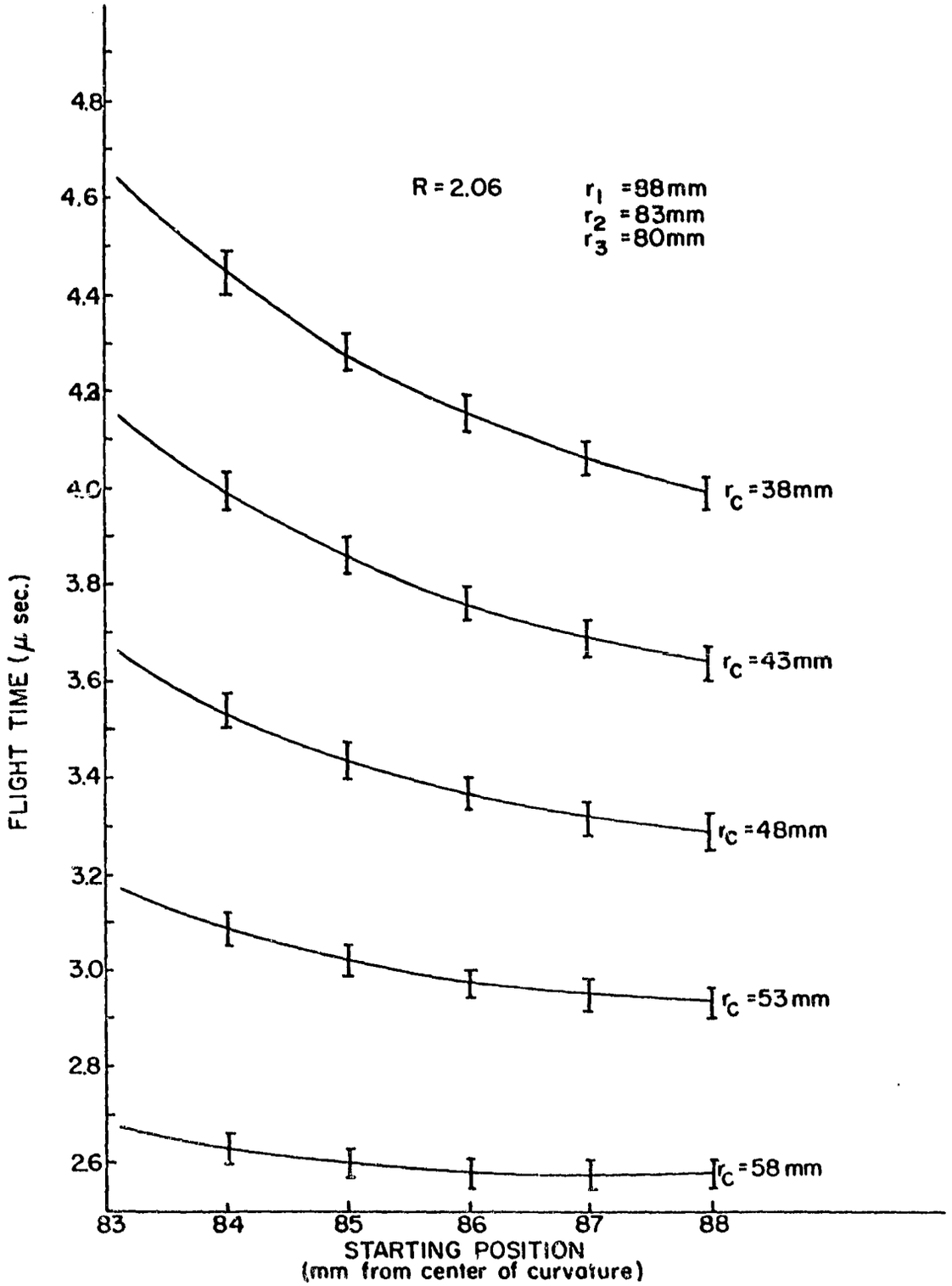

Figure 2.14 Computer Generated Space Focusing Characteristics for a Cylindrical-Electrode TOFMS Having r_1 = 88 mm, r_2 = 83 mm, r_3 = 80 mm, R = 2.06, an Ion Mass of 133 amu, and an Ion Initial Energy of 4 eV (Directed Toward the Collector), While r_c was Varied. The Bars Represent an Initial Ion Energy Spread of ± 1 eV.

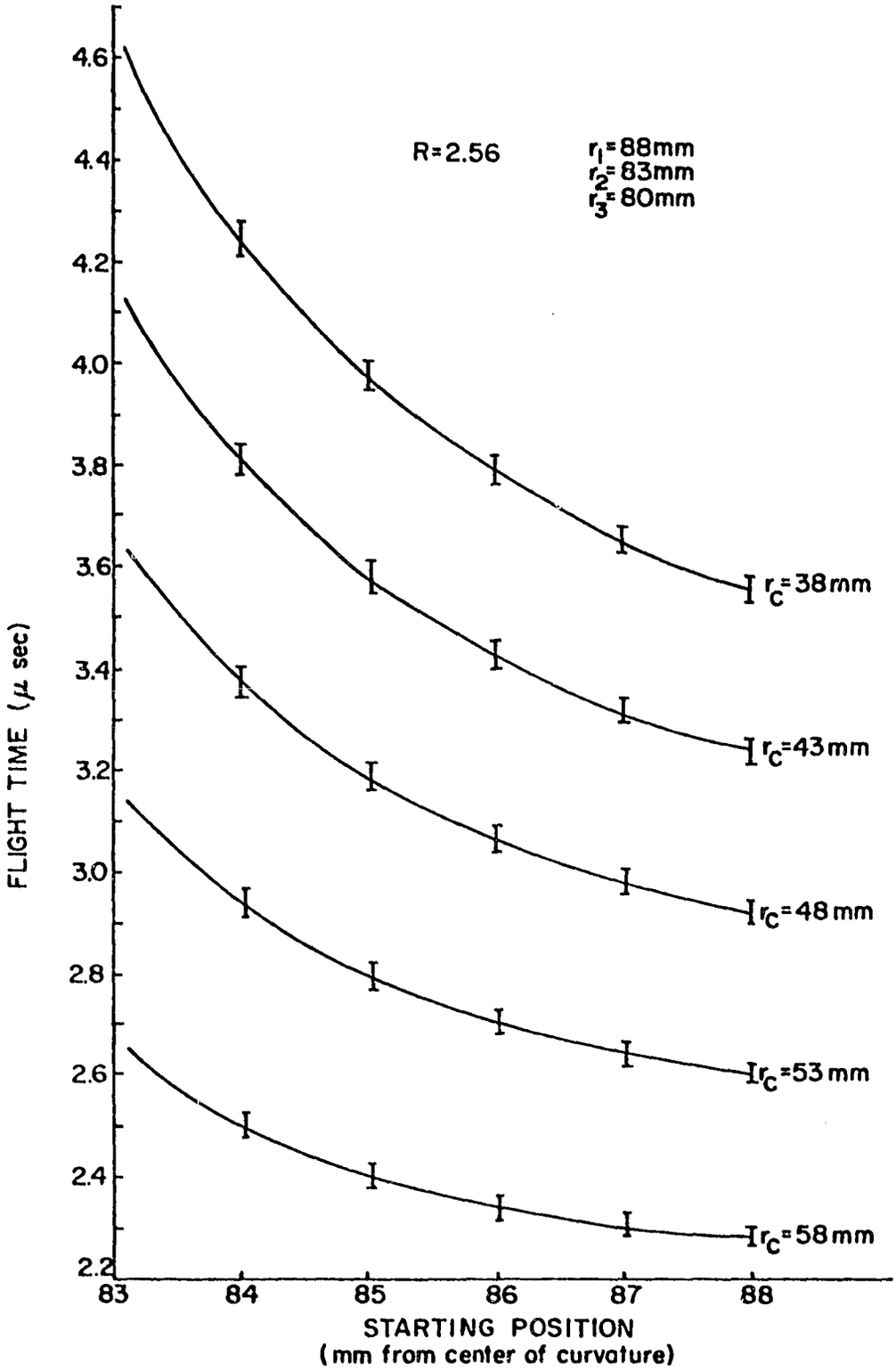

Figure 2.15 Computer Generated Space Focusing Characteristics for a Cylindrical-Electrode TOFMS Having r_1 = 88 mm, r_2 = 83 mm, r_3 = 80 mm, R = 2.56, an Ion Mass of 133 amu, and Ion Initial Energy of 4 eV (Directed Toward the Collector), While r_c was Varied. The Bars Represent an Initial Ion Energy Spread of ± 1 eV.

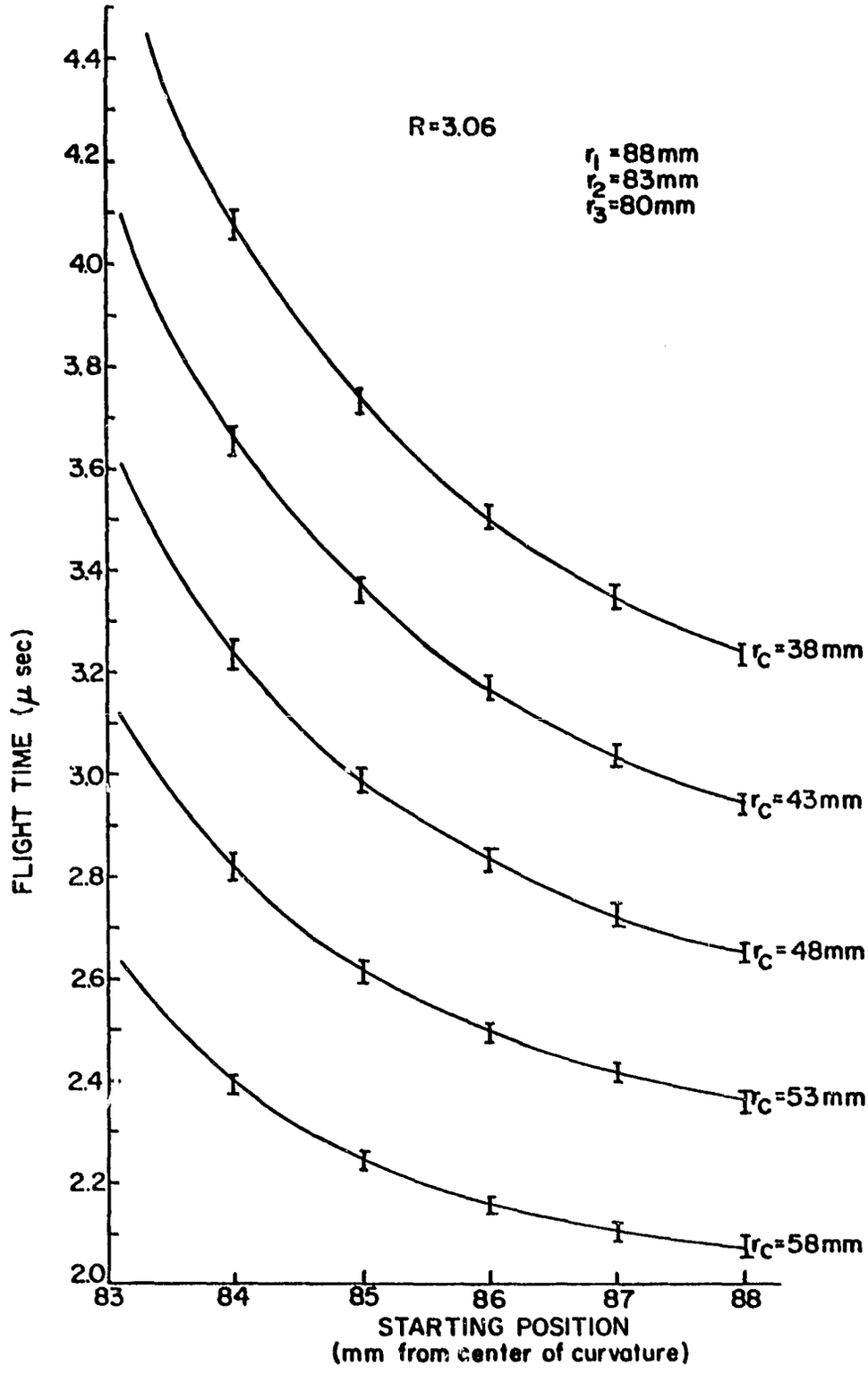

Figure 2.16 Computer Generated Space Focusing Characteristics for a Cylindrical-Electrode TOFMS Having r_1 = 88 mm, r_2 = 83 mm, r_3 = 80 mm, R = 3.06, an Ion Mass of 133 amu, and an Ion Initial Energy of 4 eV (Directed Toward the Collector), While r_c was Varied. The Bars Represent an Initial Ion Energy Spread of ± 1 eV.

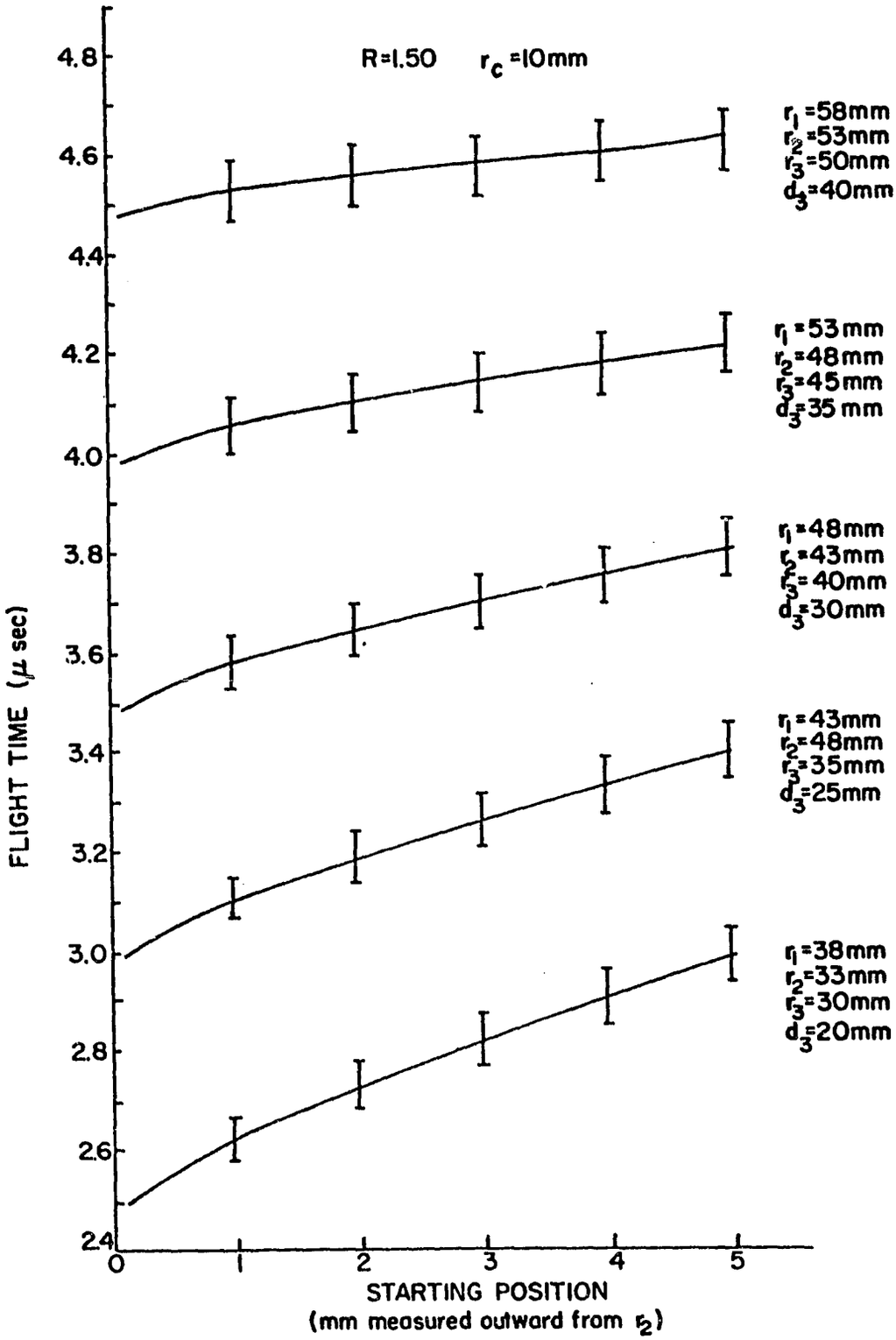

Figure 2.17 Computer Generated Space Focusing Characteristics for a Cylindrical-Electrode TOFMS Having R = 1.50, r_c = 10 mm, an Ion Mass of 133 amu, and an Ion Initial Energy of 4 eV (Directed Toward the Collector), While r_1, r_2, r_3, and the Drift Region Length (d_3) Were Varied. The Spacings Between r_1 and r_2 and Between r_2 and r_3 Were Kept Constant.[1] The Bars Represent an Initial Ion Energy Spread of ± 1 eV.

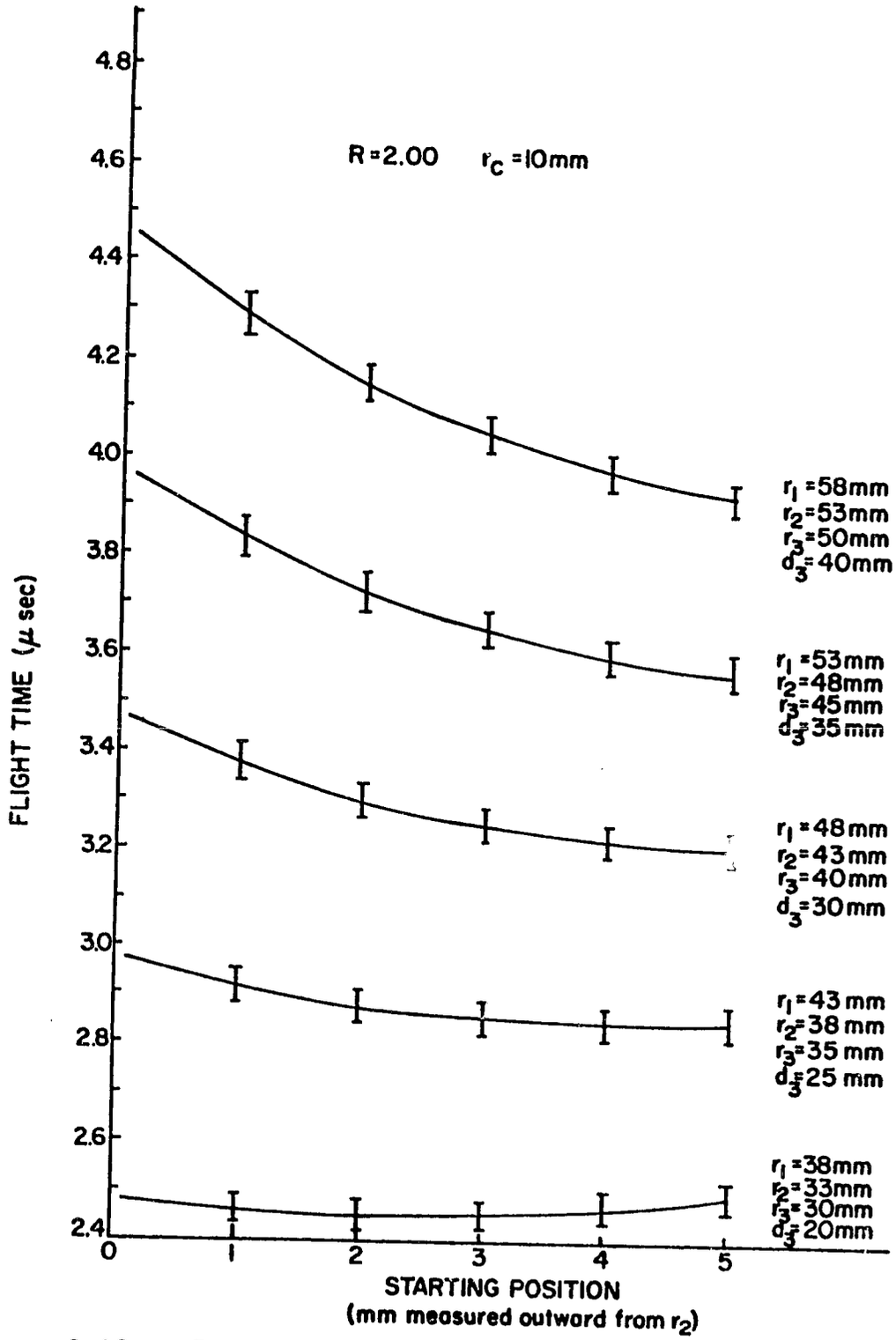

Figure 2.18 Computer Generated Space Focusing Characteristics for a Cylindrical-Electrode TOFMS Having R = 2.00, r_c = 10 mm, an Ion Mass of 133 amu, and an Ion Initial Energy of 4 eV (Directed Toward the Collector), While r_1, r_2, r_3, and the Drift Region Length (d_3) Were Varied. The Spacings Between r_1 and r_2 and Between r_2 and r_3 Were Kept Constant. The Bars Represent an Initial Ion Energy Spread of ± 1 eV.

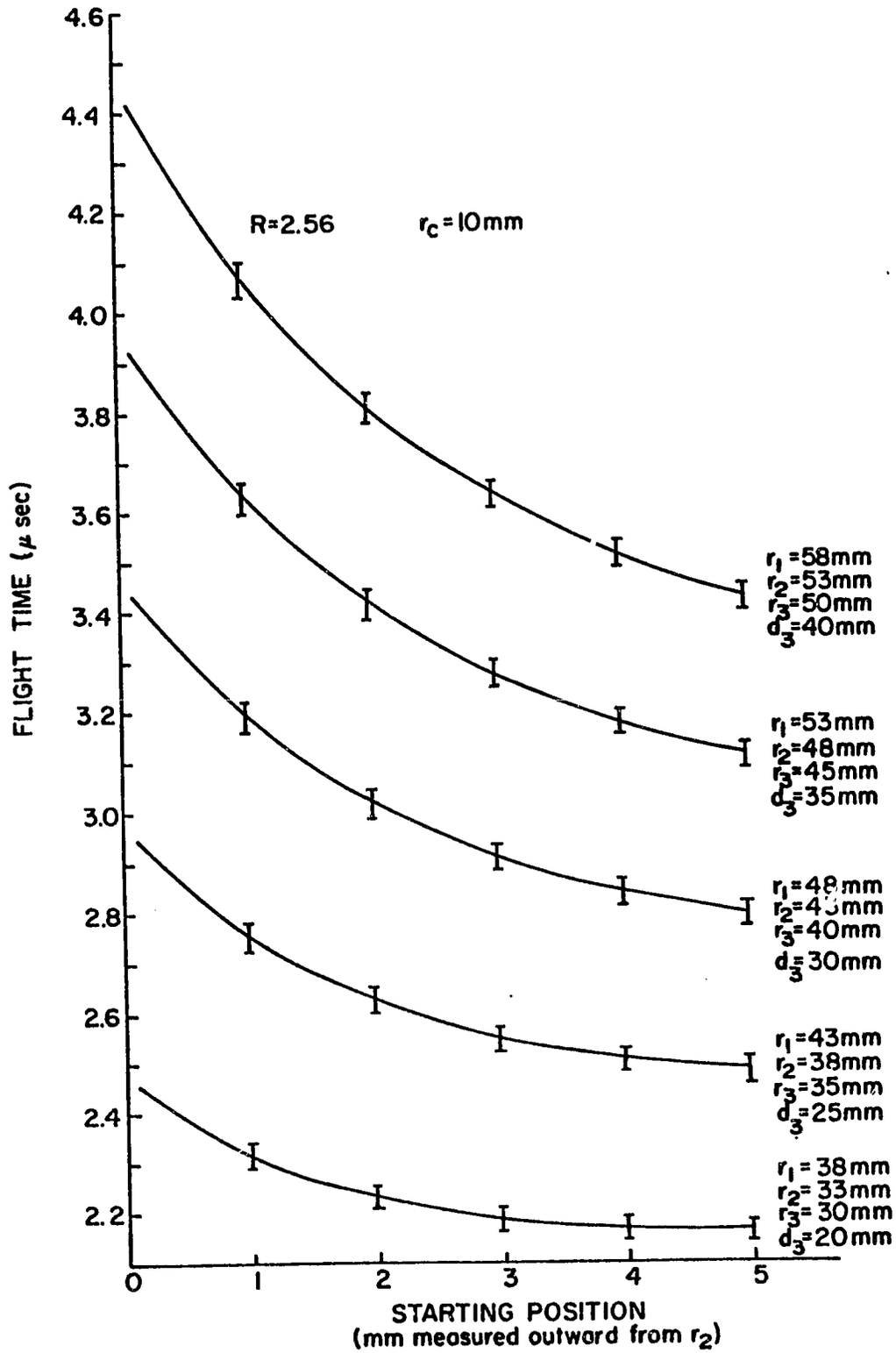

Figure 2.19 Computer Generated Space Focusing Characteristics for a Cylindrical-Electrode TOFMS Having R =2.56, r_c = 10 mm, an Ion Mass of 133 amu, and an Ion Initial Energy of 4 eV (Directed Toward the Collector), While r_1, r_2, r_3, and the Drift Region Length (d_3) Were Varied. The Spacings Between r_1 and r_2 and Between r_2 and r_3 Were Kept Constant. The Bars Represent an Initial Ion Energy Spread of ± 1 eV.

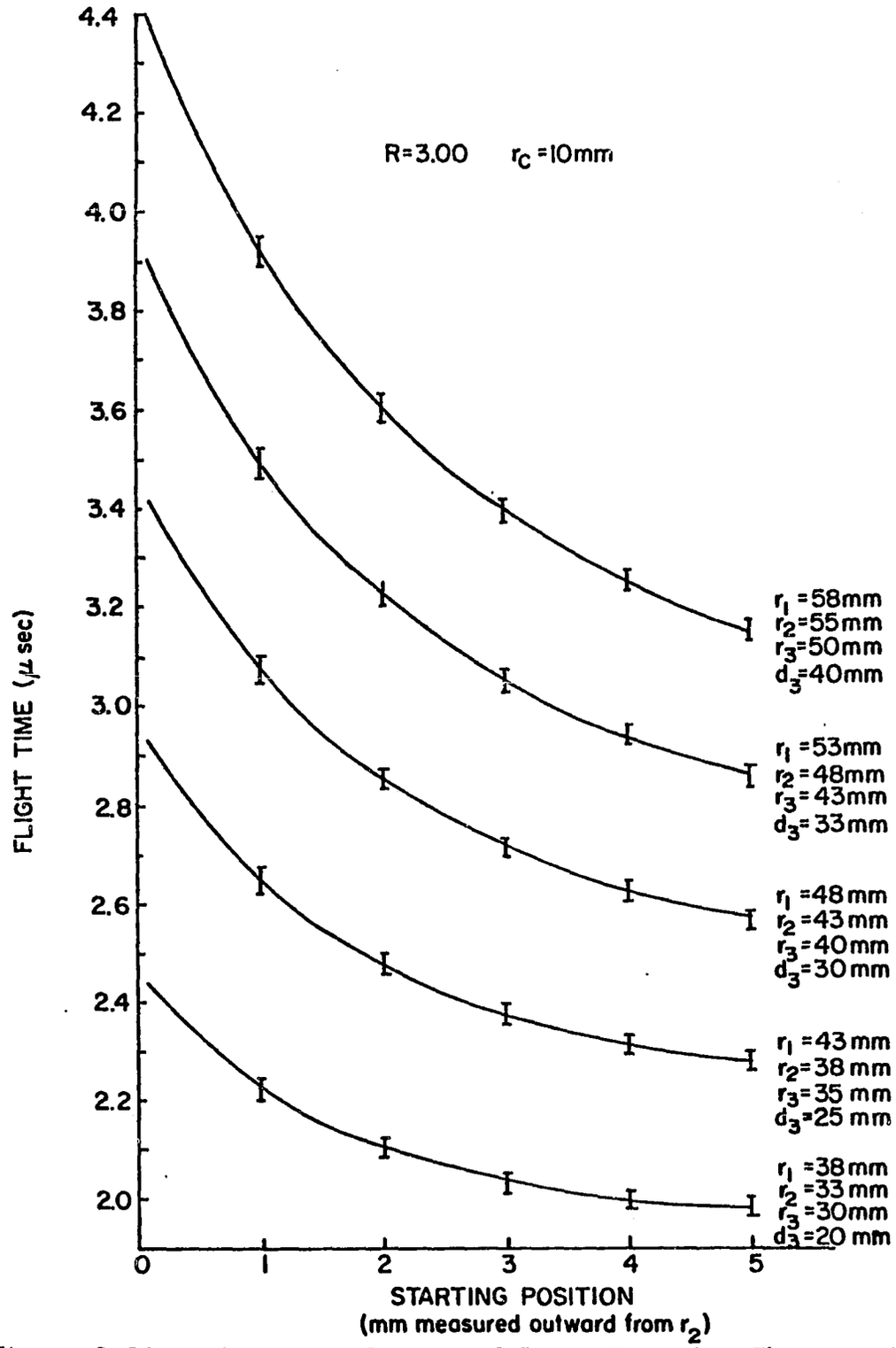

Figure 2.20 Computer Generated Space Focusing Characteristics for a Cylindrical-Electrode TOFMS Having R = 3.00, r_c = 10 mm, an Ion Mass of 133 amu, and an Ion Initial Energy of 4 eV (Directed Toward the Collector), While r_1, r_2, r_3, and the Drift Region Length (d_3) Were Varied. The Spacings Between r_1 and r_2 and Between r_2 and r_3 Were Kept Constant. The Bars Represent an Initial Ion Energy Spread of ± 1 eV.

spaced cylindrical-electrodes are less than 23 mm and 28 mm. A useful area for future study would be to examine the flight time characteristics of cylindrical and spherical TOFMS with an outer source electrode radius of less than 30 mm.

The Figures presented in this section confirm a number of observations made by previous researchers. First, inferior mass peak shapes would result if the operating voltages of a TOFMS were adjusted to allow ions starting at the inner and outer source region electrodes to arrive at the collector simultaneously (i.e. be space focused). Second, the optimum space focusing voltage ratios for a planar, cylindrical or spherical TOFMS are very nearly identical. Third, the spread in ion initial energies (velocities) is the cause for the poor resolving power at good space focusing voltage ratios in a TOFMS. Fourth, the velocity focusing characteristics can be improved by increasing the voltage ratio at the cost of degrading the space focusing if the ion initial energies and the grid spacings are not altered. Fifth, varying the drift region length is equivalent to varying the voltage ratio, as far as space focusing is concerned. Sixth, the fact that a mass peak produced by a voltage ratio near the optimum space focusing value, with no initial velocity spread, is extremely narrow with respect to the mass peak which is produced when an initial energy spread greater than about .5 eV is considered. At the optimum space focusing voltage ratio in a cylindrical TOFMS, the flight time spread, due to an initial energy spread of .5 eV, (for a specific initial energy) is about 10 times the full width at half height of a mass peak produced only by space focusing.

Since the true mass peak is a convolution of the space and velocity contributions to the flight time spread, it should be possible to deduce significant information on an unknown initial ion energy spread. For large initial energy spreads (>.5 eV), the initial energy distribution can be deduced from direct observation of the resulting mass peak shape. This is because the space focused contribution to the mass peak is similar to a delta function (for optimum voltage ratios) and the convolution of the flight time spread due to the initial energy spread and a delta function will reproduce the flight time spread directly due to the initial energy spread. It should still be possible to deduce the initial energy distribution for smaller energy spreads (<.5 eV) through deconvolution, since the space focusing flight time distribution can be easily calculated, with great accuracy, from computer programs. This last observation was originally made by Ferguson et al., (1965) and has been used, with great success, to calculate the translational energy of ions in TOFMS by Franklin et al., (1967) and by Hadley and Franklin (1975).

There are also two observations which can be made that have not been mentioned by previous researchers. The first is that the velocity focusing characteristics in a TOFMS are almost entirely determined in the source and acceleration regions since varying the drift region length has little effect on velocity focusing while having a large effect on space focusing.

The second observation was suggested by Figure (2.12). This Figure showed that it was possible to simulate a change in voltage ratio by changing the initial ion velocity distribution in the source

region. Although Figure (2.12) illustrates flight times for a low voltage ratio where there was a large flight time spread, it seems entirely possible to apply this effect to high voltage ratios. This would greatly improve the velocity focusing characteristics. The ions closest to the collector, in the source, arrive at the collector last, while ions farthest from the collector arrive there first (see Figures (2.8) and (2.9) for example). If ion initial velocities (before the buncher pulse turns on) can be produced, which are greater closer to the collector than in the outer portion of the source region, it should be possible to reduce the effective space focusing voltage ratio while still keeping good velocity focusing. This should produce greatly improved resolving power. The next two sections will discuss this resolving power improvement and present computer simulations for several examples.

CHAPTER III

ION GATING IN TIME-OF-FLIGHT MASS SPECTROMETERS

3.1 Background

The use of gating systems in time-of-flight mass spectrometers has been present for nearly as long as time-of-flight mass spectrometers. The first reported gating systems were used by Glenn (1952), Ionov and Mamyrin (1953) and Katzenstein and Friedland (1955). Glenn (1952) placed a grid with a dc potential directly in front of the collector. Ions arriving at the appropriate time were given additional energy by the gate pulse and could reach the collector. The gating system of Ionov and Mamyrin (1953) used four grids placed at the end of the ion drift tube, directly in front of the collector. The outer two grids were at the drift tube potential. The inner grid closest to the collector was set at a dc potential corresponding to the ion acceleration voltage plus a small ΔV. The other inner grid had a positive pulse which gave ions arriving at the proper time enough energy to spill over the potential barrier. In this instrument, varying the gate pulse time and varying the ion acceleration voltage produced equivalent results. Katzenstein and Friedland (1955) used an arrangement which was very similar to the system of Glenn (1952). The systems of Glenn (1952) and Katzenstein and Friedland (1955) were similar to the varied gate pulse delay time mode of Ionov and Mamyrin (1953). The grid arrangement of Katzenstein and Friedland (1955) is shown in Figure (3.1b). Other gating systems have been

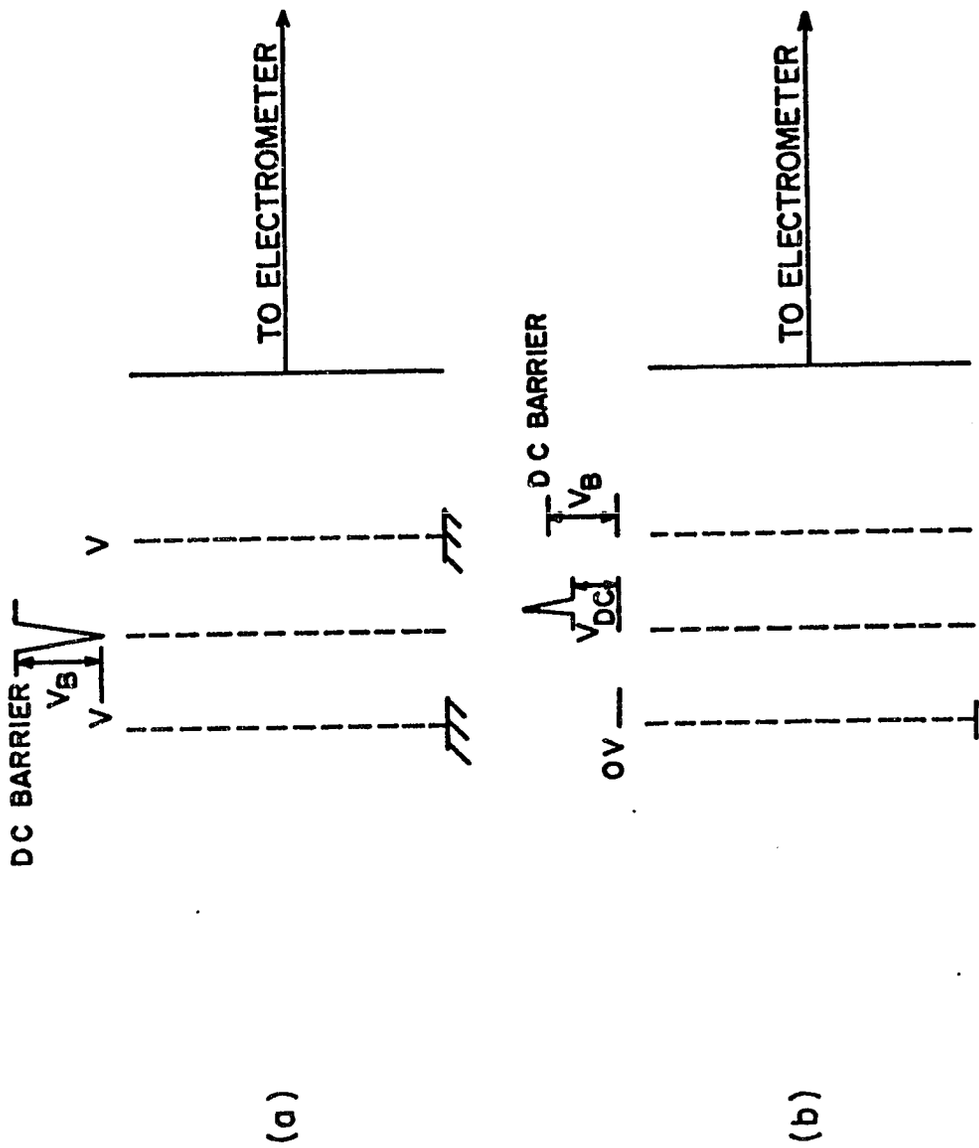

Figure 3.1 a. The Gating Arrangement Used for the Computer Simulations in Chapter III and in the Laboratory Version of the Cylindrical-Electrode TOFMS.

b. The Gating Arrangement Used by Katzenstein and Friedland (1955).

described by Wager (1960), Narcisi et al., (1966), Diem (1967) and Zabielski (1970). These systems will be described below.

Glenn (1952) used his gating system to insure that ions which did not have the appropriate flight times did not reach the collector. Ionov and Mamyrin (1953) used their gating system in order to produce enough current at the collector to be measured with the electrometers in use at that time. The gate was also used to eliminate the need for an electrometer with a high frequency response. With their gating system a dc electrometer could be used. The gating system of Katzenstein and Friedland (1955) was developed to eliminate excessive capacitive coupling to the collector plate. This improved the signal-to-noise ratio of the mass spectrum. The gating systems reported by Wager (1960), Narcisi et al., (1966), Diem (1967) and Zabielski (1970) were used in instruments carried on balloon and sounding rocket flights. The fact that time-of-flight mass spectrometers produce a spectrum in a very short time (μ sec) results in two major problems when used in atmospheric applications. The first problem is the need for an electrometer which can satisfy the severe environmental constraints imposed by a sounding rocket or balloon flight and still have a sufficiently high frequency response. The second problem is the low-bandwidth constraint imposed by the telemetry systems in use. Even if an electrometer could be developed to handle the output of a TOFMS directly, the telemetry system could not handle the electrometer output.

These problems can be solved by "slowing down" the mass spectra, without losing any of the significant features, through the

use of gating. Wager (1960) developed the necessary electronics to sample a mass spectrum after amplification and to reproduce the spectrum at a suitably slowed down time. However, a high performance (with respect to frequency response) electrometer was still required. Narcisi et al., (1966), Diem (1967) and Zabielski (1970) described gating systems which were used to sample a mass spectrum before the ions reached the collector and so introduced a slowed down spectrum to the electrometer. This second gating method greatly reduced the frequency response requirements of the electrometer and allowed a much greater electrometer sensitivity. It also satisfied telemetry constraints. The electronics used in the gating systems used by Zabielski (1970) and Diem (1967) were described by Hazelton (1968) and Barnes (1971).

The gating systems of Katzenstein and Friedland (1955) and Wager (1960) produced a significant increase in the mass spectrum signal-to-noise ratio. A partial analysis by Zabielski (1970) showed all the gating systems discussed here produce a slight decrease in sensitivity (in this thesis, sensitivity refers to the number of ions collected in mass peaks in relation to the number of ions entering the spectrometer) and no marked decrease in resolving power. The sensitivity decrease was also mass dependent. It was also mentioned by Zabielski (1970) that the gate pulse shape would have a direct bearing on the mass peak shape. Unfortunately, no further studies were made.

The difficulty in producing a gate pulse which had a variable width and was compatible with the other spectrometer electronics

prevented most direct experimental studies of the effects of gating on mass spectrometer operation in this laboratory. It is possible to study a number of gate pulse shapes, used in the gating configuration shown in Figure (3.1a), by using computer simulations. Ion transit times through the gate region can be interpreted to give the effects on sensitivity and resolving power by the gate pulse shape for any number of TOFMS operating conditions.

3.2 Computer Simulation

A typical gate pulse shape is shown in Figure (3.2). It can be approximated closely by a triangular pulse shape. The ideal gate pulse is a square pulse with infinitely fast rise and fall times. Both a triangular gate pulse shape and a square gate pulse shape can be studied with relative ease using computer models.

The important parameters in the study of a gate pulse are the gate voltages, the ion energy as it enters the gate region, the ion mass, the time the gate starts with respect to the ion arrival in the gate region, and in the case of a triangular pulse, the rise and fall times. The computer programs used for these analyses followed the path of one ion at a time through the gate region and calculated the time for the ion to pass the electrode with the gate pulse.

The flight times for ions traveling a distance corresponding to the width of the gate region are shown in Figure (3.3). The calculations carried out for this Figure and the Figures that follow were carried out by using planar electrodes for greater simplicity.

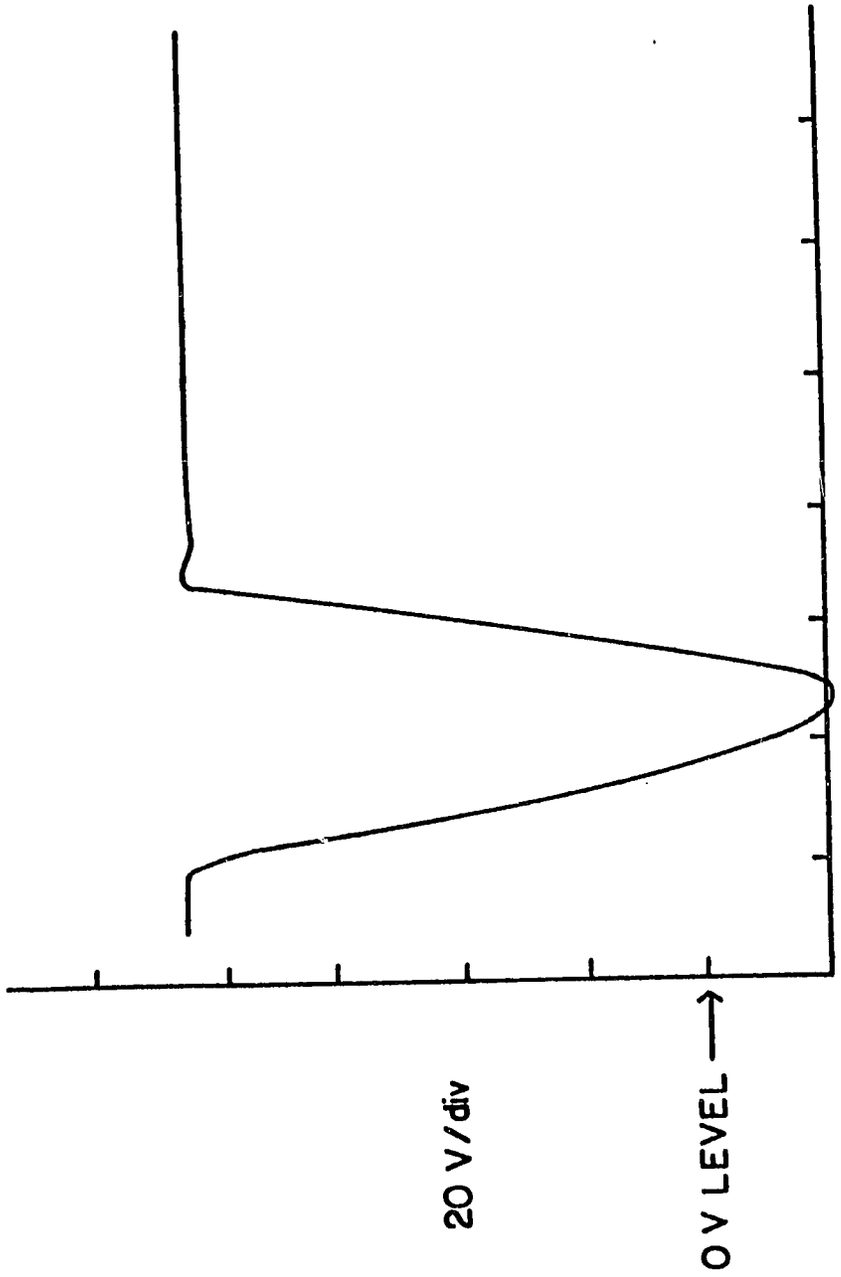

Figure 3.2 A Typical Gate Pulse Used in a Cylindrical-Electrode TOFMS with the Gating Arrangement Shown in Figure 3.1a.

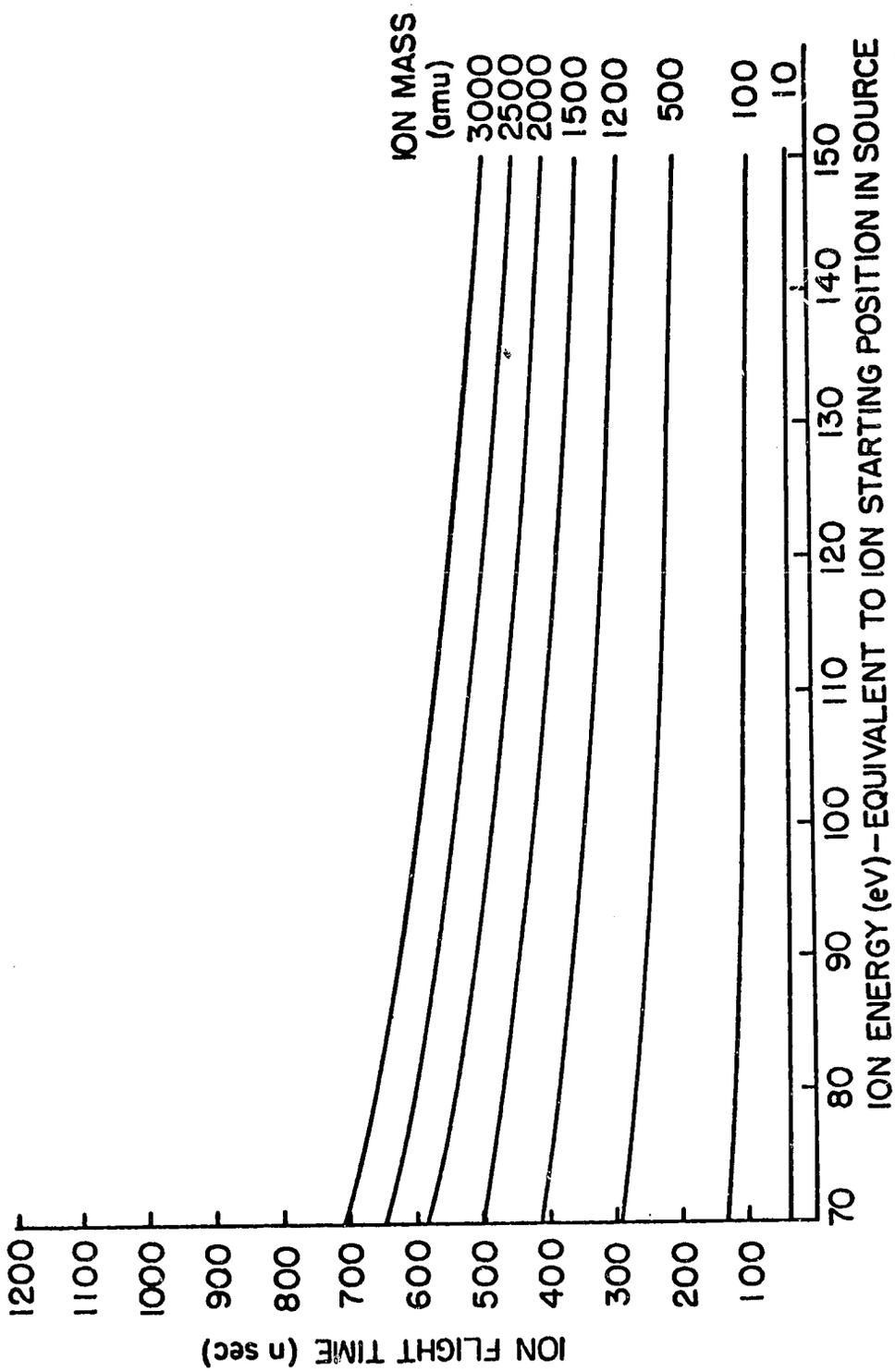

Figure 3.3 Computer Generated Ion Flight Times for the Gating Arrangement in Figure 3.1a (Width = 1.5 mm) with No Gate Pulse Present.

The ion energies considered are typical for the mass spectrometers under study. Figure (3.3) can be used as a reference for ion flight times when a gate pulse is present.

The ion flight times for a triangular gate pulse closely approximating an actual gate pulse shape (see Figure (3.2)) are shown in Figure (3.4). The flight times discussed in this chapter are only the transit times through the gate region and should not be confused with the total ion flight times in a spectrometer. The rise and fall times for the pulse were 50 nsec, the barrier potential was 155 V, the pulse amplitude was 100 V, and the gate pulse was started just as the ions entered the gate region. This Figure illustrates several interesting effects. The first effect of the gate is to produce a mass discrimination against the heavier ion masses. This should result in a sensitivity decrease as the mass of ions under study increases. For the operating conditions under study, this discrimination is not easily noticeable at masses less than 100 amu. A sensitivity decrease for K^+ (39, 41) and Cs^+ (133) was observed experimentally by Zabielski (1970) when the barrier potential was increased (which is also similar to narrowing the gate pulse). The results of Zabielski's measurements are reproduced in Figure (3.5). The presence of this sensitivity decrease at higher masses has been confirmed in measurements made by me, although exact sensitivity values were not obtained. The second effect of the gate pulse was not expected. The gate pulse also discriminated against certain ion starting positions in the source. In a typical operational cylindrical-electrode time-of-flight

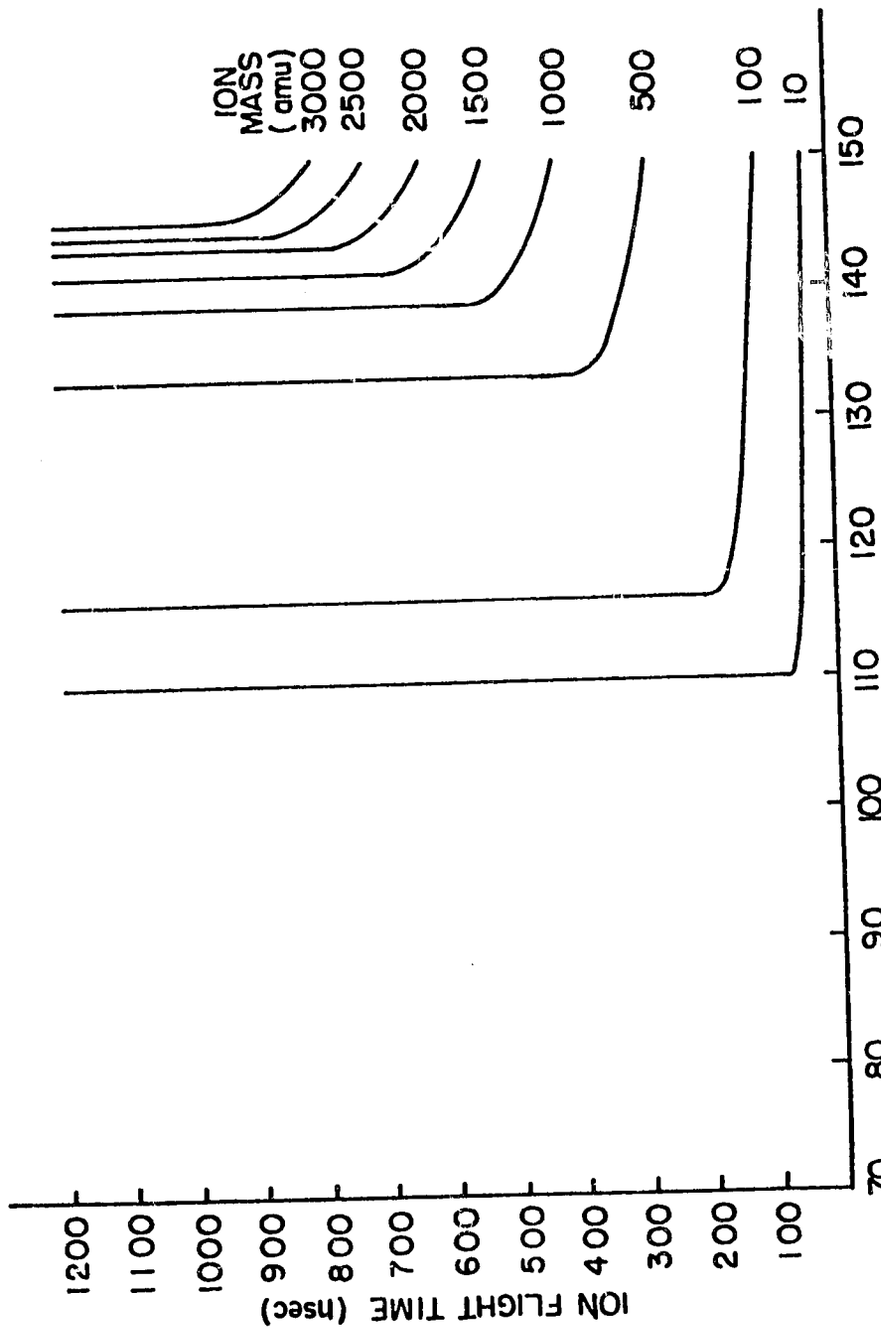

Figure 3.4 Computer Generated Ion Flight Times for a Triangular Gate Pulse. The Pulse Amplitude was 100 V, the Gate Barrier Potential was 155 V, and the Pulse Base Width was 100 nsec. The Gate Pulse was Turned on Just as Each Ion Entered the Gate Region.

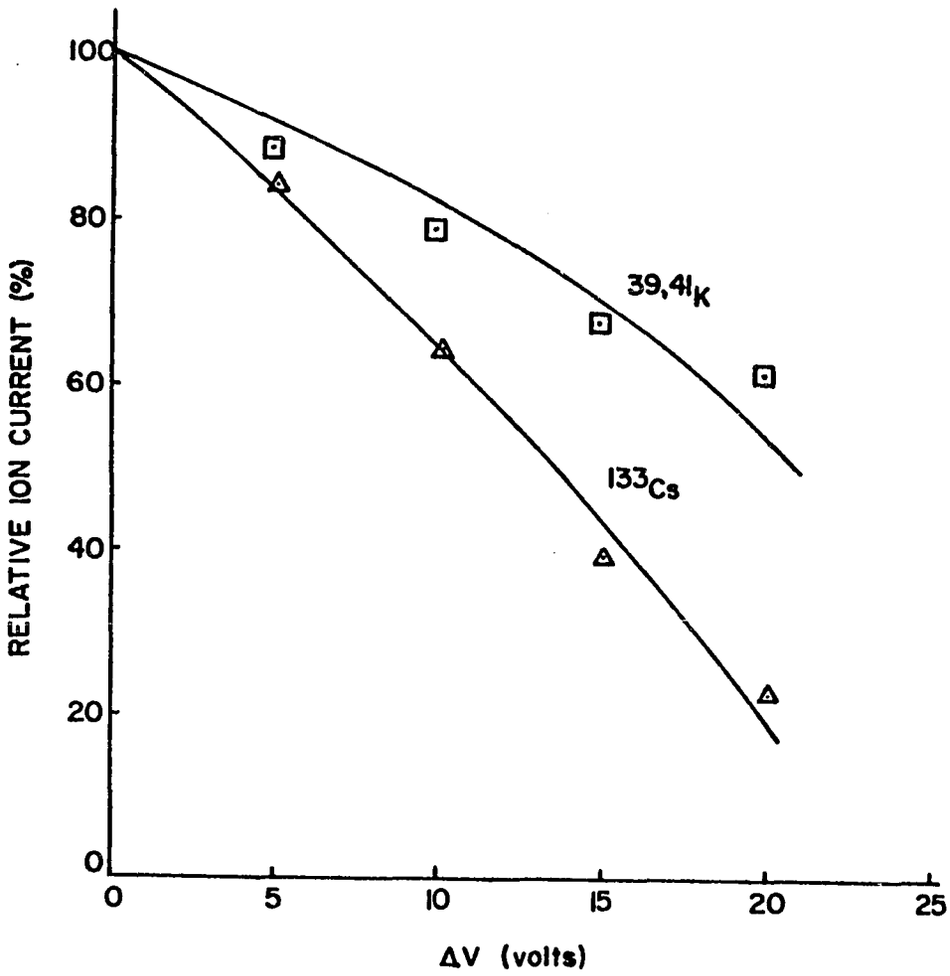

Figure 3.5 Experimentally Determined Sensitivity Decrease as the Gate Barrier Potential was Raised Above an 'Optimum Value'. (Reference: Zabielski (1970)).

mass spectrometer developed at Penn State, the various starting positions in the source produce ions with energies between 78 eV and 150 eV when they reach the gate. The lower energies correspond to a starting position closer to the collector while the higher energies correspond to ion starting positions away from the collector. As Figure (3.4) indicates, for an ion mass of 100 amu, only about 50 per cent of the ions will be collected. The 100 amu ions that are collected will only be from starting positions in the half of the source farthest from the collector.

Additional treatment of this problem is given by Reiter (1976).

CHAPTER IV

LABORATORY MEASUREMENTS WITH CYLINDRICAL AND HEMISPHERICAL-ELECTRODE TIME-OF-FLIGHT MASS SPECTROMETERS

4.1 Vacuum System and Ion Source

The primary motivation for the study of the cylindrical-electrode and the hemispherical-electrode time-of-flight mass spectrometers (TOFMS) was the need to understand the operation of these instruments for use in the D-region ionosphere. In order to simulate the vacuum environment of the D-region, the vacuum system illustrated in Figure (4.1) was used. This vacuum system included a gas inlet system and a zero pressure reference system for a diaphragm manometer. The ion source used in all the laboratory measurements was a surface ionization source identical to the one described by Diem (1967) and Zabielski (1970). The ion source and the associated electronics are shown in Figure (4.2).

4.2 Cylindrical-Electrode Two-Field TOFMS

4.2.1 Operating Voltages and Electronics

The results in these sections extend the experimental work reported by Diem (1967), Zabielski, Diem and Kendall (1970) and Zabielski (1970). The cylindrical-electrode two-field TOFMS used for laboratory analysis is shown, completely assembled, in Figure (4.3). A cross-sectional view of the spectrometer is shown in Figure (4.4) with the grid labeling and interelectrode spacings. The operating voltages are designed for positive ion collection. The voltage applied to the outermost grid, V_0, is used to draw ions into the

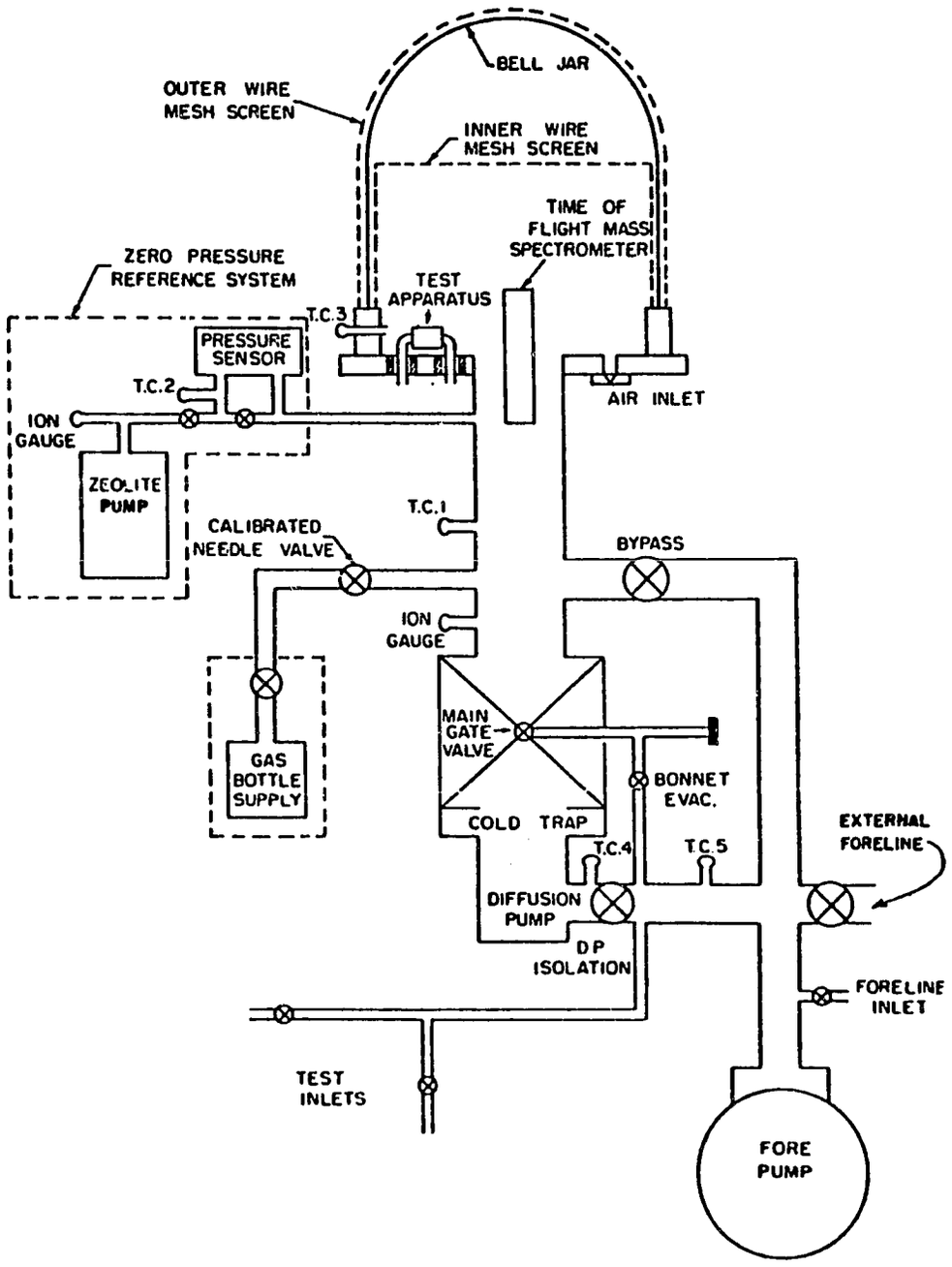

Figure 4.1 Vacuum System Used for Laboratory Studies of Cylindrical and Hemispherical TOFMS.

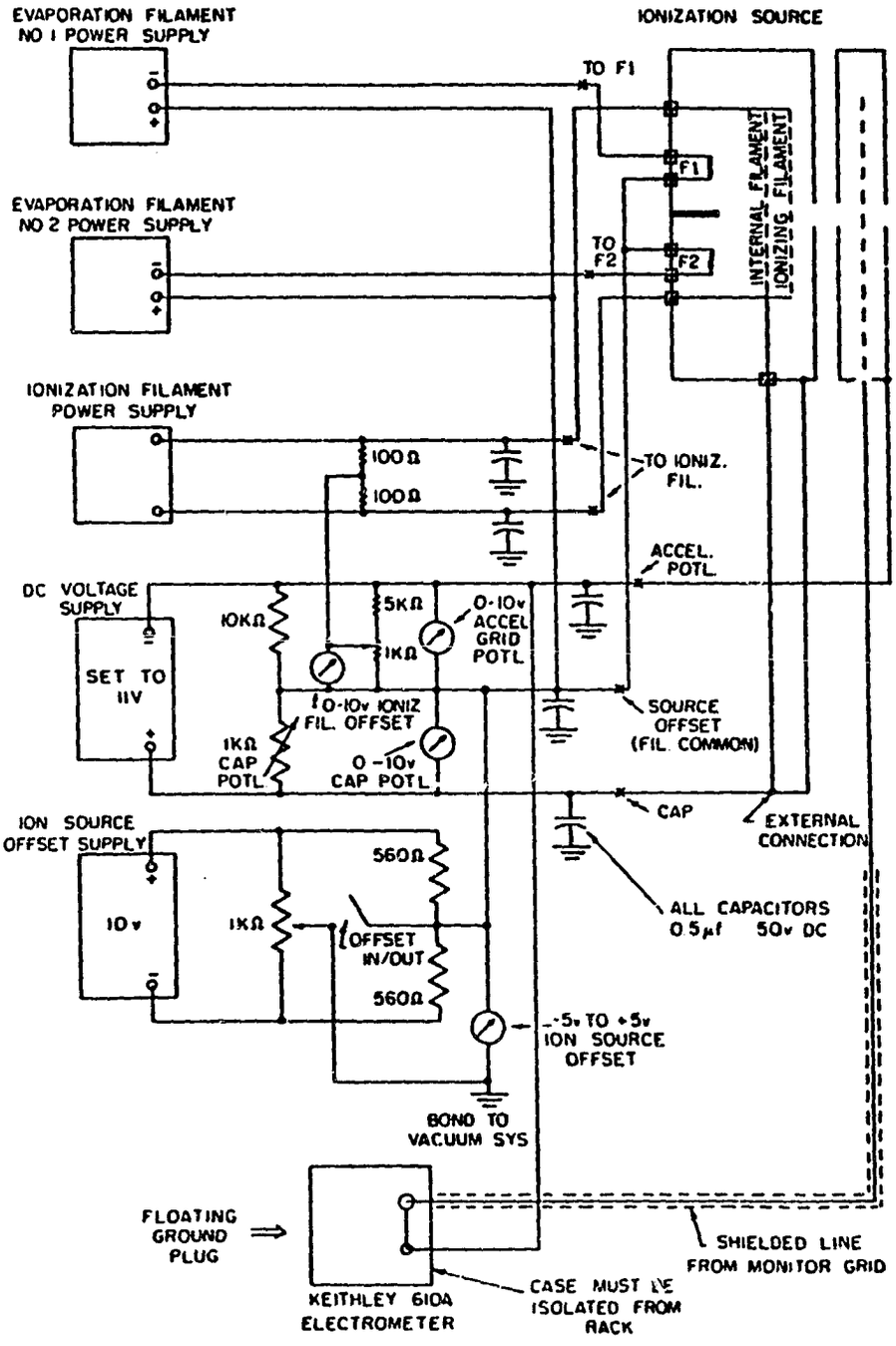

Figure 4.2 Surface Ionization Ion Source and Associated Electronics.

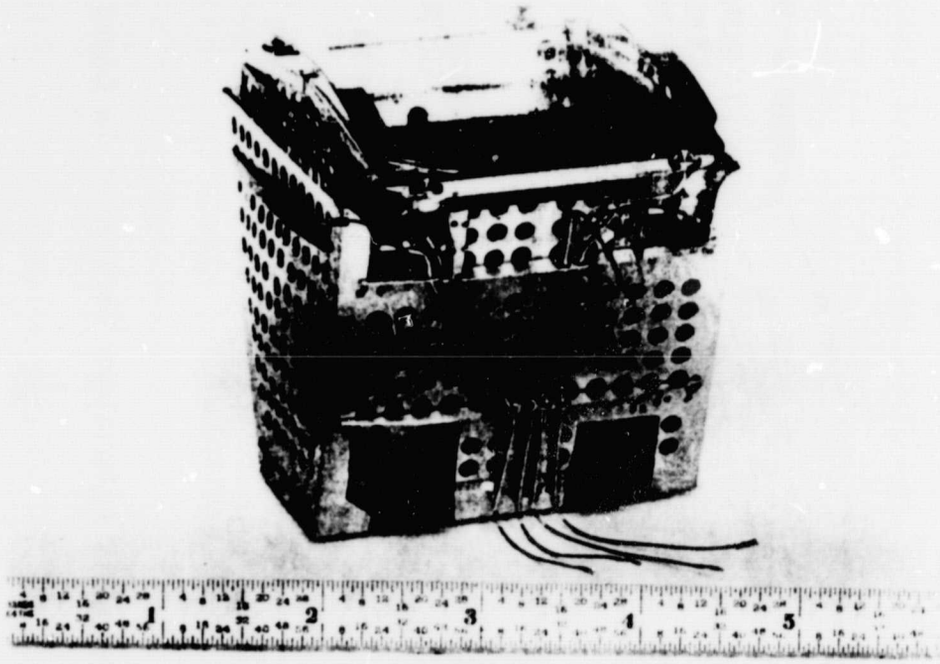

Figure 4.3 Cylindrical-Electrode TOFMS Used for Laboratory Studies.

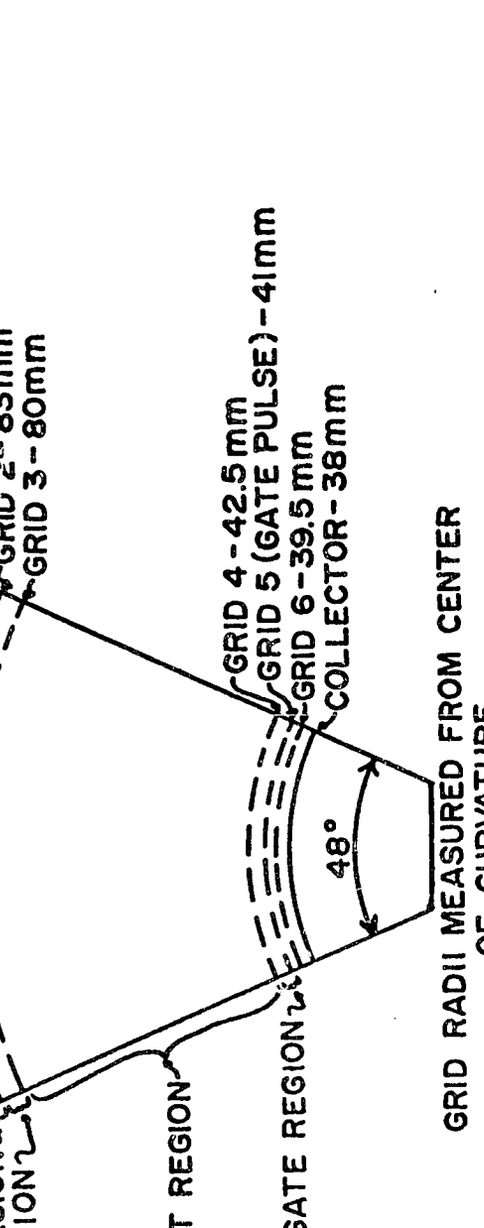

Figure 4.4 Cross-Sectional View of the Laboratory Version of the Gated Cylindrical-Electrode TOFMS.

spectrometer and to isolate the surrounding medium from the voltage pulses inside the mass spectrometer. The bunching pulse, with positive amplitude V_1, is applied to grid 1. The dc potential applied to grid 1 is usually V_0 (the same as the potential on grid 0). A dc potential, V_2, is applied to grid 2. Grid 3 carries the ion acceleration voltage, V_3. Grids 4 and 6 are also set at V_3. Grid 5 carries the dc barrier potential, V_5, and the gate pulse. The collector is also at V_3. All potentials can be varied independently. The interelectrode spacings are fixed. The electrodes were made from nickel wire mesh with 80 lines per inch and individual wire diameters of 1 mil. The grid transparency was about 89 per cent.

The electronics for the production of the voltages for this mass spectrometer were contained in a single controller built to the specifications of Dr. B. R. F. Kendall by the Electronic Services Group of the Electrical Engineering Department of The Pennsylvania State University. The controller was based on the designs of Hazelton (1968), Barnes (1971) and Zabielski (1970). Modifications were made on the controller by myself at a later date. The buncher pulse and gate pulse widths were fixed by the original controller design. A typical buncher pulse is shown in Figure (4.5). A typical gate pulse has already been illustrated in Chapter III. The gate pulse delay time could be varied at fixed scan rates of 20 Hz, .5 Hz, and .1 Hz. A manual scan was also possible.

Several electrometers were used during the study of this mass spectrometer. The first was a linear electrometer with four gain settings based on a Keithly 302 commercial electrometer. This

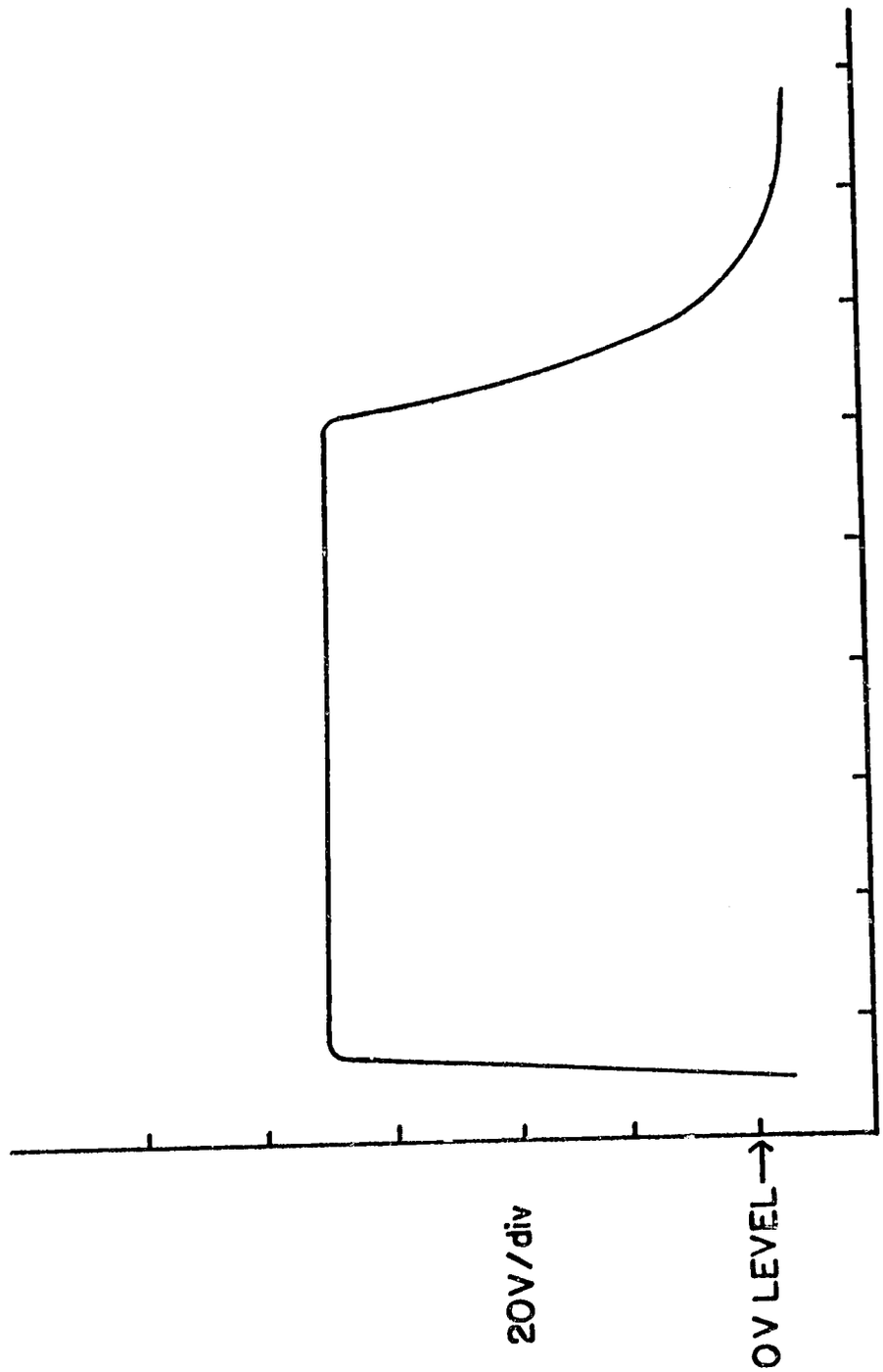

Figure 4.5 A Typical Buncher Pulse Used in the Cylindrical-Electrode TOFMS.

electrometer circuit is shown in Figure (4.6). The frequency response of this electrometer was about 100 Hz at the lowest gain setting. The second electrometer was a logarithmic electrometer, based on an Intersil 8500A commercial electrometer, designed by Locus, Inc. of State College, Pennsylvania. The frequency response of this electrometer was better than 1 kHz at the currents of interest. The third electrometer was a Keithley 610B vacuum tube electrometer. This electrometer could only be used with the manual gate sweep because of its extremely low frequency response (less than 1 Hz). Extraneous microphonic noise caused by pump vibration was a constant problem in making noise-free current measurements. The vacuum system backing pump could be shut down for short periods and a liquid nitrogen cooled zeolite pump used in its place. When this method was inconvenient, a signal averager (a Princeton Applied Research Waveform Eductor) was used. Care was needed when using the logarithmic electrometer with the signal averager since amplitude measurements could be misleading in this situation.

4.2.2 Ion Flight Times and Mass Spectrum Characteristics

Experimental flight time calibrations were obtained for a number of mass spectrometer operating conditions. A representative example is shown in Figure (4.7). The mass spectrometer operating voltages can be deduced from the buncher pulse positive amplitude, V_1, and the voltage ratio, $R = V_1 - V_3/V_2 - V_3$. The gate barrier was 155 V (V_5 = 85 V and V_3 = -70 V) and the gate pulse amplitude was typically 100 V. The $m^{1/2}$ dependence of the flight times can be seen easily. A typical mass spectrum obtained by using the

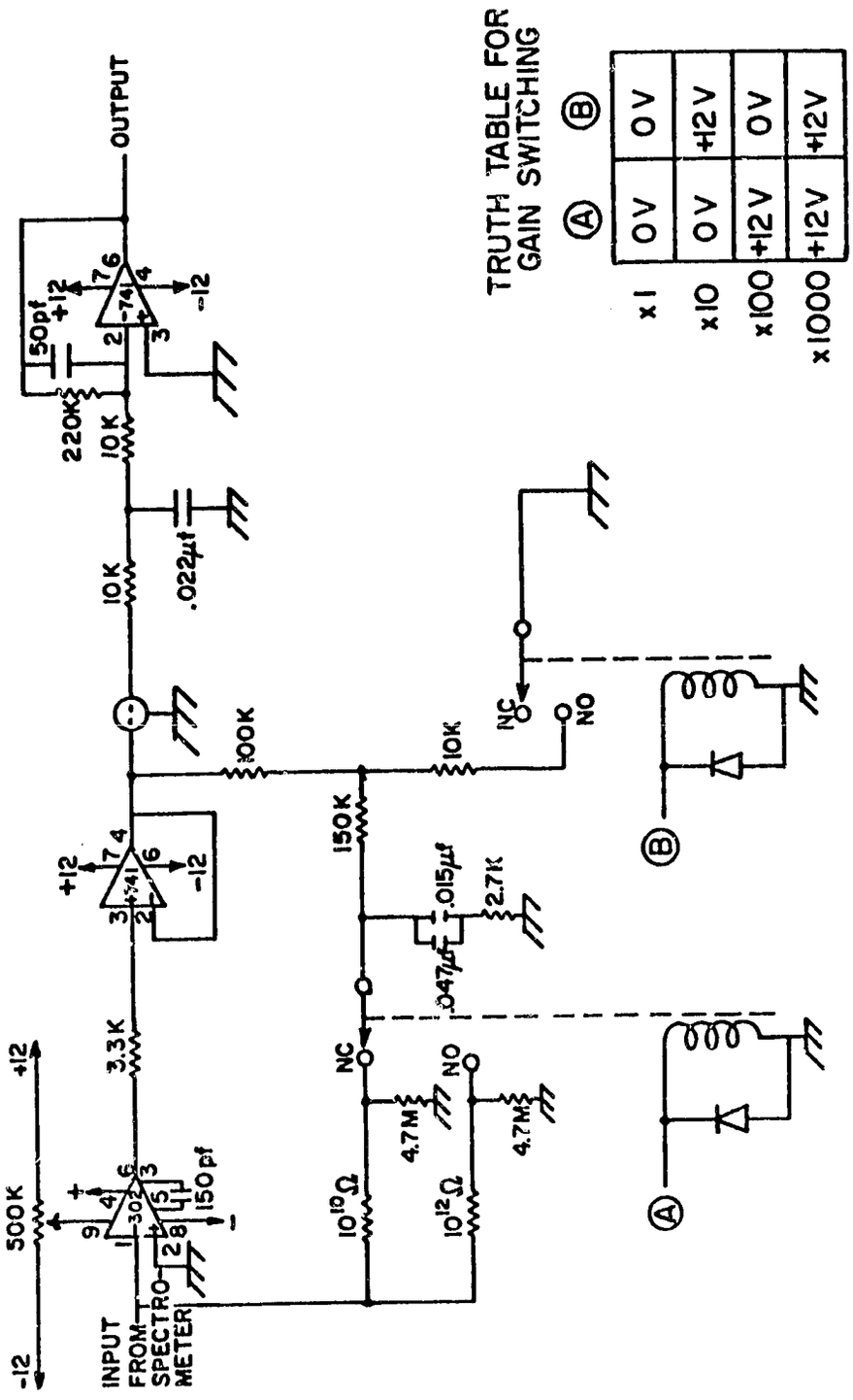

Figure 4.6 Linear Electrometer Circuit Based on a Keithley 302 Commercial Electrometer.

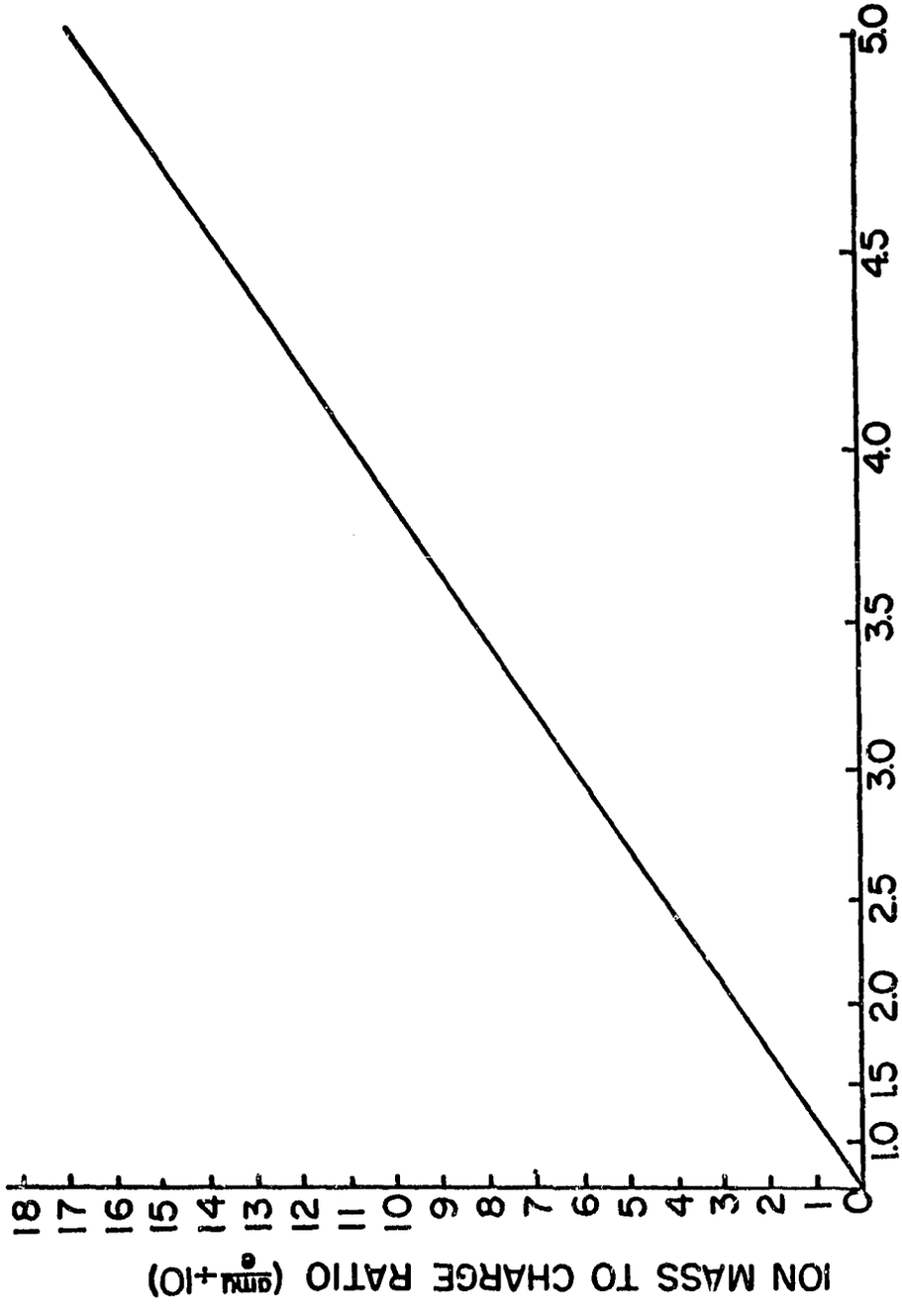

Figure 4.7 Experimental Ion Flight Time as a Function of Ion Mass-to-Charge Ratio.

surface ionization source is shown in Figure (4.8). The resolving power ($m/\Delta m = t/2\Delta t$) was 5.9 at Na^+ (23), 6.5 at K^+ (39, 41) and 9.4 at Cs^+ (133). The voltage ratio was 2.30. This voltage ratio was higher than the theoretical ratio for optimum space focusing to offset the effect of the initial ion energy spread. The variation in resolving power with mass is thought to be due to the operation of the gate and to the finite rise time of the buncher pulse. The improvement in resolving power over the results reported by Zabielski is due to improved electrometer frequency response and buncher pulse rise time characteristics (typically 10 nsec).

4.2.3 High Pressure Operation

Measurements of the mass spectrometer sensitivity at high pressure have been reported by both Diem (1967) and Zabielski (1970). However, these measurements were taken using a thermocouple pressure gauge to measure the pressure from 6.67×10^{-2} pa to 6.67 pa. A thermocouple gauge is not particularly accurate over this pressure range and requires constant calibration. The addition of a diaphragm manometer to the vacuum system used for these measurements made it possible to make extremely accurate pressure readings for sensitivity measurements. Because of this improvement in pressure accuracy, the sensitivity measurements for the cylindrical TOFMS were repeated in conjunction with the measurements of the background current ratio reported in Chapter III. The relative sensitivity as a function of pressure is shown in Figure (4.9). The sensitivity has been corrected for the distance the ions have to travel before entering the mass spectrometer. An important

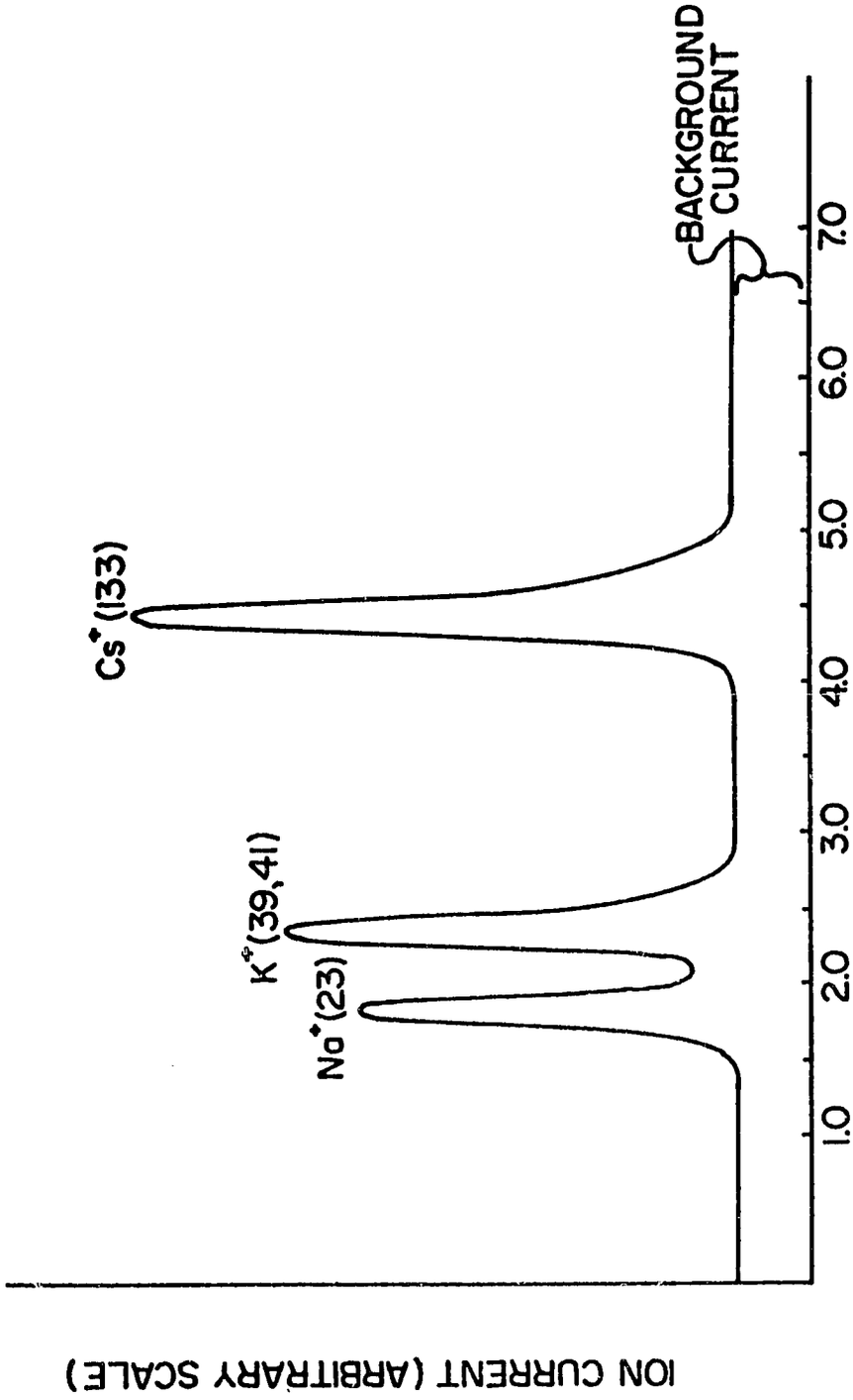

Figure 4.8 A Typical Mass Spectrum Taken with a Gated Cylindrical-Electrode TOFMS.

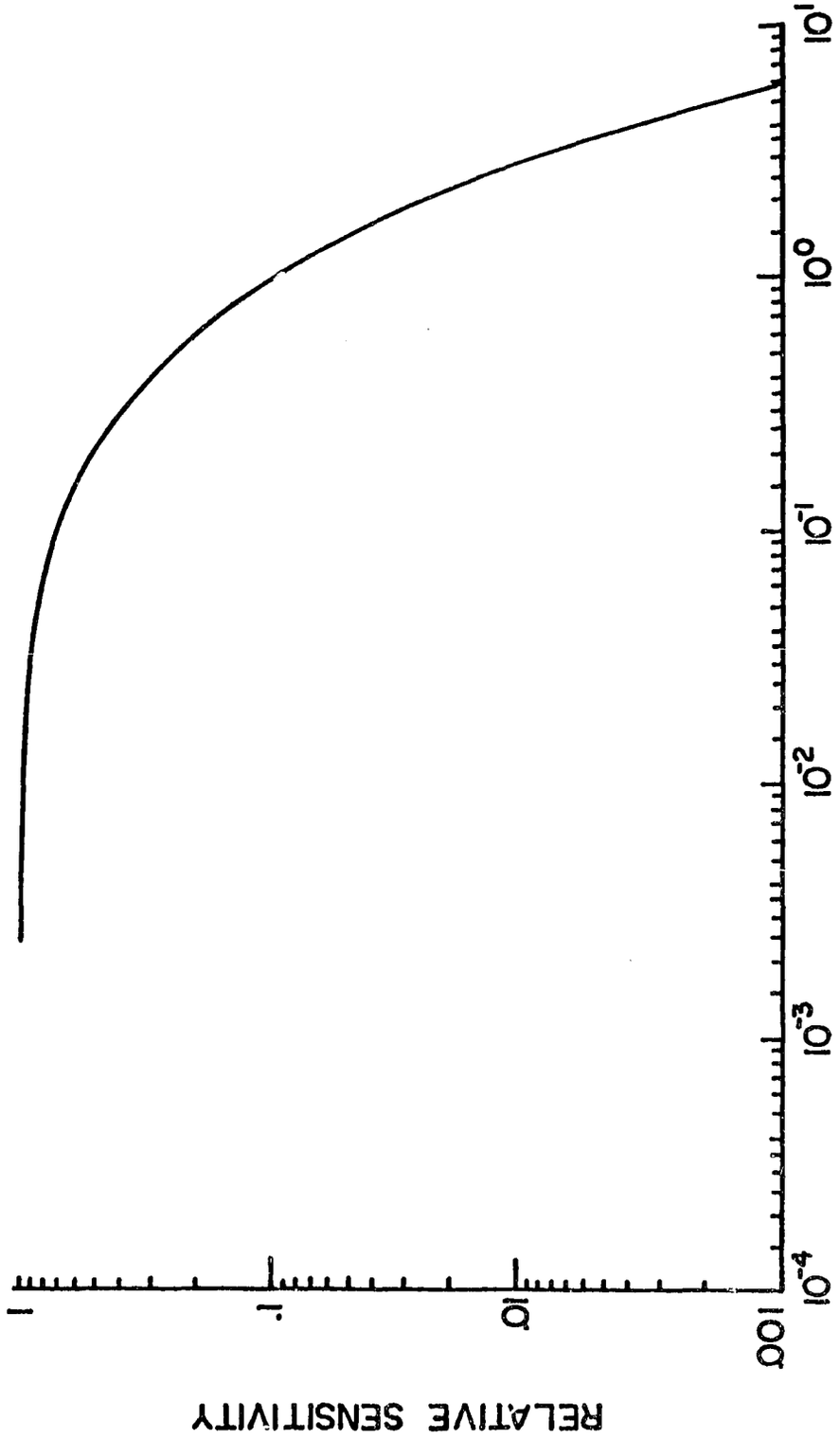

Figure 4.9 Experimentally Measured Relative Sensitivity Versus Pressure for a Gated Cylindrical-Electrode TOFMS.

observation, also reported by Zabielski (1970), was that there was no degradation in the resolving power at pressures up to 5.33 pa. This is due to the way in which a time-of-flight mass spectrometer operates. Once an ion has left the very narrow source and acceleration regions, it enters the drift region. Any ion which has its flight time altered in the drift region (due to collisions) will usually not get through the gate. Those which do undergo collisions and get through the gate will contribute to the background current instead of the proper mass peak. Therefore, it is only collisions in the source and acceleration regions which can degrade the resolving power. Above 5.33 pa the ion mean free paths become shorter than the width of the source and acceleration regions. The extremely high sensitivity of this spectrometer and the lack of resolving power degradation at high pressures makes it an excellent instrument for D-region ionosphere measurements.

4.2.4 Resolving Power Improvements; Variable Source Velocity

The numerical studies in Chapter II showed the possibility of improving the resolving power in time-of-flight mass spectrometers. A cylindrical-electrode TOFMS was used to test these studies experimentally. The principle was to make the ion velocities in the source proportional to their distance from the collector before the buncher pulse turns on. While operating in a high voltage ratio mode these ion initial velocities should make it possible to correct for the poor space focusing characteristics inherent in the high voltage ratio mode. The new ion initial velocities were produced by making

$V_2 < V_0$ while altering the other operating conditions to produce the desired voltage ratio. The results of these measurements are illustrated in Figure (4.10). The voltage difference across the source region is plotted horizontally as $\Delta V = V_0 - V_2$. The resolving power is plotted vertically. For these measurements R = 2.30 was used. The resolving power maximum occurred at a ΔV which was within the range of ΔV's predicted in Chapter II for a voltage ratio of 2.15. The difference in the voltage ratios between the computer studies in Chapter II (see Figure (2.22)) and the ratio used in this section will not make a significant difference in this discussion. The effect in Figure (4.10) which does not agree with computer results in Chapter II is the immediate decrease in the resolving power for ΔV's greater than the ΔV corresponding to the maximum resolving power. There should be a broad range of ΔV's, from $\Delta V \cong 25$ V to $\Delta V \cong 35$ V, where the resolving power is maximized. The resolving power decrease for $\Delta V > 25$ V can be easily explained when computer studies of gating in TOFMS in Chapter III are considered (see Figure (3.4)). Only ions starting in the outer half (approximately) of the source when the buncher pulse is turned on are collected for Cs^+ (133). Therefore, when the minimum in the flight time curves (Figure (2.22)) moves inward toward r_2 (as V_2 is made more negative) and passes the center of the source region, the resolving power should decrease rapidly. The behavior of the K^+ (39, 41) resolving power curve should exhibit a broader resolving power maximum and a slower resolving power decrease above the optimum ΔV values because gating will discriminate

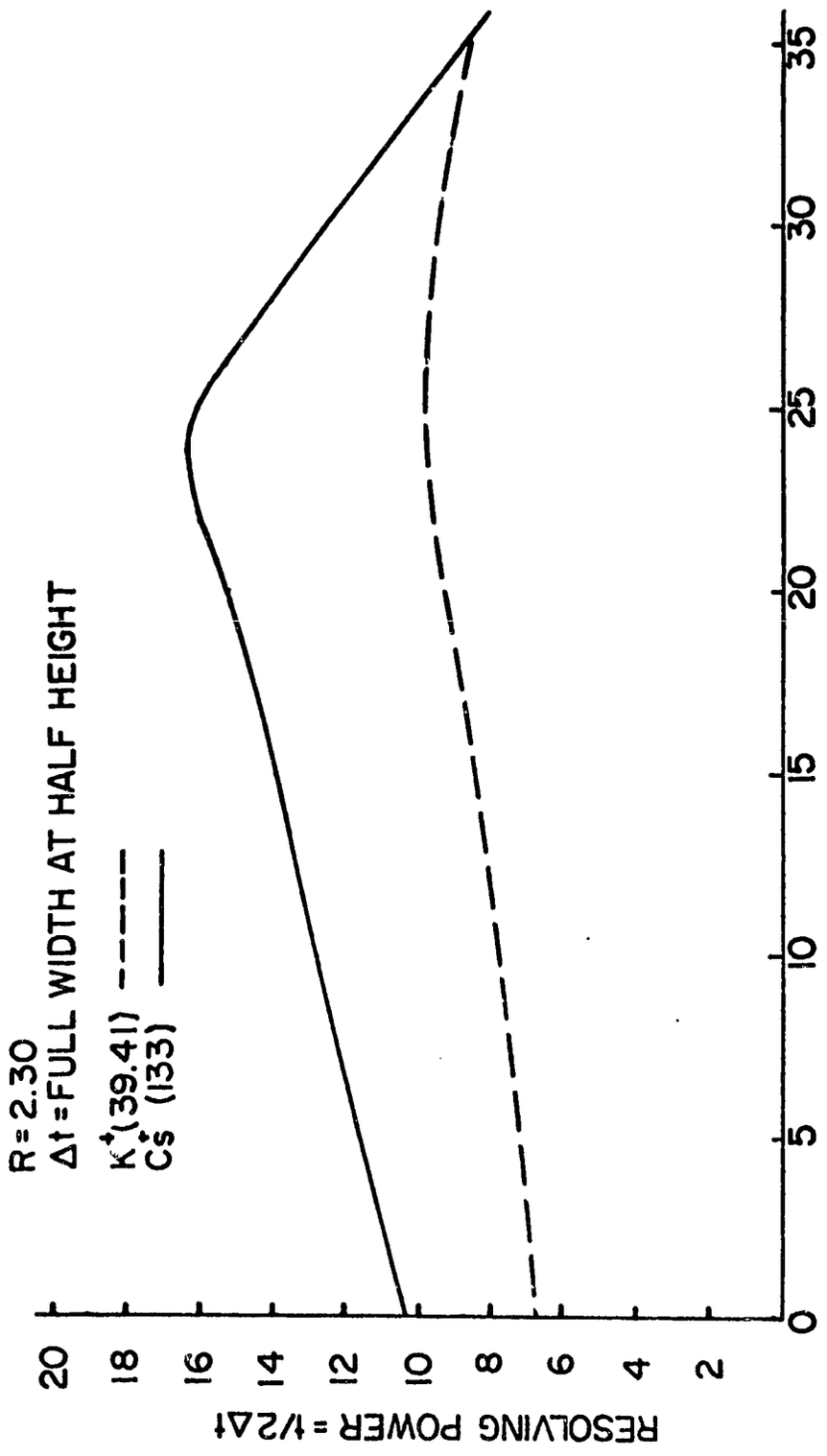

Figure 4.10 Experimentally Measured Resolving Power Versus the Voltage Difference Across the Source Region for a Gated Cylindrical-Electrode TOFMS.

against only the innermost source starting positions. This is, in fact, the behavior which is observed in Figure (4.10). This discussion shows that the computer simulations of Chapter II and Chapter III can be combined to accurately explain the experimental measurements with a gated cylindrical-electrode TOFMS.

A resolving power maximum of 21 for Cs^+ (133) had been obtained at a slightly lower voltage ratio (R = 2.03) in other studies using source position dependent initial ion velocities.

4.3 Hemispherical-Electrode Two-Field TOFMS

4.3.1 Instrument Dimensions and Electronics

The theoretical calculations carried out in Chapter II were for a spherical-electrode TOFMS. In order to experimentally test the results of Zabielski (1970), Zabielski, Stein and Kendall (1972/1973), Stein (1974) and myself, it was decided to use a TOFMS constructed with hemispherical electrodes because the construction of hemispherical electrodes was thought to be simpler (than spherical electrodes) and could be accomplished quickly. It also simplified the proper spacing of the electrodes. The hemispherical TOFMS used for these measurements is shown in Figure (4.11). The effects of fringing fields were bypassed by taking care that ions entered the spectrometer at the center of the outer electrode. This was accomplished by injecting the ions through a cover which had a hole at the center. This cover was maintained at the same potential as the outermost spectrometer grid before the buncher pulse was applied. Ion detection was made using a 16 stage venetian blind

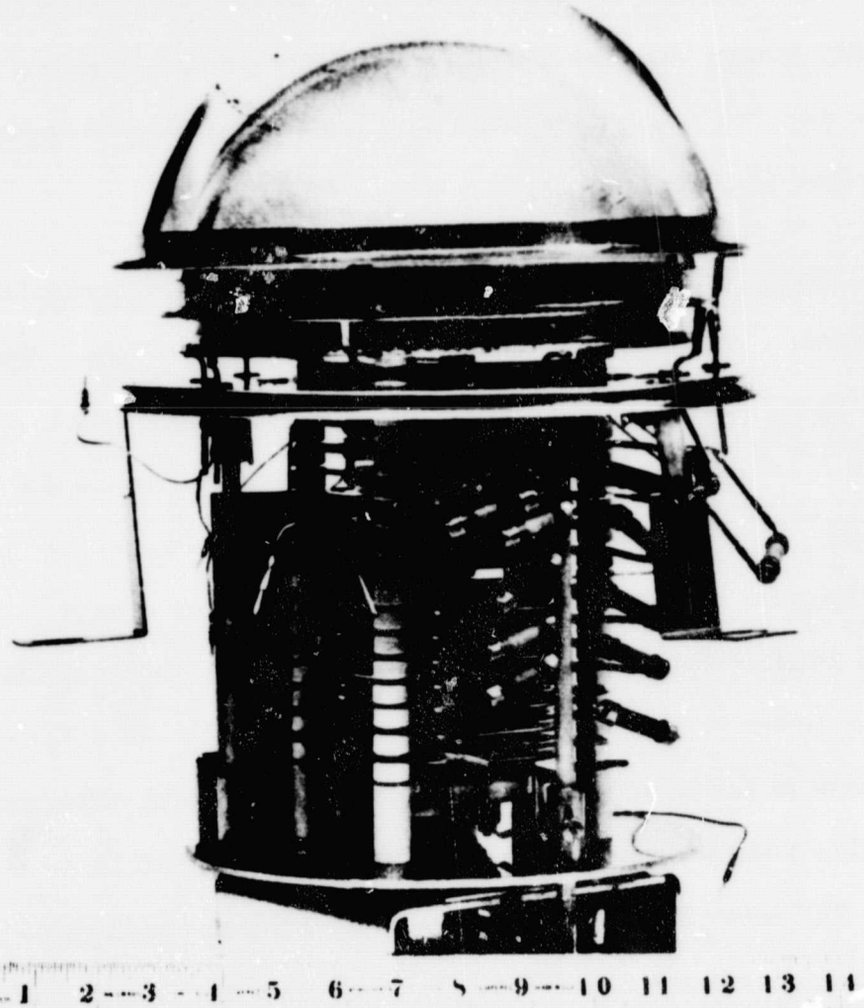

Figure 4.11 Hemispherical-Electrode TOFMS. A 16 Stage Electron Multiplier Used for Ion Detection is Shown.

electron multiplier with unactivated Be-Cu dynodes. The spectrometer cover also performed the same task as grid 0 did for the cylindrical TOFMS. The associated electronics and spectrometer grid spacings are shown in Figure (4.12). The hemispherical TOFMS did not use any form of gating. Because a commercial pulse generator was used for these studies, the buncher pulse rise time was considerably longer than the cylindrical TOFMS buncher pulse rise time. The buncher pulse rise time was typically 150 nsec in the hemispherical TOFMS studies.

4.3.2 Ion Flight Times and Mass Spectrum Characteristics

A composite mass spectrum is shown in Figure (4.13). This mass spectrum illustrates a number of characteristics which might not be visible on any one mass spectrum. The ion mass peaks represent Na^+ (23), K^+ (39,41) and Cs^+ (133). The resolving power at these particular mass peaks are 8.2 at Na^+ (23), 9.2 at K^+ (39,41) and 10.1 at Cs^+ (133). The significantly lower resolving power at the lower ion masses is thought to be due to the relatively long rise time of the buncher pulse. Another important observation is the smaller resolving power variation with mass than in the cylindrical TOFMS. This is undoubtedly because of the lack of gating in the hemispherical device. It is obvious that the use of gating does have a significant effect on resolving power. Also notice the overall improvement in the resolving power at all masses over the cylindrical TOFMS operating with normal voltages as reported in this thesis and by previous researchers. Some of this improvement must be due to the lack of gating. The extremely high

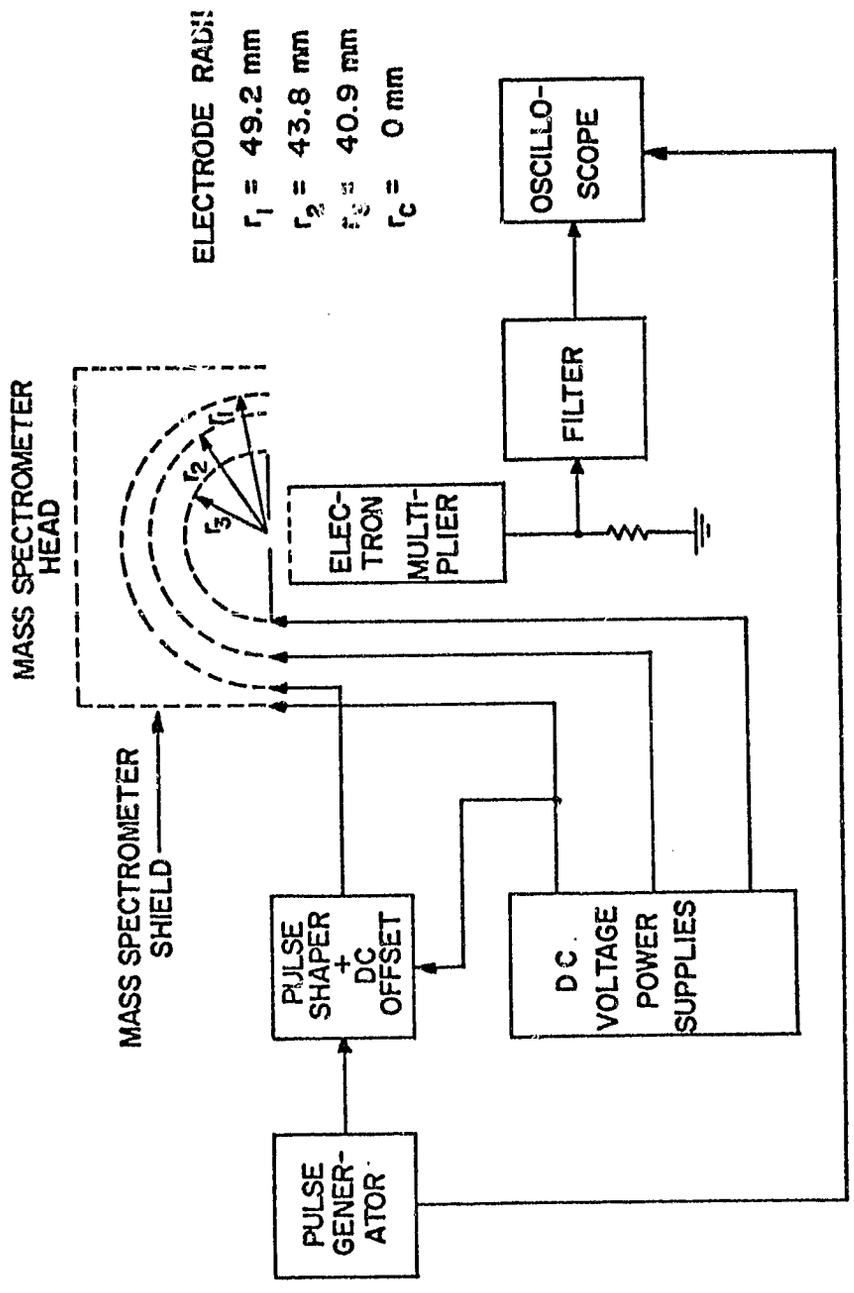

Figure 4.12 Hemispherical-Electrode TOFMS Electrode Radii and Associated Electronics.

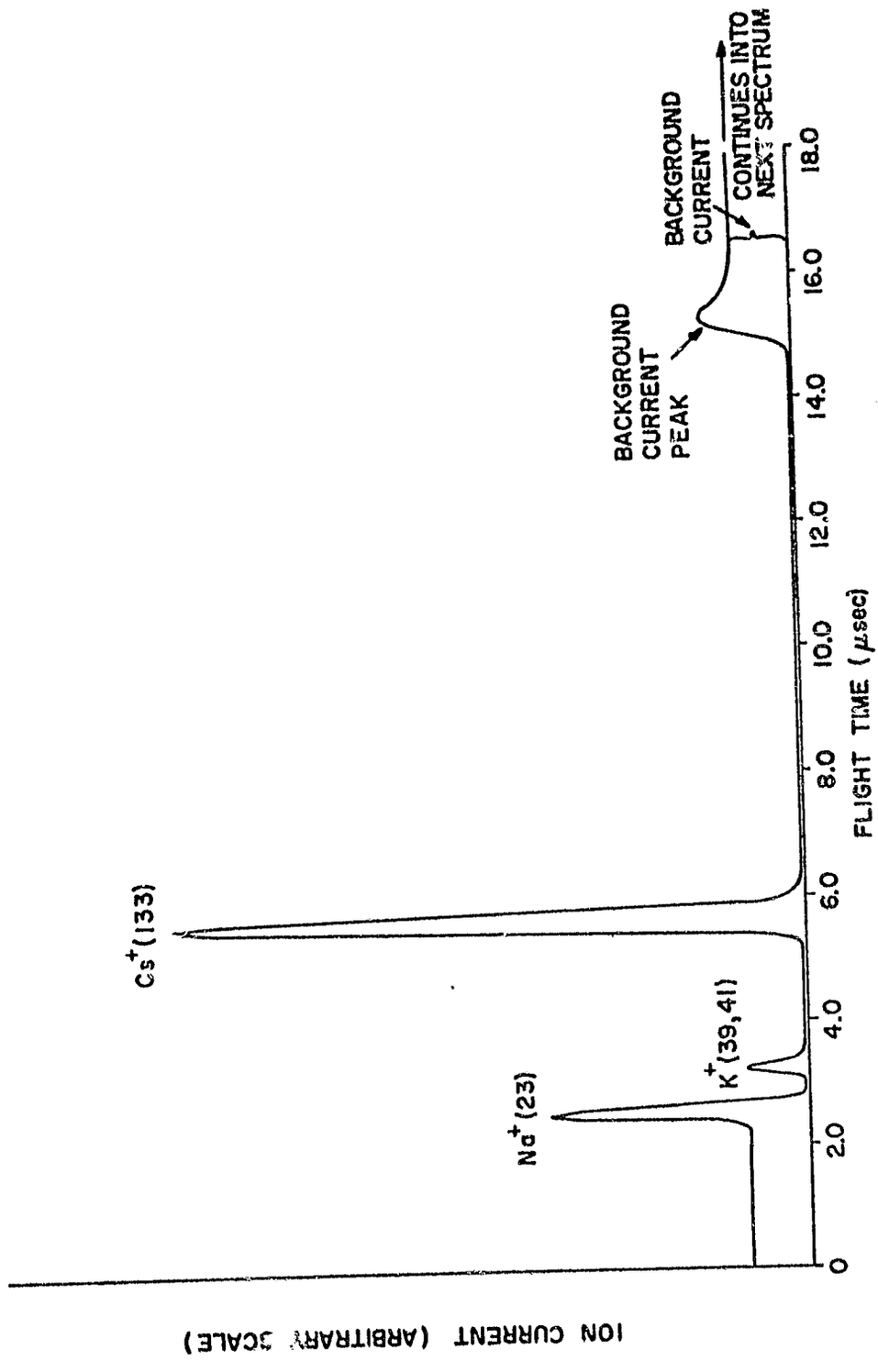

Figure 4.13 Composite Mass Spectrum for the Hemispherical-Electrode TOFMS.

frequency response of the electron multiplier might also contribute to this resolving power improvement. The finite depth of the conversion dynode of the electron multiplier could produce an ion flight time spread corresponding to as much as 17 per cent of the observed Cs^+ (133) mass peak (and a correspondingly larger amount for the lighter ion mass peaks) if the ions were not properly focused at the collector. This lack of proper focusing could easily result if the hemispherical TOFMS electrodes were improperly centered or if the electron multiplier conversion dynode was not placed in the correct position. In actual fact, an examination of the conversion dynode showed the ions had been focused onto a spot which covered only about 25 per cent of the depth of the conversion dynode.

The background current starting to the right of the Cs^+ (133) mass peak is produced by ions entering the mass spectrometer after the buncher pulse turns off. These ions pass through the source region before the next buncher pulse starts and are eventually collected. The lack of background current up to this point is due to the buncher pulse repelling ions about to enter the source. This explanation for the background current was verified by varying the width of the buncher pulse, which caused a corresponding change in the starting flight time for the background current, and by varying the spectrometer potentials, which again caused a corresponding variation in the background current starting time. One feature of the background which could not be explained immediately was the small current peak at the beginning of the background current. It was concluded that this small peak was caused by ions which were

just at the turn around point outside the spectrometer as the buncher pulse turns off. Since the current density of the ion beam from the ion source is conserved, the ion density (charge density) at the turn around point is enhanced and produces the small peak when they are eventually collected.

A best resolving power of about 13 was obtained with the hemispherical TOFMS at Cs^+ (133) with a voltage ratio of 2.46. This is the best resolving power obtained with a hemispherical spectrometer operating with the normal operating voltages. The resolving power improvement method using a variable initial source velocity has not been attempted with the hemispherical TOFMS to this date. The high voltage ratio required for best resolving power is probably due to the slightly larger source region width and the shorter drift region length combined with the large initial energy spread (see the discussion of high initial energy spreads in Stein (1974)). The smaller radii of curvature of the hemispherical-electrode TOFMS used for these studies will not make a significant difference in the resolving power compared to the cylindrical-electrode TOFMS (see the discussion of radius of curvature in Chapter II). Some of the results presented in this chapter have been previously reported by Reiter and Kendall (1974), Kendall and Reiter (1975) or were used as examples in Stein (1974).

CHAPTER V

BOOSTED ARCAS SOUNDING ROCKET EXPERIMENTS

5.1 Aims

The launch vehicle chosen for the first flight applications of the new miniature time-of-flight mass analyzer was the Boosted Arcas II. This is a small two-stage sounding rocket made by Atlantic Research Corporation. Two flight packages were prepared and successfully put through shake and impact testing to both Arcas and Nike-Tomahawk specifications. The Nike-Tomahawk is considered to have one of the most violent vibrational profiles relative to other sounding rockets of its class. The aim of the experiment was to study the ion composition of the D-region and lower E-region with an instrument which was radically different in design from the pumped quadrupole mass spectrometers used by most other experimenters, and therefore not necessarily subject to the same sources of error. Of special interest was the distribution as a function of mass of the protonated water clusters $H^+ \cdot (H_2O)_n$ which have been observed in the mesosphere by Narcisi and Bailey (1965), Goldberg and Blumle (1970), Goldberg and Aikin (1971) Krankowsky et al. (1972), Johannessen et al. (1972), Johannessen and Krankowsky (1974), and others.

5.2 Experiment Package

The layout of the experiment package and a summary of its operating characteristics is shown in Figure 5-1. The entire package was hermetically sealed and special precautions were taken

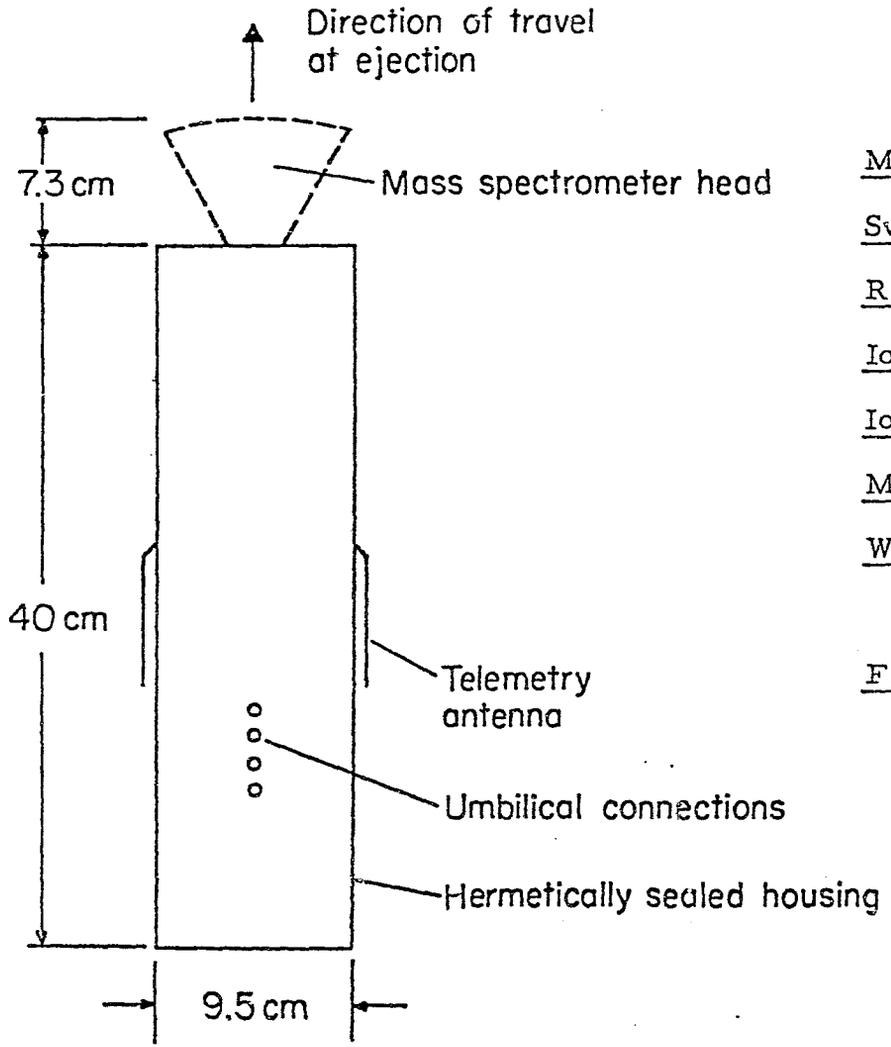

Mass range: 2-280

Sweep Rate: 1 mass scan/second

Resolving Power: 9

Ion Flight Time: 2.5 μsec at mass 40 amu

Ion Entrance Aperture: 6.4 x 5.0 cm

Minimum Detectable Ion Current: $\sim 10^{-13}$ amp

Weights: Mass analyzer head ~ 125 gm

Total, including batteries and transmitter 5 Kg

Frequencies: 1680 MHz F.M. transmitter; 70 KHz and 52.5 KHz F.M. Subcarriers

Figure 5-1. Ejectable rocket-borne experiment package consisting of external time-of-flight mass spectrometer head with cylindrical mesh electrodes, and sealed housing containing mass spectrometer power supplies, electrometer, telemetry equipment, transmitter and batteries.

to minimize outgassing of water vapor from its exterior during flight (Kendall and Weeks, 1974). It was intended to be ejected from the burnt-out second stage of the vehicle at approximately 70 km altitude to further reduce contamination effects. Nosecone ejection and removal of a protective nitrogen-filled cap over the mass spectrometer occurred at the same time. The total weight of the experiment package, including batteries, telemetry equipment and transmitter, was 5 kg.

The ion mass spectrometer used in this experiment used the time-of-flight principle with curved focusing electrodes and a short ion path length of 4.5 cm. This allowed operation at ambient pressures up to about 4 Pa without a vacuum pump. The focusing electrodes and a 32 cm^2 ion inlet aperture gave high sensitivity without the need for an electron multiplier detector. A relatively low draw-in voltage of -7 V was used to reduce possible break-up of ion clusters. For the same reason, the pulsed region of the ion source projected beyond the bow shock of the ejected instrument package and was bounded by high-transparency mesh. The resolving power was set at approximately 9. This was considered adequate to distinguish between the main water cluster species. Mass peaks were superimposed on a uniform background current which was proportional to the total current of ions collected, including those having masses beyond the 275 amu upper mass scan limit of the instrument. Extensive testing and calibration were carried out in a laboratory simulator at pressures up to 4 Pa using an alkali surface-ionization ion source. A

theoretical analysis of the ion dynamics of this mass analyzer was given by Zabielski et al. (1970).

5.3 Flight Results: 15.42

The first experiment package was launched at 1605 E.S.T. on 29 October, 1969 from Wallops Island, Virginia. The flight designation was NASA Arcas 15.42. Supervision of vehicle preparation was by personnel from NASA Goddard Space Flight Center. The vehicle was tracked by Wallops Island radar and the 1680 MHz telemetry transmissions were received by the Wallops Island Weather Station and the Ballistic Research Laboratory telemetry van. The first and second stages of the rocket performed excellently. However, payload separation never occurred because the explosive charge was not present in the second stage. Due to an error on NASA's part, the wrong type of second-stage motor was used. Because separation did not occur, the spectrometer was never exposed to the ionosphere; hence, no spectra were obtained.

On the brighter side, this flight provided proof that most of the electronics can function well throughout a flight. Telemetry records of the temperature in the electrometer region, electrometer calibrations, mass scan, time marks, and range change marks during electrometer calibration were obtained.

5.4 Flight Results: 15.46UI

A similar experiment package was prepared and launched at 1916 UT on 3 August 1971, again on a Boosted Arcas II, and again from Wallops Island. The flight designation was 15.46UI

and vehicle preparation in this case was in the capable hands of Wallops Station personnel.

About one minute after a normal launch of this experiment, defects appeared in the telemetry link. By the time the experiment package was ejected at +80 seconds and a velocity of 973 m/sec, only fragments of data were being collected and subsequent signals appeared at the time to consist almost entirely of noise. Apogee was 117 km.

A continuing effort to extract the small amount of useful data present in these signals has recently been successful. Two effects which were discovered in analyzing the flight records were nonlinearity of the ground-based telemetry equipment and the appearance of amplitude modulation in the frequency-modulated data link at low signal levels. Allowance for these effects made it possible to determine the signal strength levels above which reliable data could be expected. The distribution of electrometer range changes as a function of mass, electrometer range settings, and temperature data from an internal thermistor could then be determined. In this way it was possible to build up a semi-quantitative picture of the mass spectrometer outputs in the 72-80 km height range.

The data finally extracted showed a large background current without any clear mass features below 275 amu. This indicated that the majority of the collected charged particles had masses greater than 275 amu. It appeared that, of the ions which were within the instrument's mass range, most were around mass 19 or

above mass 100, except for metallic ions which were present in at least two thin layers.

It can be argued that the high background ion current might have been the result of the fine grids at the input of the mass spectrometer rupturing during the outrush of dry nitrogen following removal of the mass spectrometer cover. However, tests in a vacuum chamber with an identical mass spectrometer showed that there was a large safety factor even when the cover was intentionally over-pressurized. Studies of movies of the ejection process and records of numerous shake tests on the flight instrument all pointed to the data having been obtained with a physically intact instrument.

CHAPTER VI

NIKE-APACHE AND NIKE-CAJUN SOUNDING ROCKET EXPERIMENTS

6.1 Mechanical

6.1.1 Vehicle

In 1969 the initial plans for second-generation sounding rocket experiment packages were developed. At NASA's suggestion, it was decided to fly these experiments on Nike-Apache or Nike-Cajun two-stage sounding rockets. The mechanical configuration of the experiment package was then designed by Electronic Services (a special projects group associated with the Electrical Engineering Department of The Pennsylvania State University).

6.1.2 Experiment Package

The actual experiment package was a combination of two sections. One half of the package was made at Penn State University and contained the electronics for the instruments carried by the package. These instruments were to be a cylindrical-electrode time-of-flight mass spectrometer, three ion probes of various geometries, a thermocouple vacuum gauge and two thermistors for temperature measurement. The mass spectrometer and two of the probes were forward facing. The remaining probe and the thermocouple gauge inlet ports were facing to the side. One temperature thermistor was placed in contact with the inside of the experiment package skin while the second thermistor was placed in contact with the hottest part of

the electronics inside the experiment package. The other half of the package was made at Wallops Island, Virginia by NASA personnel. This second half of the package contained telemetry equipment, batteries, a magnetometer, solar sensors and thermistors. When both sections were combined, the complete experiment package was hermetically sealed. This was considered essential for two reasons. First, outgassing from the interior of the package would be a serious source of contamination to the measurements contemplated in the ionosphere. A discussion of this effect can be found in Kendall and Weeks (1974). Secondly, the loss of conductive dissipation of heat that would be a result of a reduction in pressure around the electronic components could cause component failure. The exterior of the complete experiment package was also gold plated to reduce both outgassing effects and photoelectron emission. Figures (5.1), (5.2) and (5.3) show photographs of the Penn State portion of the experiment package.

6.1.3 Mass Spectrometer Vacuum Cap

A vacuum cap made of aluminum and stainless steel was designed to be placed over the front end of the experiment package, covering the mass spectrometer, the two forward facing ion probes and the inlet ports to the thermocouple gauge. The purpose of this cap was to keep the enclosed instruments, and the front end of the package in general, under partial vacuum until the payload (the complete experiment package will be called the payload) was ejected into the ionosphere and began taking measurements. The volume under this cap

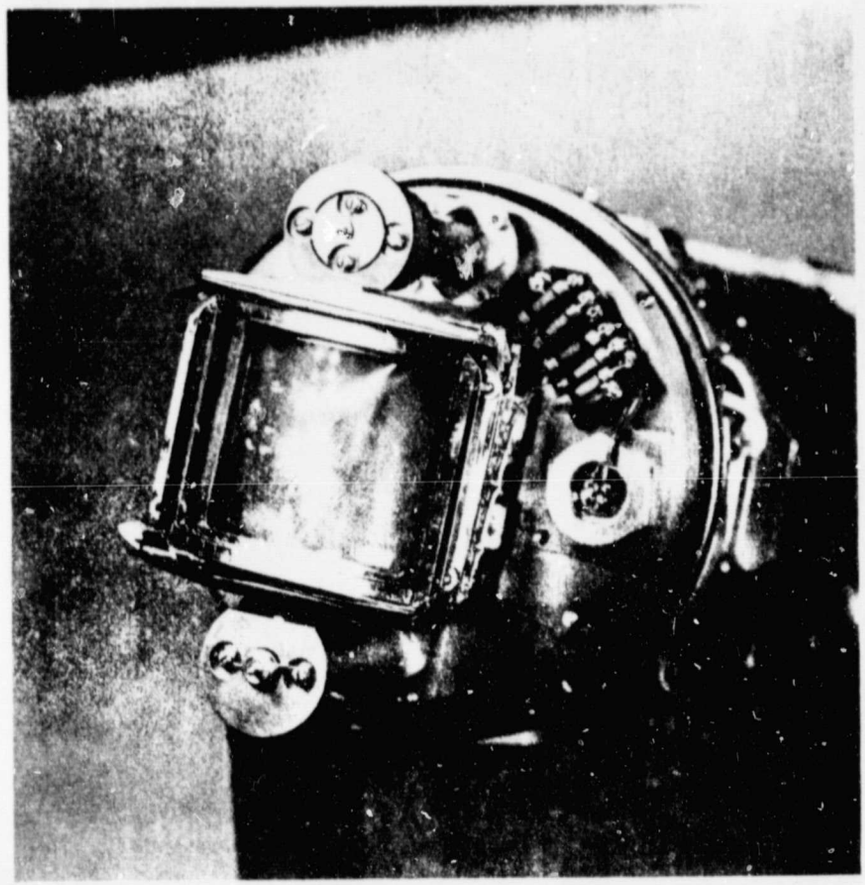

Figure 6.1 Front View of the Nike-Apache Experiment Package Showing the Cylindrical-Electrode TOFMS and Two Ion Probes.

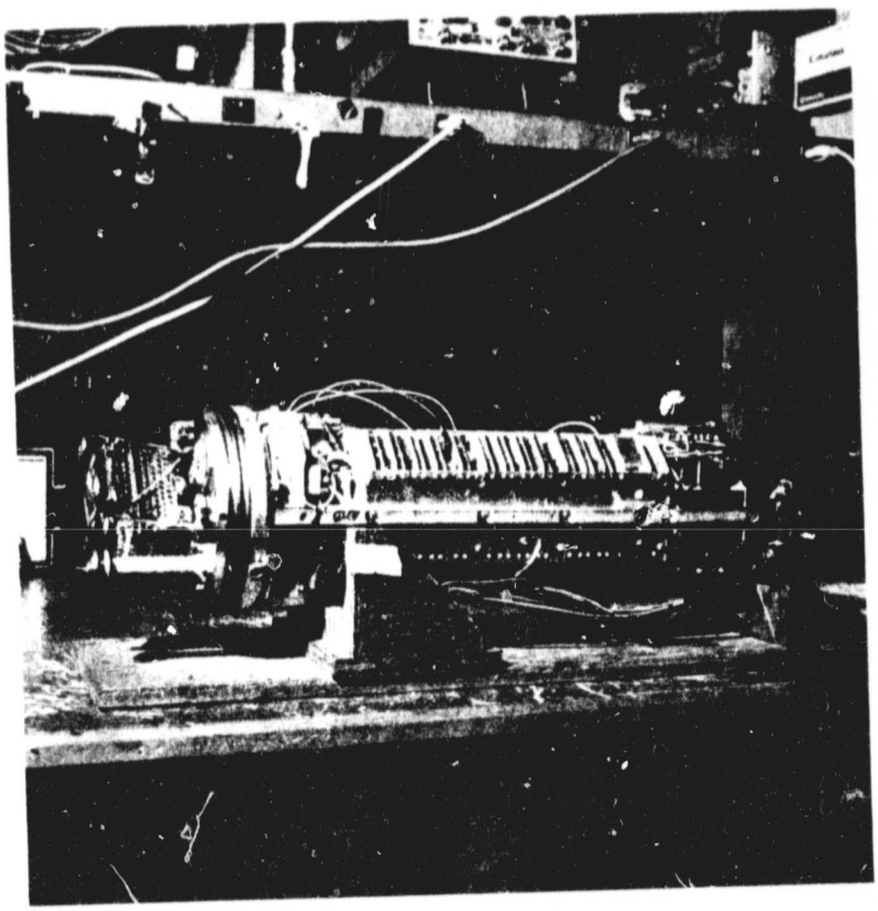

Figure 6.2 Side View of the Nike-Apache Experiment Package Showing the Arrangement of the Electronics.

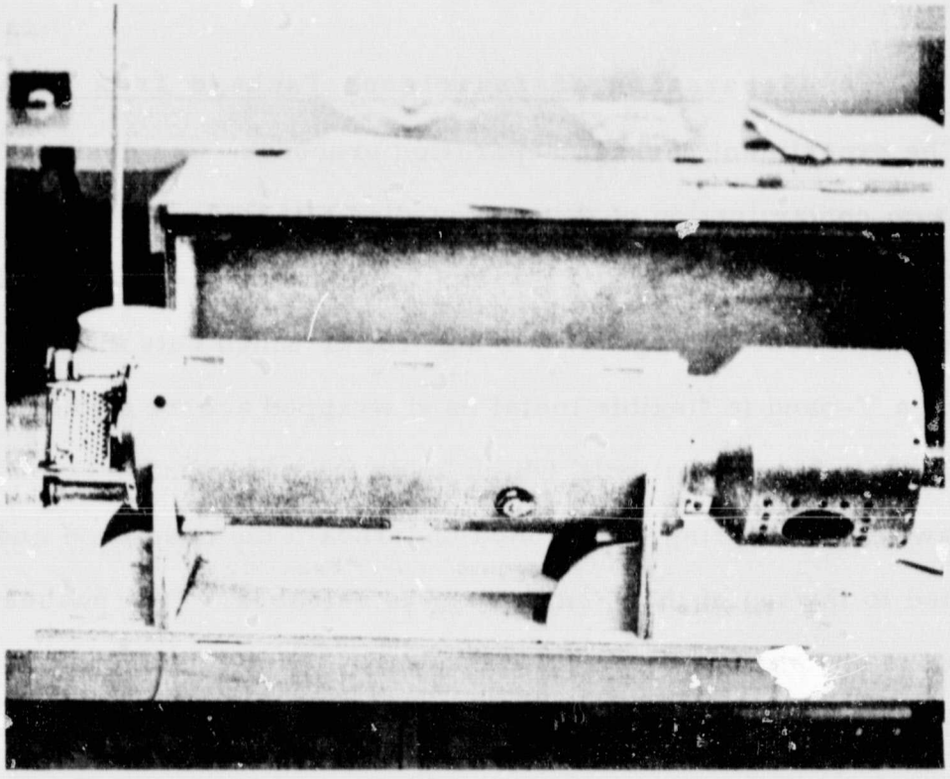

Figure 6.3 Side View of the Nike-Apache Experiment Package in the Outer Skin Showing the Side Probe Connector. An Adapter for Shake Testing is Shown Attached to the Bottom of the Experiment Package.

was to be pumped for approximately 24 hours and then backfilled to near atmospheric pressure with dry Nitrogen. A pressure valve was added to the cap to keep the pressure differential to about 1.38×10^4 pa during the rocket ascent.

6.1.4 Separation of Experiment Package from Vehicle

The experiment package separation procedure was designed for minimum contamination of the surrounding atmosphere. The separation takes place in two stages. The first stage starts when a sealed pyrotechnic charge fires a bolt cutter which cuts a bolt holding a V-band (a flexible metal band wrapped around a joint and held in place by a metal bolt) which holds the nose cone. The V-band flies away and a spring, positioned underneath the nose cone and attached to the top of the vacuum cap, is released. This pushes the nose cone ahead of the experiment package. When the spring reaches full extension, the vacuum cap is also jerked off. All the experiment package instruments are exposed at this time. However, the package is still resting in a short sleeve attached to the second stage motor. After the first stage of the payload ejection, the experiment package is no longer directly attached to the rocket motor. The second stage of the payload ejection takes place at this time. A second sealed pyrotechnic charge fires a second bolt cutter. This releases an air spring, located beneath the experiment package, which has been pumped out and then backfilled to about 1.03×10^5 pa with dry Nitrogen. The piston of the spring then pushes the experiment package out of the sleeve on Teflon skids. A strap is attached to the

piston to keep it from escaping. The experiment package is then completely separated from the rocket motor and nose cone and follows its own trajectory. See Figure (6.4) for a diagram of the ejection sequence.

The pyrotechnic charges were designed to be completely sealed when the charge is fired. Three versions of the charges were tested in the vacuum laboratory at The Pennsylvania State University by Dr. B. R. F. Kendall and John O. Weeks. The final version was found to have a satisfactory leak rate. The initial leakage from the successful charge was 2.00×10^{-3} pa-liters at firing and 4.44×10^{-6} pa-liters/sec. thereafter.

An important design parameter was the altitude at which separation was to take place. This altitude needed to be high enough so that the dynamic forces which the mass spectrometer grids are subjected to would not tear the grids. Studies, using high speed films, were made by Dr. B. R. F. Kendall and J. O. Weeks of the reaction of the mass spectrometer grids to sudden decompression. Static pressure tests made by myself were also made. Results of these studies showed the minimum ejection altitude to be about 65 km. An ejection altitude of 70 km was decided on to include a safety factor..

6.2 Environmental Testing

6.2.1 Shake Testing

In order to qualify for launch on the Nike-Apache sounding rocket, the experiment package had to undergo several shake tests. The first shake test was with just the Penn State section of

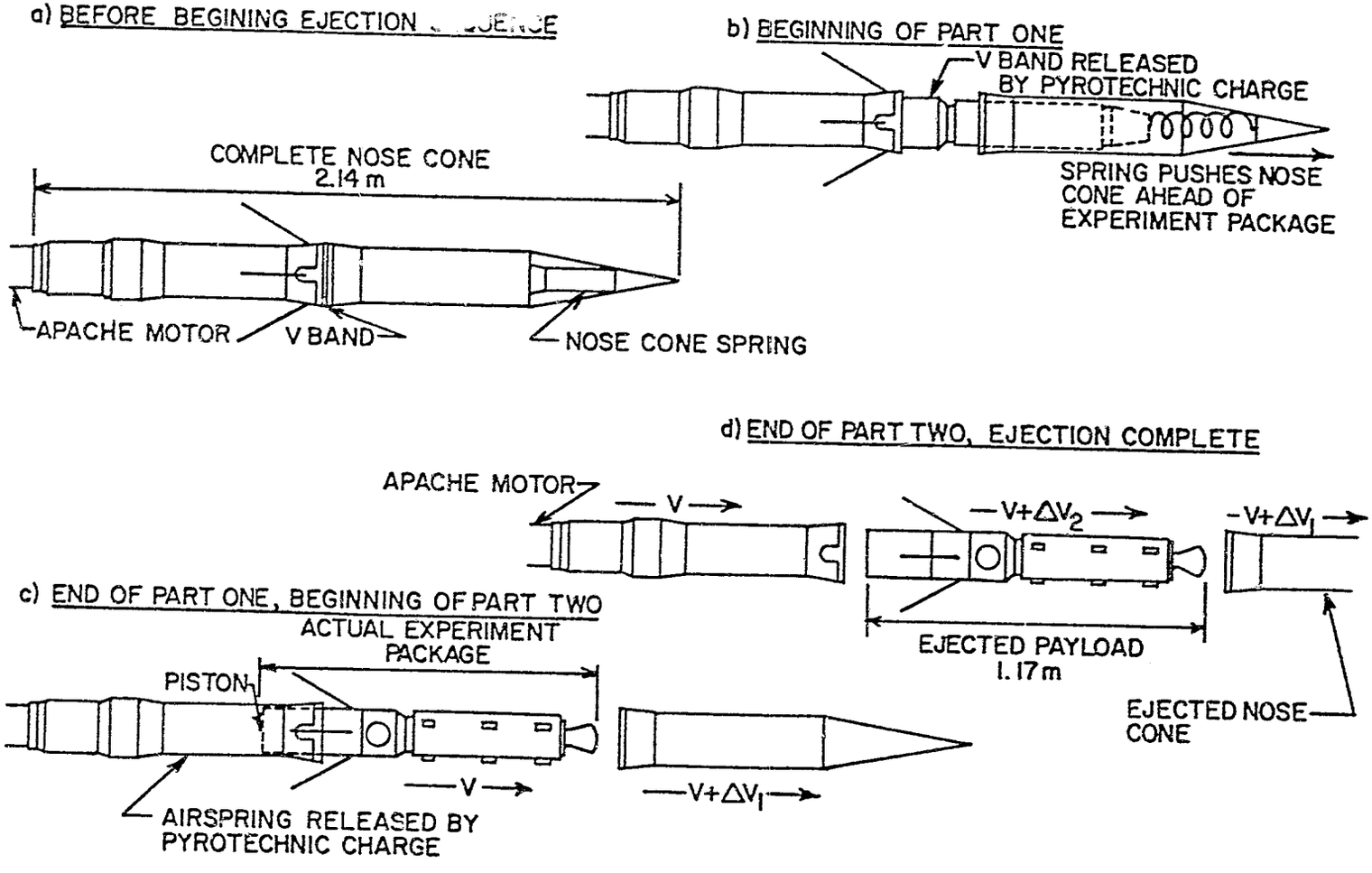

Figure 6.4 Experiment Package Ejection Sequence.

the payload. The second test was with the complete payload installed inside the nose cone. The shake tests were conducted at the Wallops Island, NASA, facility. These tests were conducted on the three axes of the payload, the thrust axis (z-z axis) and the two axes perpendicular to the thrust axis (the x-x axis and the y-y axis). The thrust axis shake tests included a low level sine-wave shake test, a simulated flight level shake test, a random noise shake test, and a transient shake test (to simulate the shock of a Nike booster ignition). The shake tests for the other axes included a low level sine-wave shake test, a simulated flight level shake test, and a random noise shake test. The details of the simulated flight level shake tests are shown in Table (5.1).

The experiment package electronics and telemetry were run during all the shake tests to monitor the behavior of the payload instruments. The electrometer outputs showed severe microphonic effects during the actual shake tests but this was not considered important to the operation of the electronics after payload ejection.

6.2.2 Payload Weight, Center of Gravity, Pitch and Roll Moments

In order to accurately determine the altitude to be attained by the payload and the precise trajectory to be followed by the payload and the nose cone after ejection, the weight and center of gravity of the complete payload had to be determined. The payload weight of the complete experiment package was 23 kg. The center of gravity was found to be 50.3 cm from the rear of the combined experiment package (the total package length was about 117 cm).

Table 6.1: Shake Test Parameters for the Nike-Apache Experiment Package

Axis	Frequency	g Level or Displacement	Sweep Rate
Z-Z (Thrust)	10-120 Hz	3g	4 octaves/min
	120-200 Hz	10g	
	200-350 Hz	20g	
	350-2000 Hz	5g	
X-X and Y-Y (Lateral)	7-11 Hz	1.02mm	4 octaves / min
	11-20 Hz	0.508mm	
	20-30 Hz	0.203mm	
	30-40 Hz	0.408 mm	
	40-120 Hz	0.06mm	
	120-200 Hz	0.0187mm	

note: Lateral g levels were limited to 30g's at the center of gravity.

Two other important parameters to the payload trajectory are the pitch and roll moments of the payload. These were measured at the same time as the center of gravity.

6.2.3 Spin Test

A dynamic spin test of the experiment package and the complete payload and nose cone assembly was carried out to determine the dynamic stability. The stability was found to be such that it would produce a 2^{o} - 3^{o} coning angle for the experiment package from after payload ejection until the payload reaches about 70 km on the downleg.

The behavior of the experiment package electronics were monitored during the spin test to determine the effect of the projected spin rate. The outputs of the electronics showed severe microphonic effects. This was considered more important than the microphonics caused by the shake tests since the experiment package would be spinning throughout the flight.

After a careful analysis for possible reasons for the severity of the microphonics, it was found to be caused by the slight instability of the experiment package acting through the fixed base of the spin table to cause vibration. Since the base of the experiment package would not be fixed after it was ejected from the rocket motor, this effect would not be important. However, it was decided to apply a potting compound to the sensitive electronics in any future experiment packages. Microphonic noise was found to be negligible during the actual flight after the second stage rocket motor stopped

firing. It decreased even further once the atmospheric pressure had decreased to the point where the experiment package trajectory was ballistic.

6.2.4 Outgassing and Ion Collection Tests

A special vacuum chamber which could hold the entire experiment package was built to study the outgassing from the surface of the package and any leakage from the interior of the package. A surface ionization ion source was included so to be able to check ion collection of the mass spectrometer and ion probes.

The results of several measurements show the outgas/leak rate of the clean, complete experiment package to range between 5.2×10^{-2} pa-liters/sec and 1.6×10^{-1} pa-liters/sec. The spread in the outgas/leak rate is due to the cleaning and handling methods for the experiment package.

Ion collection by the mass spectrometer and the ion probes was confirmed by using the ion source in this vacuum chamber. The telemetry operation was tested at this time to compare the data outputs with previous results hard wired out of the experiment package.

6.3 Experiment Package Electronics

6.3.1 Determination of Mass Spectrometer Repetition Frequency and Electrometer Requirements

The volume of the pulsing region of the flight version of the cylindrical-electrode mass spectrometer is 16.34 cm^3. The fill time of this pulsing region is dependent on the ion draw-in potential, the

vehicle velocity and the experiment package angle-of-attack (defined as the angle between the package velocity vector and the package spin axis). The fill time for the minimum vehicle speed ($\sim$300 m/sec), smallest draw-in voltage (-5 V) and maximum angle of attack is about 5 μsec for 500 amu ions (this is the worst possible case and would never be found in flight). To analyze heavy ions up to 500 amu in this mass spectrometer, a sufficiently long initial pulse width needs to be selected. A pulse width of 3 μsec was calculated to be more than sufficient. The total mass sweep time would then be 8 μseconds. A repetition frequency of 90 kHz was selected for the sounding rocket flight.

The dominant fill mechanism for up to 500 amu ions will be the draw-in potential at all times after payload ejection until the experiment package reaches about 50 km on the downleg. At the lowest draw-in potential (-5 V) the radially directed ion velocity due to the draw-in potential will be at least twice the thermal and ram filling velocity contributions at altitudes above 70 km.

Calculations of the total ion concentration for any measured ion peak can be made, assuming the source region is completely filled. If we define the sensitivity correction for the increased pressure behind the vehicle shock wave as S, the correction for grid transparency as T, and t_s as the length, in time, of each mass spectrum then for a measured ion current, in a mass peak, I;

$$n = \frac{S \times T \times I \times t_s}{(16.34\ cm^3)\,(1.6 \times 10^{-19}\ coul/ion)} \qquad (6.1)$$

S and T are dimensionless constants, I is in amperes, and t_s is in seconds. Singly charged ions are assumed.

For example, suppose the peak ion current for NO^+ at 85 km is measured to be 3.0×10^{-11} a and t_s is 11.1×10^{-6} seconds. S can be found from the pressure vs. sensitivity curve discussed earlier in this thesis. At 85 km the ambient pressure is about .333 pa. The pressure behind a normal detached shock wave calculated for this experiment package will be 6.19 pa (see Cuirle (1976)). This corresponds to $S \cong 75$, where S is the inverse of the relative sensitivity. For 90 per cent transparency grids T = 1.69, where T is the inverse of the transmission fraction for the spectrometer when all the grids are considered. Substituting these values into equation (5.1) yields $n = 1.61 \times 10^4$ ions/cm^3.

The minimum detectable current for the mass spectrometer electrometer was originally set for 1×10^{-13} a. However, because of difficulties with oscillations, the minimum detectable current was altered to 3×10^{-13} a. The original calculations of Zabielski showed that a current of 3×10^{-13} a would give a sensitivity of about 150 ions/cm^3 at 75 km and 6 ions/cm^3 at 90 km for an 8.9 cm diameter blunt nosed cylinder travelling at Mach 1.5. Recently revised pressure enhancement calculations by Cuirle (1976) for a 15 cm diameter blunt nosed payload travelling at about Mach 3 show that 3×10^{-13} a would correspond to a sensitivity of about 215 ions/cm^3 for NO^+ at 90 km. The revised sensitivity versus pressure data will be discussed in greater detail in the next chapter.

6.3.2 Mass Spectrometer Stepping Ground

In order to study the effect of a varied potential gradient used to draw ions into the mass spectrometer, the ground to which all the mass spectrometer voltages were referenced was stepped from +3 V to +1 V to -1 V to -3 V. The mass spectrometer was run at each offset level for one second before shifting to the next offset level. Hopefully, the study of the effects of these various offset levels superimposed on the dc draw-in potential on the pulse terminator grid will shed some light on chemical reactions that might be induced by the draw-in potential.

6.3.3 Potential on the Pulse Terminator Grid

The dc potential on this grid shields the surrounding plasma from the pulses inside the mass spectrometer and acts as the ion draw-in grid. This grid is called grid 0 because it is not essential to the mass spectrometer operation. The potential was set at -8 V with respect to the mass spectrometer offset ground. With respect to the payload skin, this voltage will step from -5 V to -11 V.

6.3.4 Potential on the Pulsed Grid and Grid 2

The dc potential of the pulsed grid, which will be called grid 1, was set at -7 V with respect to the mass spectrometer ground. This potential produces a nearly field-free region between grid 0, grid 1 and grid 2 when the pulse is not applied to grid 1. This reduces the possibility of electric field induced chemical events occurring in this region. The dc potential of the third grid, called grid 2, was set at -8 V.

The performance of the mass spectrometer is very dependent on the energy spread of the ions in the source region. The -8 V dc potential on grid 2 can produce an ion energy spread in the source up to 5eV to 11eV (depending on the mass spectrometer offset ground). This initial energy spread requires the operating voltages of the spectrometer be set for better velocity focusing. This means a larger pulse voltage will be required than for optimum space focusing. A positive pulse amplitude, applied to grid 1, of 72 V with respect to the offset ground (from now on all mass spectrometer voltages will be referenced to the offset ground) was decided on as the optimum voltage. The energy spread in the source region could be lowered by lowering the dc potentials on grids 0, 1 and 2. There were two reasons for choosing the dc potentials that were actually used. First, the effect of larger draw-in potentials was of interest and this required draw-in voltages of -10 V or larger (more negative). Secondly, there was a possibility of the payload skin swinging positive with respect to the surrounding plasma. This necessitated a draw-in potential at least several volts negative. As a compromise between these two requirements, the flight voltages were decided on.

6.3.5 Remaining DC Potentials and the Gate Pulse Height and Width

The potential of the fourth grid, called grid 3, was set at -70 V. This voltage was a result of the need to produce the proper velocity focusing characteristics and to give ions a reasonably fast flight time in order to measure ions up to 500 amu. Grid 4 (the fifth

actual grid) defines the beginning of the gate region. The potential on this grid is common to the sides of the drift region (between grids 3 and 4) and grid 3. Grid 4 shields the drift region from the gate pulse. The gate dc potential was set to + 85 V (grid 5) with gate pulse amplitude at about 100 V. The base width of the gate pulse was set at about 110 nsec. The grid terminating the gate region (grid 6) was common with the sides of the mass spectrometer inner shield and was at -70 V. In future experiment packages this grid will be set at a slightly more negative potential and isolated from the sides of the wedge in order to suppress secondary electron emission from the collector. Finally, the collector was set at -70 V. The collector was gold plated to reduce possible photoemission effects.

The gate pulse was swept from .8 μsec to 8.7 μsec which sweeps over a mass range of 7 amu to 500 amu. This scan occurr twice in a one second interval. One scan was over a .95 sec interval and a fast retrace occurred in .05 sec. The slower sweep was from light to heavier ions; the fast retrace was from heavier to lighter ions.

6.3.6 Spectrometer Shields

A shield was placed around the mass spectrometer in order to prevent the spectrometer sides and bottom from being exposed to the plasma. This shield was held at the mass spectrometer offset ground (it steps from +3 V to -3 V with respect to the payload skin). This outer shield had a number of holes cut in it to allow the ambient atmosphere to flow through part of the mass spectrometer.

An inner shield at -70 V with respect to the offset ground was placed inside the shield at the offset ground. This inner shield covered the mass spectrometer from grid 3 to the collector.

6.3.7 Summary of Flight Mass Spectrometer Voltages

A listing of the flight voltages is shown in Figure (5.5).

6.3.8 Payload Electronics

Figure (5.6) shows a block diagram of the mass spectrometer electronics. The portion of Figure (5.6) showing the dc voltage buss is self-explanatory and the voltages have been discussed in the previous sections. The buncher pulse production begins by putting the output of the 1.11 MHz clock through the $\div$ 10 multivibrator. The output of this multivibrator is then used to trigger the buncher multivibrator after passing through a delay window. The delay window produces a trigger every 11.1 μsec. The buncher multivibrator is set to produce a pulse width of 3 μsec. This pulse is then amplified and biased to the proper level and applied to grid 1. The gate pulse is produced by putting the fast and slow sweep generator outputs into a comparator. This produces a trigger pulse which occurs at varying intervals after the buncher pulse starts. This trigger pulse then triggers the gate multivibrator. The gate multivibrator produces a negative pulse with a width of about 110 nsec. This pulse is amplified by the gate pulse amplifier and biased to the proper voltage level. The pulse is then applied to grid 5.

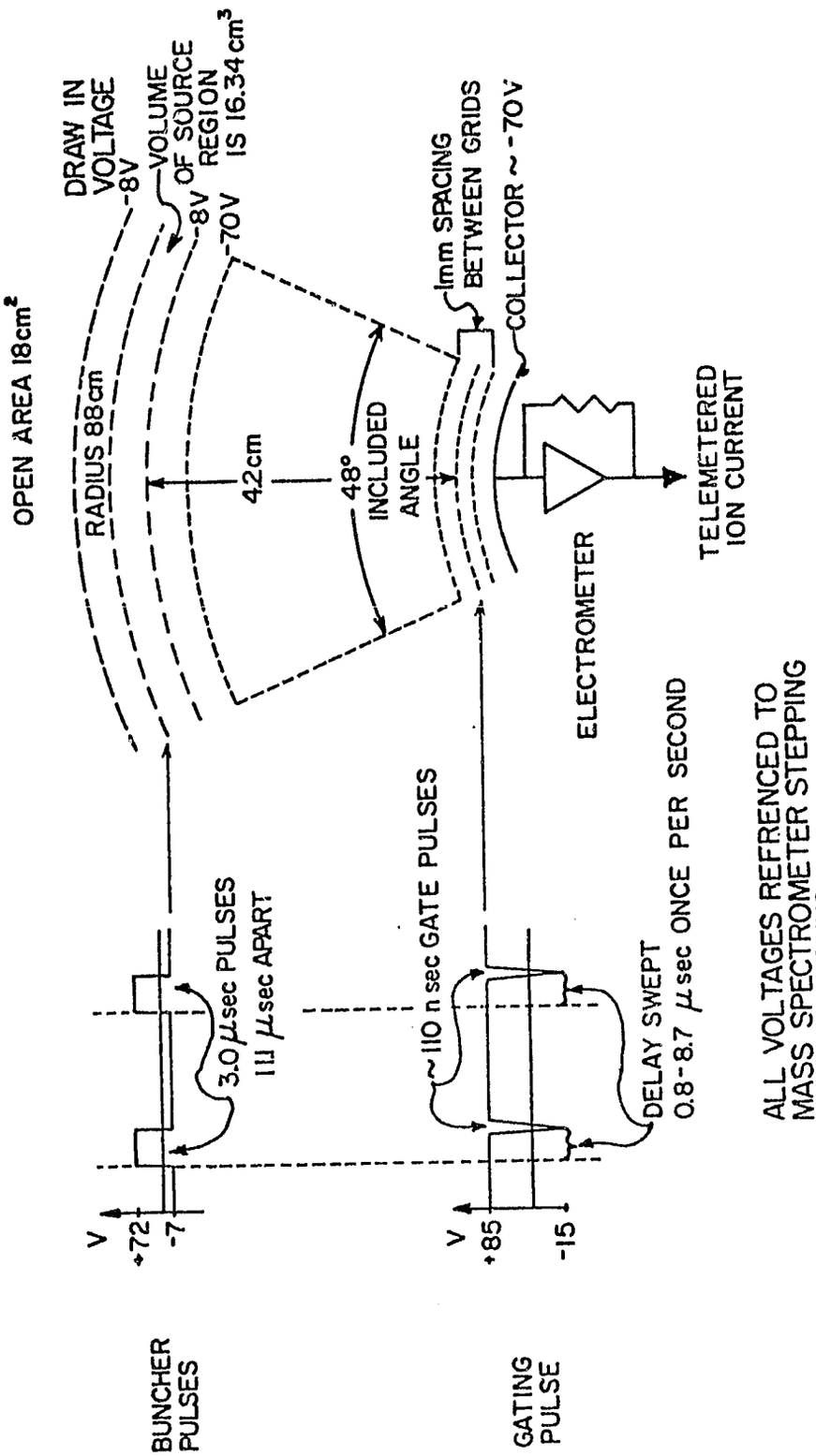

Figure 6.5 Operating Voltages for the Cylindrical-Electrode TOFMS Carried on the Experiment Package.

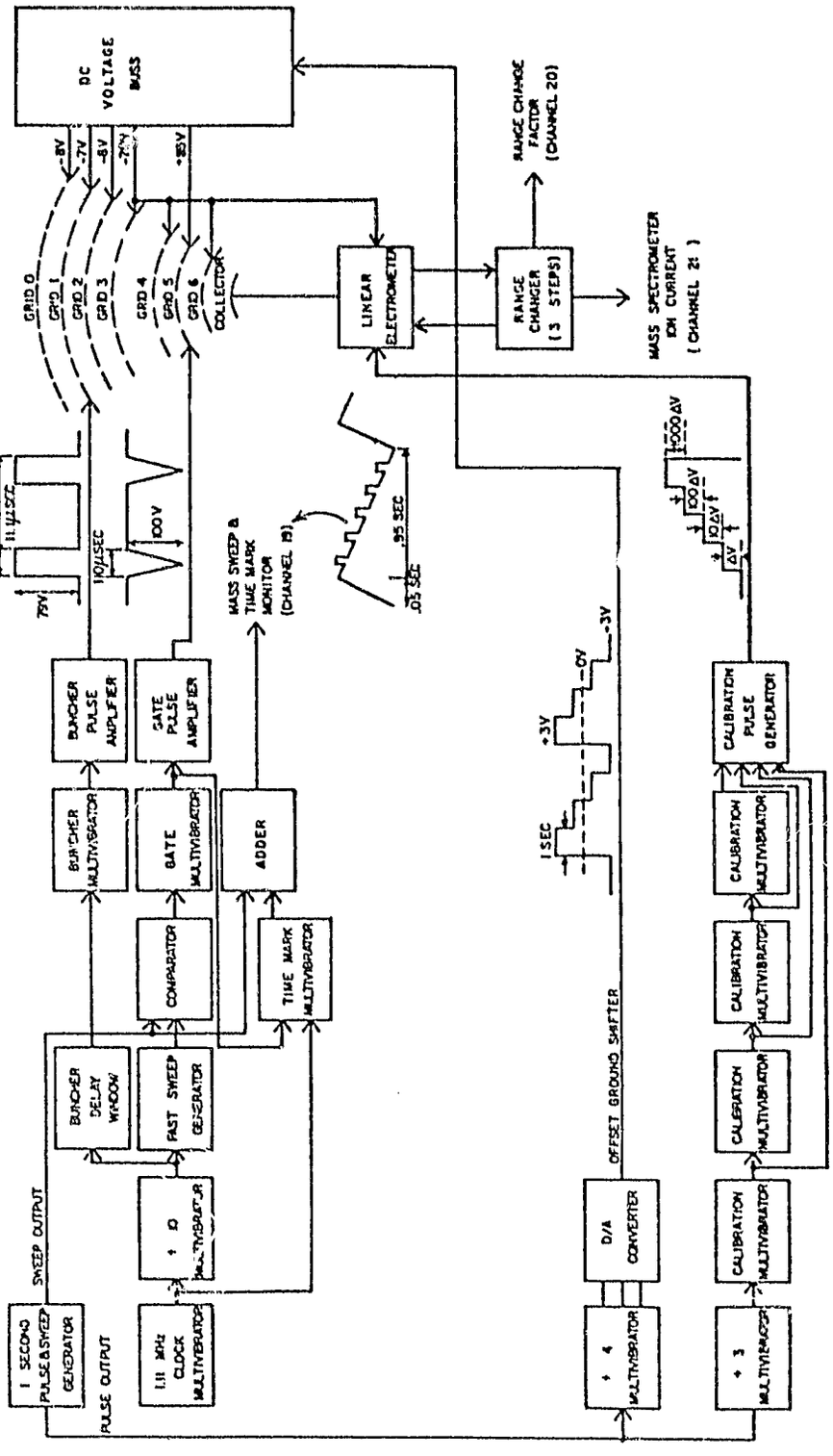

Figure 6.6 Block Diagram of the Nike-Apache Experiment Package Electronics for the Cylindrical-Electrode TOFMS.

There are a number of additional functions illustrated in Figure (6.6) which are not directly related to the mass spectrometer voltages. The first of these is the production of a signal which contains mass sweep information and timing marks for the calculation of ion flight times. The output of the slow sweep generator is a fast increasing ramp and a slow decreasing ramp. The fast ramp corresponds to the fast flyback and the slow ramp to the normal mass spectrum. The time mark multivibrator, when triggered by the 1.11 MHz clock, generates positive pulses which represent ion flight times measured from the beginning of the buncher pulse. The first time mark represents an ion flight time of 1.85 μsec. Each succeeding time mark represents an additional flight time of .925 μsec. The ramps and the time marks are combined in an adder.

The second function is the production of the mass spectrometer offset ground. The pulse output of the 1 second pulse generator triggers the $\div$ 4 multivibrator. The outputs of this multivibrator are combined in the D/A converter. This produces the 4 step offset ground which is then used to bias the mass spectrometer voltages and the electrometer ground.

The third function is a calibration signal which was originally designed to make it possible to determine the relationship between the electrometer output voltage and the collector current. Every third sweep the calibration signal is added to the collector current. The calibration signal was deliberately out of step with the 4 step offset ground so that the signal would not appear during mass sweeps with the same offset ground voltage throughout the flight. This

method of calibrating the electrometer was found to be inadequate because of the difficulty in determining absolute current values. However, the calibration signal was left in operation as a general check on the operation of the electrometer. The revised calibration procedure will be discussed in the Mass Spectrometer Calibration section.

The last function is the presence of an automatic gain changer which determines the gain to be applied to the electrometer signal. When the spectrometer current exceeds certain levels, the signal gain is decreased. Similarly, when the current falls below certain levels, the gain is increased. The switching levels had a hysteresis built in to prevent oscillations from occurring during a gain change (referred to as a range change). The original design was for a linear electrometer which had four range levels. However, the most sensitive range level had to be eliminated because of excessive electrometer noise. The electrometer used was a Keithley 302 commercial electrometer.

6.3.9 Telemetry

The telemetry system used for this payload was designed and installed by NASA personnel at Wallops Station, Virginia. The carrier frequency was 240.2 MHz. This is a standard P-band carrier frequency. The total telemetry system was a PAM/FM/FM system. Analog signals from the payload electronics drive voltage controlled oscillators (VCO's) which then are used to frequency modulate the carrier. The subcarrier channel assignments and frequencies are listed in Table (6.2). IRIG (Interrange

Instrumentation Group) channel 21 carried the mass spectrometer ion current. IRIG channel 20 carried the mass spectrometer electrometer gain indicator. Channel 19 carried the slow sweep or fast retrace indicator and ion flight timing marks. IRIG channels 13 and 14 carried both the Penn State monitor lines and the NASA monitor lines. The Penn State monitor lines are listed in Table (6.3). These two telemetry channels were commutated channels with 30 segments, each sampled at 5 times/sec. The payload antennas were 4 Vega bent spikes phased 90° apart.

6.3.10 Mass Spectrometer Calibration

Ion flight times were calibrated against ion mass-to-charge ratios for the experiment package on several occasions. Calibrations were done with the Penn State portion of the payload run off an external power supply. They were also done with complete payload run off external power. As a final check the calibrations were repeated with the complete payload run off battery (internal) power. The mass spectrometer outputs were measured while hard wired out of the vacuum test chamber and then measured using the telemetry equipment. The results of these calibrations were consistent and are as shown in Figure (6.7).

The mass spectrometer electrometer output could not be properly equated with a collector current by using calibration signals described in the Payload Electronics section because of the difficulty in determining absolute current values. An alternative method for calibrating the electrometer was developed. Artificial ion currents were fed directly onto the collector through a connector in the side of the mass spectrometer. The artificial currents were produced

Table 6.2: Telemetry Channel Assignments for the Sounding Rocket Flight

IRIG CHANNEL	CHANNEL OUTPUT	SUBCARRIER FREQ.	LOW PASS FILTER CUTOFF
21	MASS SPECTROMETER CURRENT	165 KHz	3720 Hz
20	MASS SPECTROMETER RANGE FACTOR	124 KHz	3720 Hz
19	MASS SWEEP AND TIME MARK MONITOR	93 KHz	1395 Hz
18	PROBE 1 ION CURRENT	70 KHz	1200 Hz
17	PROBE 1 RANGE FACTOR	52.5 KHz	1200 Hz
16	SOLAR SENSORS 1 + 2	40 KHz	790 Hz
15	PROBE 2 ION CURRENT	30 KHz	600 Hz
14	COMMUTATED CHANNEL #1	22 KHz	330 Hz
13	COMMUTATED CHANNEL #2	14.5 KHz	330 Hz
12	PROBE 2 RANGE FACTOR	10.5 KHz	220 Hz
11	PROBE 3 ION CURRENT	7.35 KHz	110 Hz
10	PROBE 3 RANGE FACTOR	5.4 KHz	110 Hz
9	CALIBRATE SEQUENCE	3.9 KHz	110 Hz
8	ACCELEROMETER	3.0 KHz	110 Hz
7	MAGNETOMETER ROLL	2.3 KHz	35 Hz
6	MAGNETOMETER PITCH	1.7 KHz	25 Hz
5	SOLAR SENSOR #2	1.3 KHz	20 Hz

Table 6.3: Monitor Outputs on the Commutated Channels

GRID 0 DC VOLTAGE

GRID 1 BUNCHER PULSE

GRID 1 BUNCHER DC VOLTAGE

GRID 2 DC VOLTAGE

GRIDS 3,4&6 DC VOLTAGE

GRID 5 GATE PULSE

GRID 5 GATE DC VOLTAGE

GATE PULSE LOGIC

BUNCHER PULSE LOGIC

FAST SWEEP INPUT

1-SEC PULSE GENERATOR

CALIBRATION SEQUENCE

15A POWER SUPPLY

15B POWER SUPPLY

15C POWER SUPPLY

15D POWER SUPPLY

15E POWER SUPPLY

90 VOLT POWER SUPPLY

MASS SPECTROMETER OFFSET GROUND

PROBE OFFSET GROUND

THERMOCOUPLE HEAD CURRENT

THERMOCOUPLE OUTPUT

SKIN TEMPERATURE

POWER SUPPLY TEMPERATURE

MAIN CURRENT SUPPLY

MAIN VOLTAGE SUPPLY

by picking a voltage off a battery through a potentiometer and putting the voltage through high valued resistors chosen to simulate ion currents. The battery and potentiometer were placed in a grounded box. A coaxial cable carried the voltage to the high value resistor. The resistor was shielded by a specially designed grounded sheath. In addition, the entire procedure was carried out in a grounded wire mesh cage.

6.4 Flight Results - 14.482

6.4.1 Launch Conditions

The experiment package described in Chapter V was launched on a Nike-Apache two-stage sounding rocket on May 15, 1974 at 21:37 GMT. The launch site was Wallops Island, Virginia (latitude -37.85°N, longitude -75.47°W). The NASA identification number for the flight was 14.482 and the experiment package will be referred to by this number. May 15, 1974 was classified as a disturbed day according to the Kp index (Journal of Geophysical Research, 76, 3886, 1974). The Kp index at near the launch time was 4.3, the Ap index was 30 and the Ca^{II} index was 8.7. The sunspot number was 24. Electron densities for May 15, 1974, for near the 14.482 launch time, were calculated from an ionogram taken by the Wallops station facility and are shown in Figure (6.8). The ionogram was reduced using the Ionosphere Research Laboratory reduction program. Electron densities calculated by Dr. H. S. Lee from wave interaction data, taken at State College, Pennsylvania on May 15, 1974 are shown in Figure (6.9).

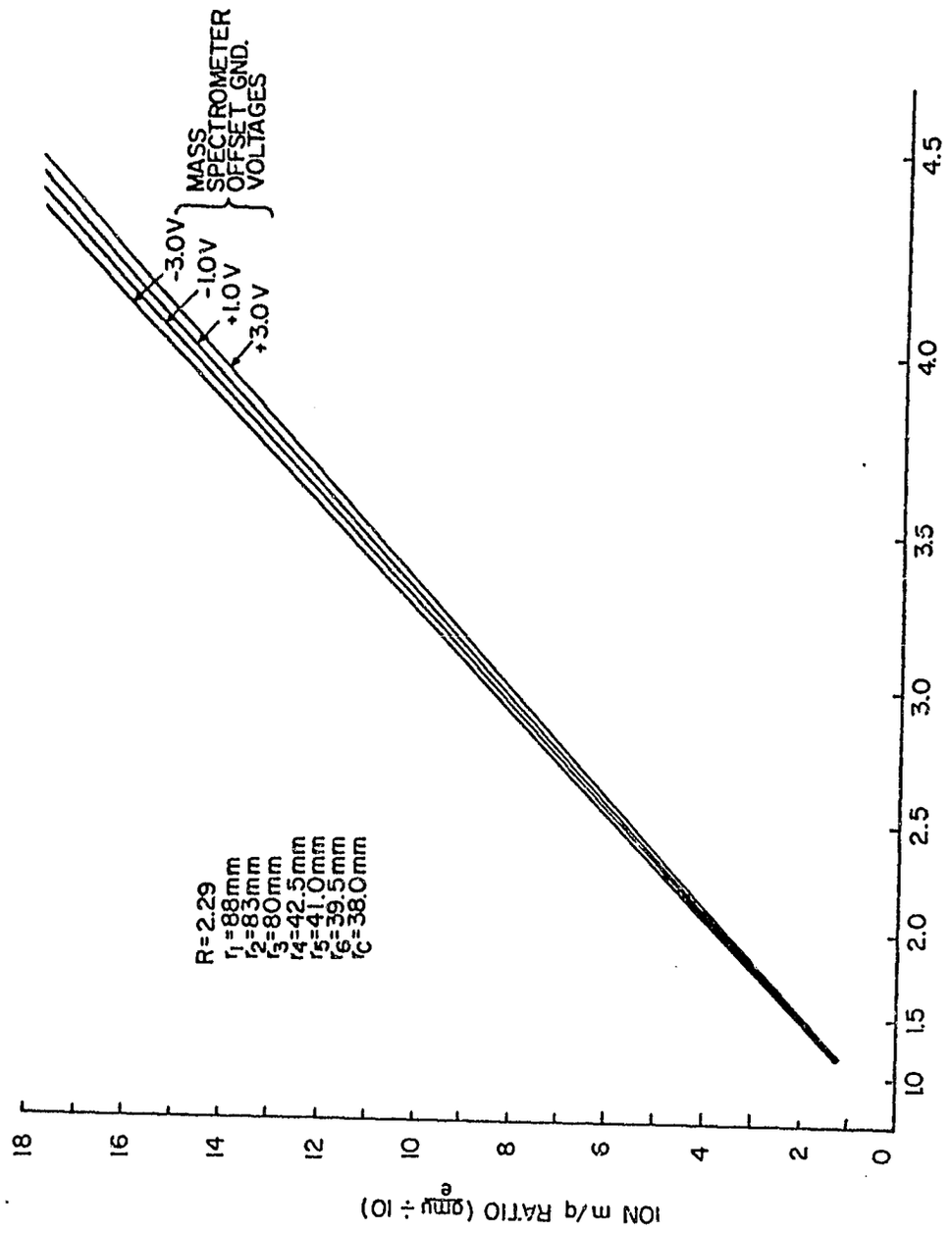

Figure 6.7 Ion Flight Times Versus Mass-to-Charge Ratios for the 14.482 Cylindrical-Electrode TOFMS.

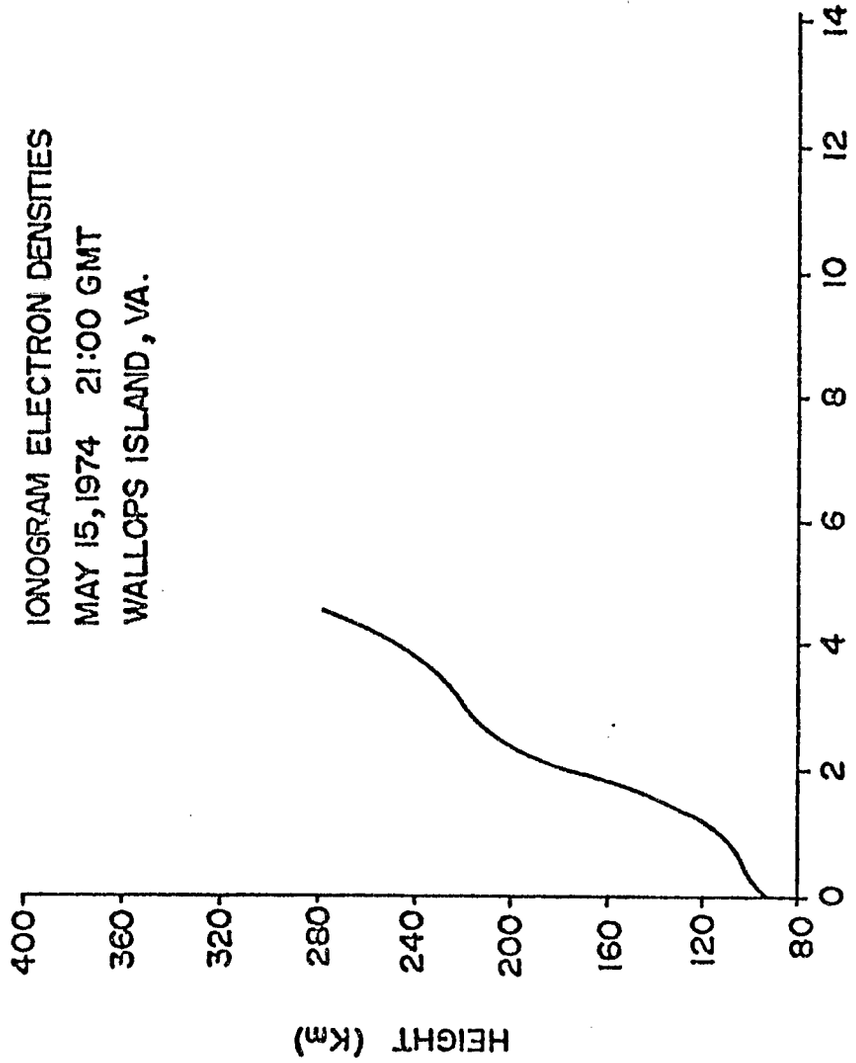

Figure 6.8 Electron Densities at Wallops Island, Virginia Taken from an Ionogram Made at 21:00 GMT on May 15, 1974.

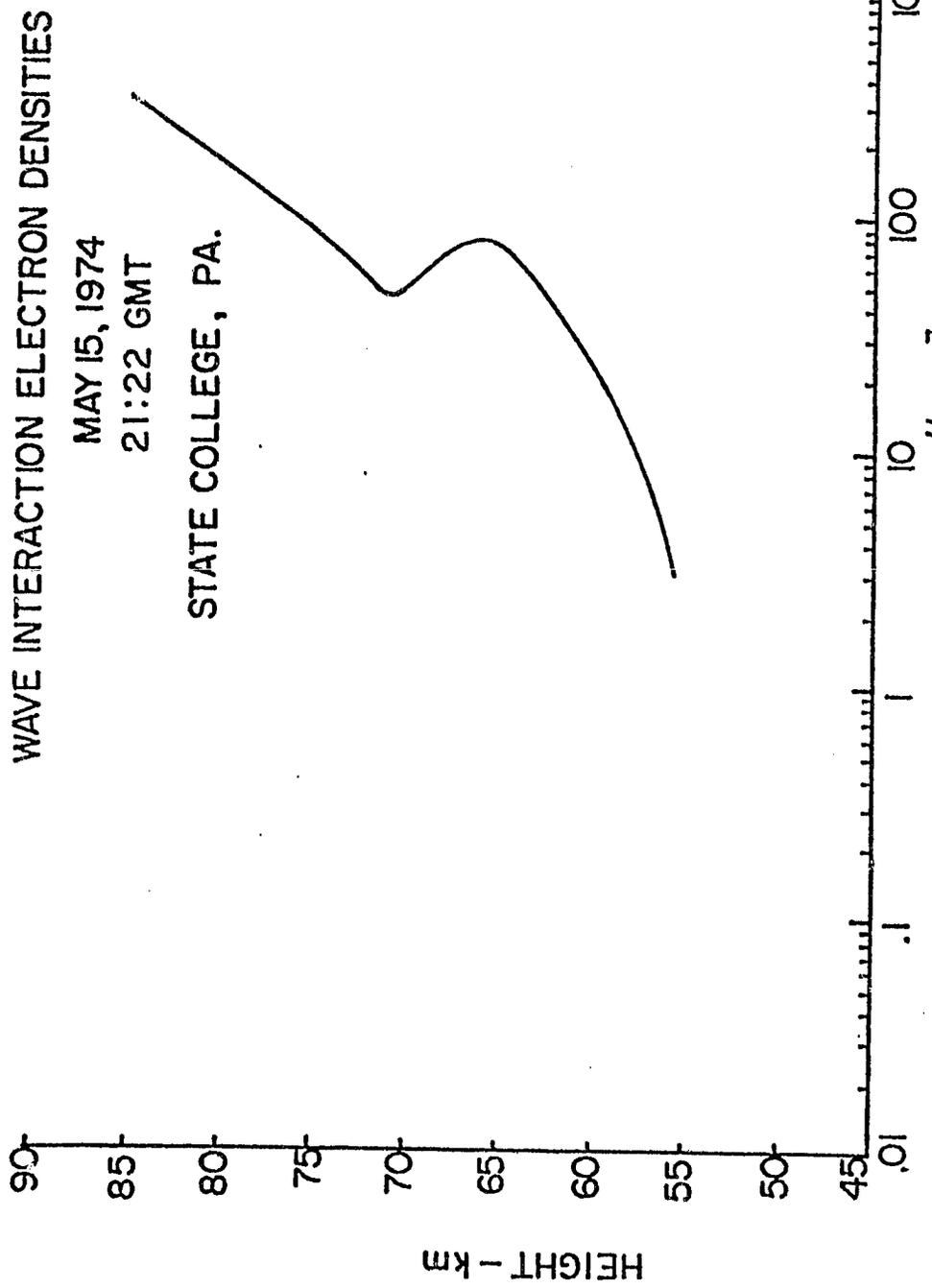

Figure 6.9 Wave Interaction Electron Densities Measured at State College, Pennsylvania at 21:22 GMT on May 15, 1974.

6.4.2 Sounding Rocket Flight

The 14.482 sounding rocket had a number of difficulties during the flight. The output transistor of the NASA transmitter failed about three seconds into the flight, corresponding to the end of the Nike booster burn. The transmitter operated at six per cent of its normal power output for the remainder of the flight. This reduced power output was still sufficient for telemetry reception with only small portions of data loss due to telemetry dropout. It has been suggested by Wayne Powell (1976) of the Computer Science Corporation that this failure might have been caused by the discharge of a large potential, on the rocket, through the pointed telemetry antennas. The antennas on the 14.482 package were capacitively coupled to the transmitter and the failure of the coupling capacitor would allow excess current to flow through the transmitter output transistor. The large potential on the rocket could be the result of charged particles being carried away from the rocket during the firing of the Nike booster. Such charging effects have been observed on jet airplanes (Nanevicz (1974)) and rockets (Nanevicz (1972)). There have been eight transmitter failures on recent NASA sounding rocket flights with pointed, capacitively coupled, antennas. Since switching to inductively coupled antennas, no transmitter failures have been observed due to this charging problem.

The second stage (Apache) burn was uneventful. The nose cone ejection occurred at the proper time (about 65 seconds after launch) and all the 14.482 experiment package instruments were exposed. However, the experiment package failed to separate from the second stage motor. This was probably caused by the failure of the bolt

cutting mechanism which was supposed to release the air spring ejection mechanism (see the explanation of the experiment package ejection sequence). This problem did not directly affect the data collection by the 14.482 instruments. However, it could have provided a serious source of contamination for any large angle-of-attack; the angle between the experiment package spin axis and the experiment package velocity vector.

Data was collected by all the experiment package instruments from nose cone ejection at about 70 km on the upleg, to about 70 km on the downleg. One of the ion probes operated down to about 40 km.

A typical portion of the 14.482 time-of-flight mass spectrometer (TOFMS) raw data is shown in Figure (6.10). A portion of the slow mass sweep, lasting about 950 msec, is shown. The slow mass sweep is from low mass-to-charge ratios to high mass-to-charge ratios. The fast mass sweep, called the flyback, is not shown in Figure (6.10). One mass peak is visible at the mass of 30 amu, assuming singly charged ions. This spectrum was taken at an altitude of 138.6 km. Also shown in Figure (6.10) are the timing marks for ion flight time calculations and the gain multiplier for the mass spectrometer electronometer.

The experiment package altitude versus time after launch, also called flight time but not to be confused with the ion flight time in the mass spectrometer, is shown in Figure (6.11). The experiment package apogee occurred at 138.7 km. The experiment package angle-of-attack versus altitude for the 14.482 flight is shown in Figure (6.12).

Two thermistors were carried in the 14.482 experiment package to monitor the temperatures inside the experiment package. One thermistor was in contact with the experiment package skin. The other thermistor

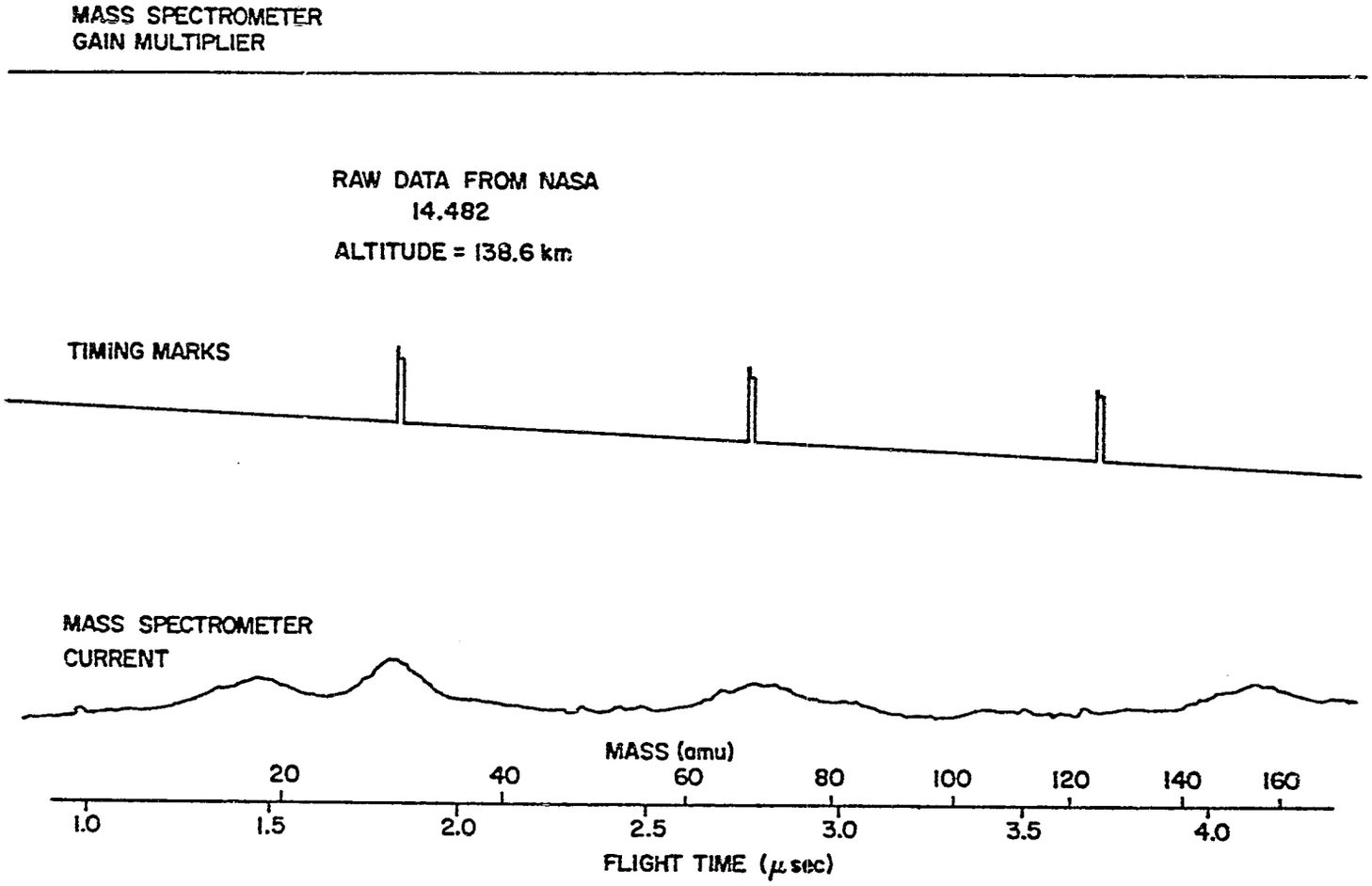

Figure 6.10 Typical Portion of 14.482 Mass Spectrometer Raw Data.

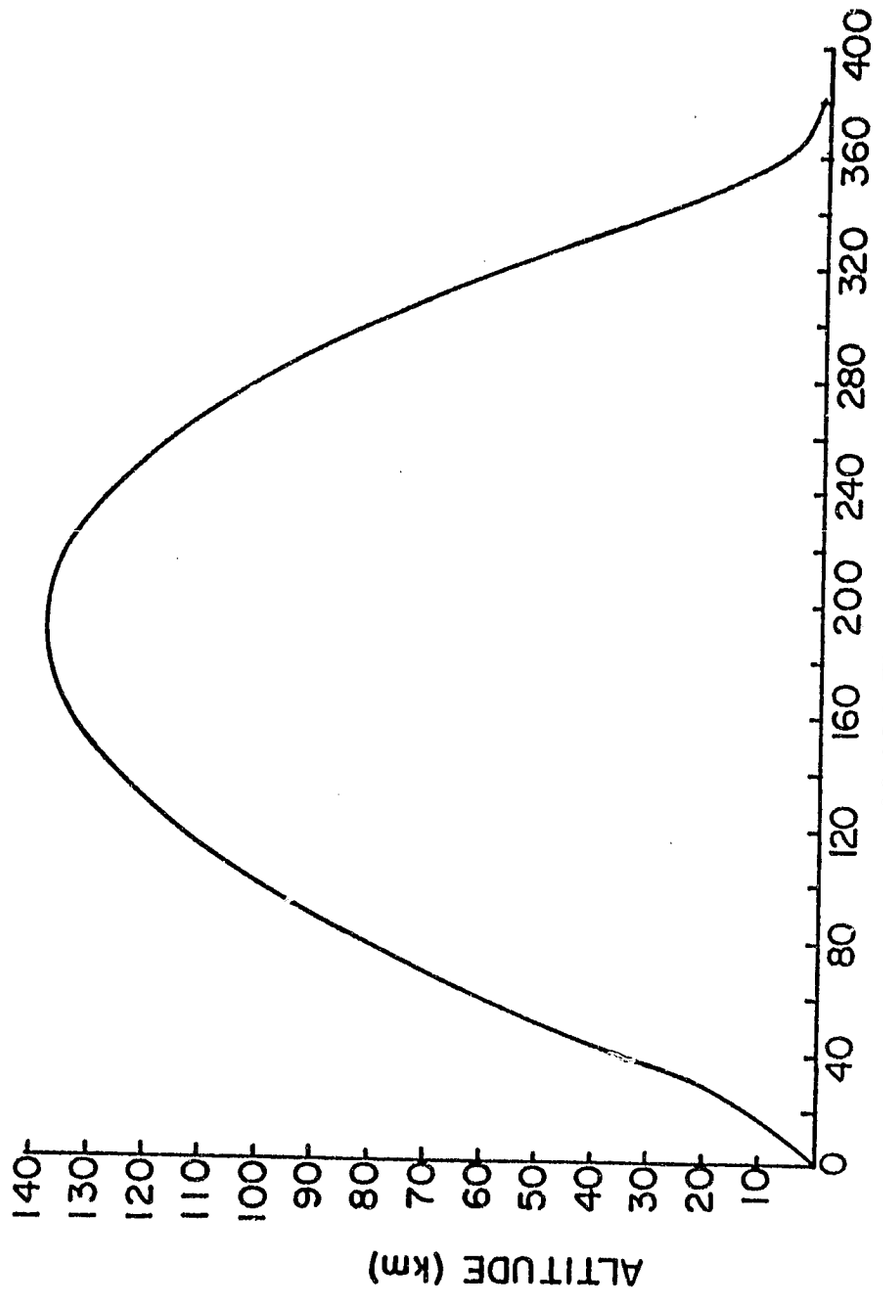

Figure 6.11 Experiment Package Altitude Versus Time for the 14.482 Flight.

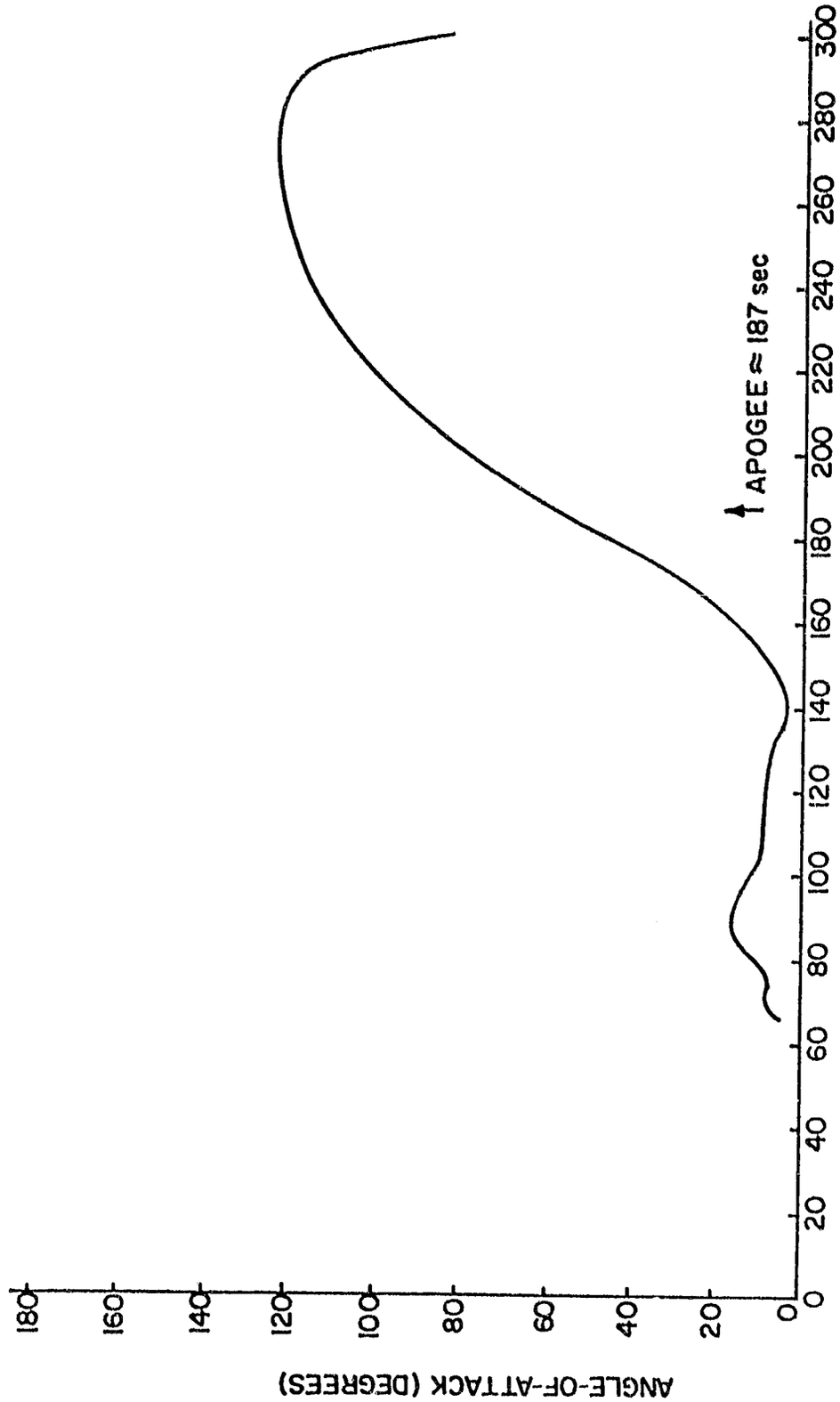

Figure 6.12 14.482 Experiment Package Angle-of-Attack Versus Flight Time.

was in the power supply section of the experiment package to monitor the largest source of heat inside the package. The results of the thermistor measurements during the 14.482 flight are shown in Figure (6.13). The skin temperature was nearly constant until re-entry heating occurred and then the skin temperature increased rapidly until impact. The experiment package power supply temperature showed a small but steady increase during the flight. The internal temperature of the package stayed well within permissible levels, for proper operation of the package electronics, during the flight.

Variations in the vehicle potential relative to the plasma were deduced by analysis of the swept ion probe data and are plotted in Figure (6.14).

6.5 Detailed Analysis of Mass Spectrometer Data from 14-482

The proper examination of the mass spectra required the removal of the spin modulation. This was accomplished by using autocorrelation to normalize the spin modulation. One spin modulation period near the end of each mass spectrum was used to normalize that mass spectrum. Since the spin modulation varied from one mass spectrum to the next, due to the changing draw-in voltages on the spectrometer, the normalization needed to be done for each individual mass spectrum. Care was taken to make sure there were no mass peaks in the spin modulation periods used for normalization. The complete normalization procedure was to digitize each mass spectrum, convert telemetry voltage to ion current, average the digitized current data using a three point average, and then use autocorrelation to remove the spin modulation. These calculations were done partly by hand, partly at the Hybrid Computer facility of The Pennsylvania

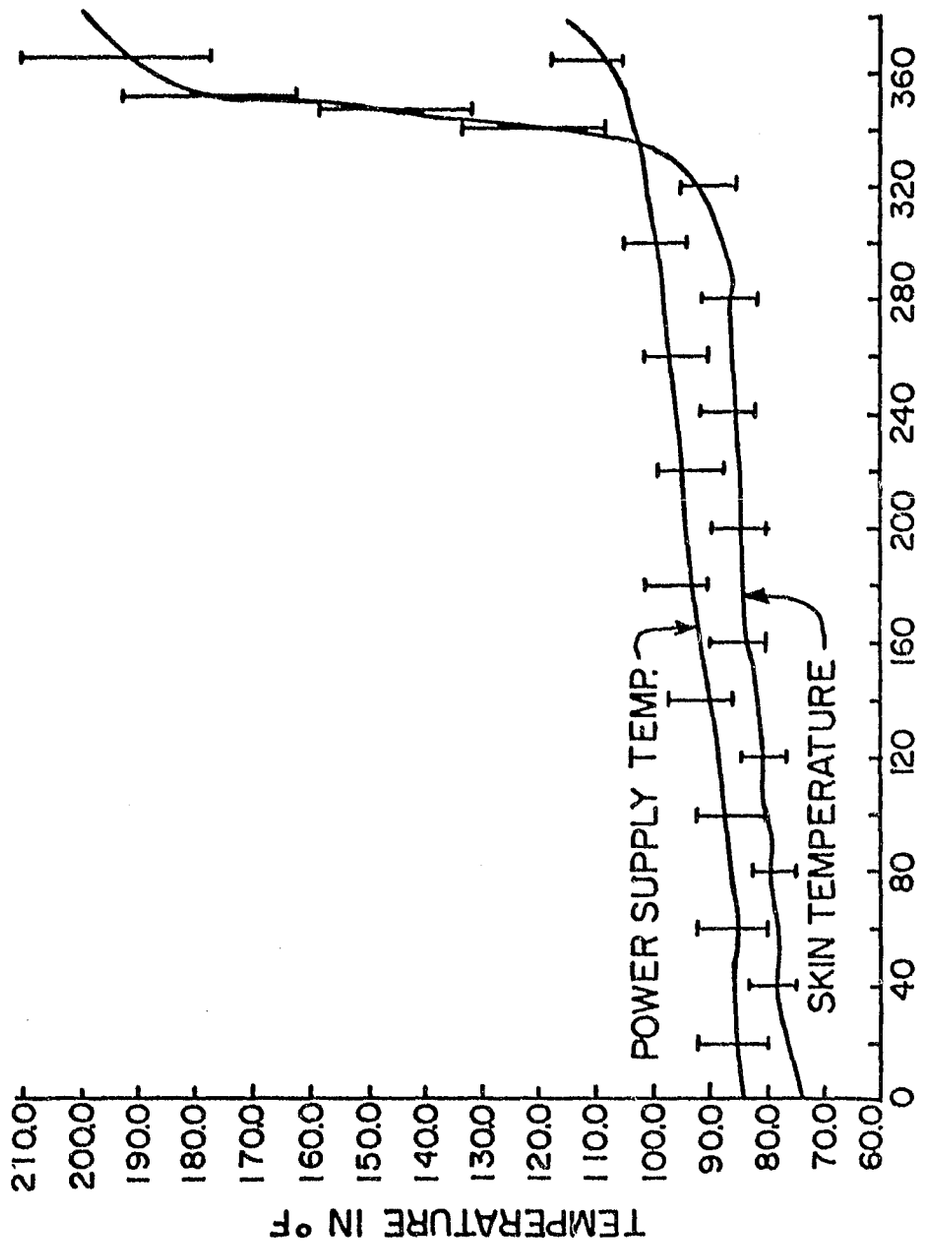

Figure 6.13 Temperatures in the 14.482 Experiment Package During the Flight.

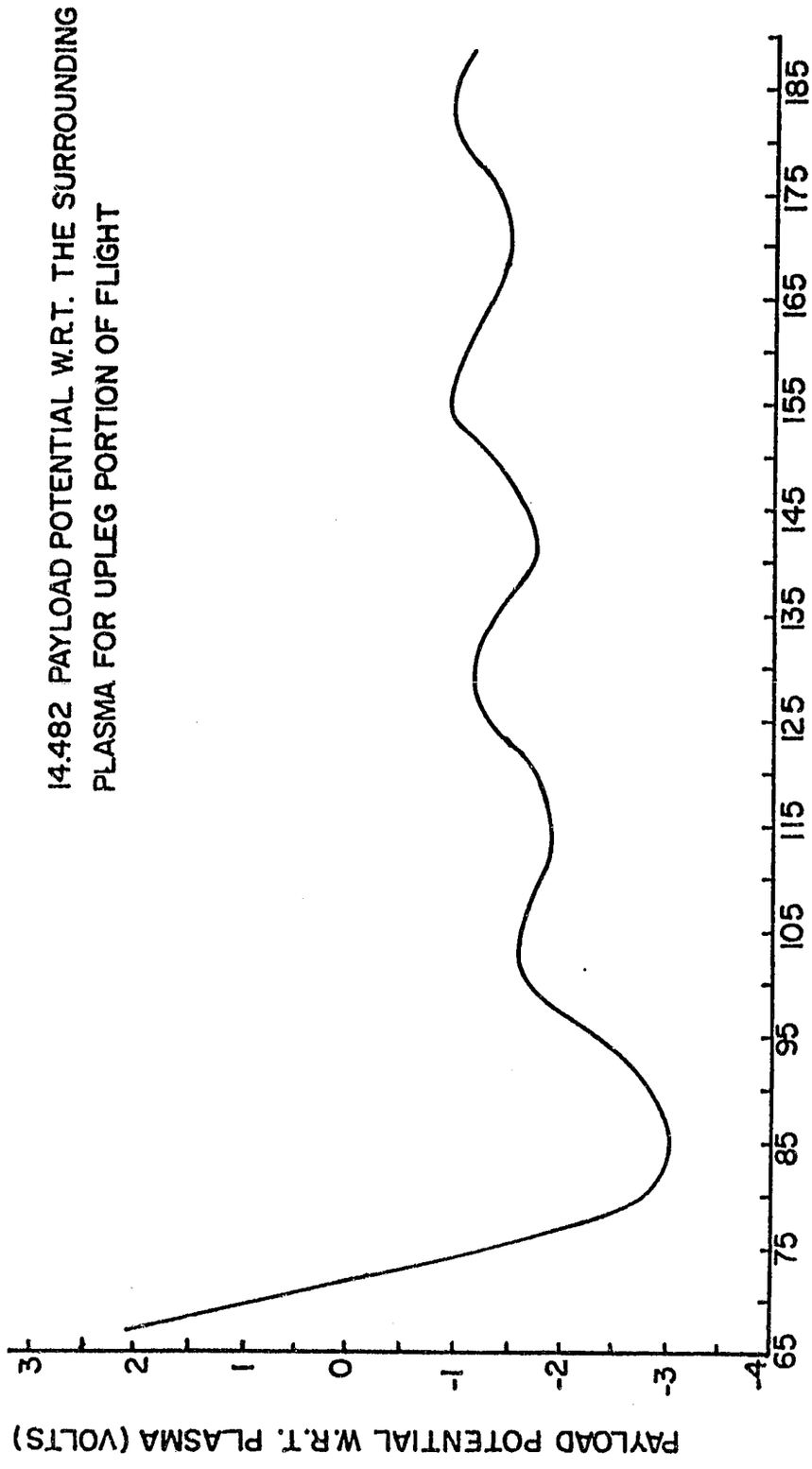

Figure 6.14 The 14.482 Experiment Package Potential with Respect to the Surrounding Plasma for the Upleg Portion of the Flight.

State University and partly on an IBM 360/175. Brad Kuhn was primarily responsible for the hybrid computer programming.

A portion of a 14.482 time-of-flight mass spectrometer (TOFMS) mass spectrum with the spin modulation and background current removed is shown in Figure (6.15). This mass spectrum was taken at about 95 km on the upleg. The mass peaks present are at mass-to-charge ratios of about 30 and 56. The mass peak at m/e = 30 is presumably NO^+ (30) and O_2^+ (32). The resolving power of the spectrometer was insufficient to separate these two peaks. The peak at m/e = 56 is probably Fe^+ (56) based on the results of other researchers.

The altitude profiles of the positive ions detected during the upleg portion of the 14.482 flight are shown in Figure (6.16). The positive ion densities were calculated assuming ambient atmospheric pressure inside the 14.482 mass spectrometer. The relative ion densities at any particular altitude are accurate. However, since only a fraction of the ions in any bunching cycle will actually be collected (Glenn (1952)) the cylindrical-electrode TOFMS should not be used to calculate absolute ion densities. The 14.482 spectrometer, as well as other types of mass spectrometers, are only accurate in relative ion density measurements. The minimum sensitivity, translated to ions/cm^3, is indicated by the dashed line in Figure (6.16) as a function of altitude.

A significant feature of Figure (6.16) is the lack of any clearly defined peaks corresponding to hydrated ions of the form $H_3O^+ \cdot (H_2O)_n$ with m/e ratios less than 500. This statement is subject to the

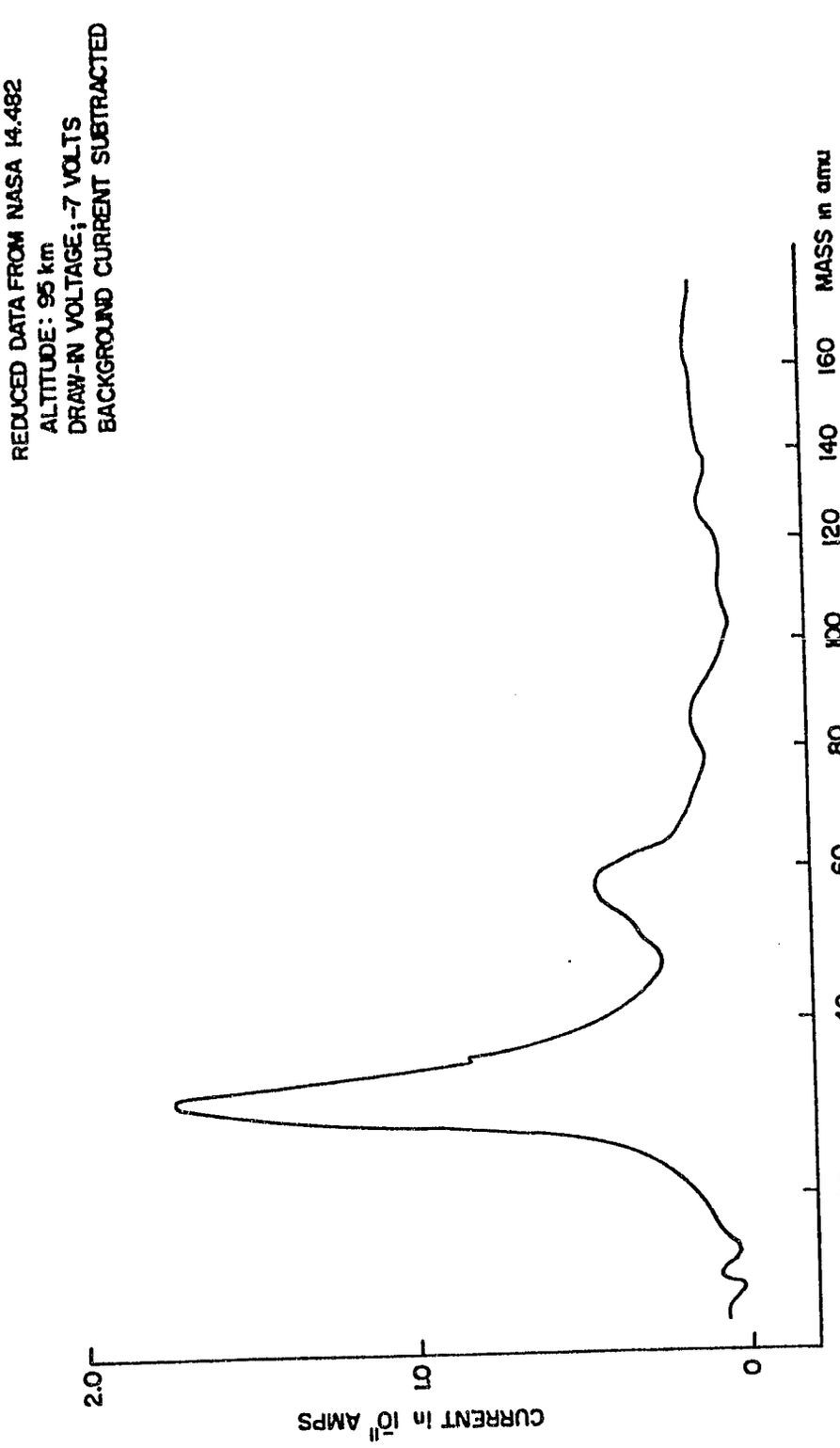

Figure 6.15 Portion of the 14.482 TOFMS Data with the Spin Modulation and Background Current Removed. This Mass Spectrum was Taken at 95 km on the Upleg.

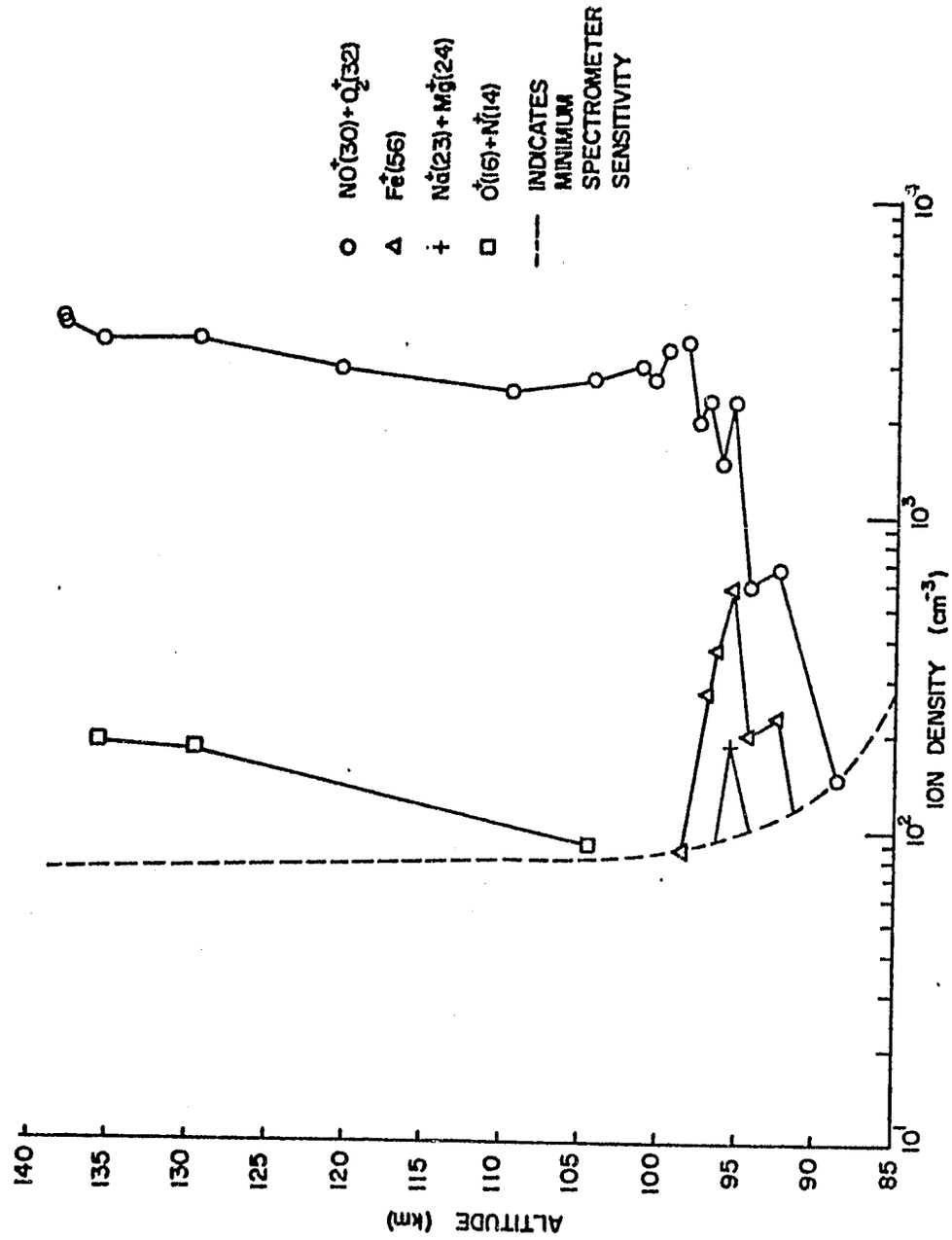

Figure 6.16 Major Positive Ion Species Detected During the Upleg of the 14.482 Flight.

constraint of lower than expected sensitivity due to the larger than expected background current. In the small portions of the downleg data which have been normalized there was a similar lack of hydrated ions with m/e ratios less than 500.

A metallic ion layer was observed at about 95 km which was made up of Fe^+ (56). Mg^+ (24) (or Na^+ (23)) was observed in one spectrum at about 96 km. These observations correspond to the results of numerous investigators (for example, see Krankowsky et al., (1972c)). The metallic ion layer at about 115 km reported by some investigators was not seen.

6.6 Flight Results - 10.317

The second of the second-generation experiments was prepared for flight on a Nike-Cajun vehicle. Flight designation was 10.317. It had numerous improvements to the instrumentation, and provision was made for parachute braking. This would have reduced the velocity to below Mach 1 for part of the trajectory and allowed air-snatch recovery so that the experiment package could be used again. Launch took place at 1930 UT on 6th October 1976 from Wallops Island.

Failure of the second-stage motor to fire caused the complete loss of this payload. Attempts to salvage the rocket from the seabed were unsuccessful.

Telemetry indicated correct operation of all of the scientific equipment up to the time of impact.

CHAPTER VII

CONCLUSIONS

Both flights in which payload ejection occurred showed substantial background ion currents in the 70-90 kilometer height range. These ions were not in the swept mass range of the instruments, which extended to about 275 amu on the first flight, and about 500 amu on the second flight. The expected low-mass water cluster ions which have been seen by other workers were not observed, although they may have been present but obscured by the background current.

One possibility put forward after the first (Boosted Arcas) flight was that a malfunction in the mass spectrometer circuitry may have occurred, and might not have been identified because of the defective telemetry. However, the successful Nike-Apache flight had elaborate telemetry to confirm correct operation of the mass spectrometer circuitry. That flight gave results for the lower E region completely in accordance with data obtained by other workers. The ions NO^+ and O_2^+ dominated, with layers of Fe^+ and other metallic ions also being observed.

Another remote possibility is that photoelectrons produced by ultraviolet radiation may have produced the spurious indicated ion currents at the collector. To reduce this possibility, the launches took place towards the east and late enough in the afternoon that direct rays from the sun could not penetrate the mass spectrometer electrode assembly. The Nike-Apache flight, to further reduce this effect, used a gold plated ion collector and the final Nike-Cajun version used suppressor fields as well. Each version of the ion collector was tested in air and vacuum with ultraviolet sources with negligible effect, even when ultraviolet rays were

shone directly onto the instrument. The photoelectric effect is therefore unlikely to have been a factor.

A final and more likely possibility is that the time-of-flight mass spectrometer was reacting to heavy charged particles to which the instruments used by other researchers are insensitive. Work by Reiter (1976) and subsequent work on mass dependence of the sensitivity of time-of-flight mass spectrometers shows that their ion current output may rise by an order of magnitude at very high masses, finally reaching a point where fast-moving charged dust particles, for instance, can penetrate to the collector independently of the fields in the instrument. All other D-region mass spectrometers use electron multiplier collectors which lose sensitivity at very high masses, and ultimately they are completely insensitive to large charged particles. This point is discussed in more detail in Appendix 1.

It seems reasonable to conclude that the choice of this unconventional type of mass spectrometer, with its enhanced sensitivity at high masses, has led to the detection of heavy charged particles in the height range below about 95 kilometers. The actual fraction of the charge in the D region residing on these heavy particles may be as little as a few percent. The particles may be meteoritic dust particles, ice clusters, or a combination of the two. They may consist of a nucleus surrounded by adsorbed water and the electrical charge may be so small that the mass-to-charge ratio of the particle, regarded as an ion, may form a distribution reaching from the typical mass spectrometer range of tens of amu up to tens of thousands of amu.

It would be interesting to fly special mass spectrometers with greatly extended upper mass ranges in both the stratosphere and the D region of the

ionosphere. Useful progress has recently been made in reducing mass discrimination in the sampling process associated with pumped mass spectrometers. Furthermore, a constant sensitivity mode of operation has been developed for quadrupole mass analyzers. Extension of the sampling and analyzer mass ranges in these ways must be accompanied by extension of the ion detector mass range, for instance by using very large post-analyzer accelerating voltages. Alternatively, consideration might be given to large-area mass analyzers, which operate at ambient pressure and do not need particle multipliers. A recent example of an instrument of the latter type is the Eiber-Loeb mass filter, which is discussed in Appendix 2.

ACKNOWLEDGEMENTS

This work would not have been possible without the efforts of R. F. Reiter, M. F. Zabielski, and J. O. Weeks. Major portions of this report are based on the Ph.D. thesis of R. F. Reiter, which summarizes the contributions made by him and by preceding students who worked on this project. Others who made important contributions at various times included F. Schwab, B. Lightfoot, W. F. Cuirle, T. Collins, G. Yanow, D. Breckenridge, and J. A. Panitz. L. W. Gurkin and J. J. Neville (NASA Wallops Station, Virginia) and W. Cruikshank (Ballistic Research Laboratory) gave invaluable aid in launch preparations and in the provision of special telemetry facilities for the flight. The work was sponsored by NASA Grant NGL 39-009-032.

REFERENCES

Agishev, E. I. and N. I. Ionov, The pulsed mass spectroscope, Sov. Phys.-Tech. Phys., 1, 201, 1956 (translated from Zh. Tekh. Fiz., 26, 203, 1956).

Aikin, A. C. and R. A. Goldberg, Metallic ions in the equatorial ionosphere, J. Geophys. Res., 78, 734, 1973.

Aikin, A. C., Private communication, 1976.

Allen, L. B. and J. L. Kassner, Jr., The nucleation of water vapor in the absence of particulate matter and ions, J. Colloid. Interface Sci., 30, 81, 1969.

Arnold, F., W. Berthold, B. Betz, P. Lammerzahl and J. Zahringer, Mass spectrometer measurements of positive ions and neutral gas between 100 and 223 km above Andoya, Norway, Space Res. IX (Ed. K. S. W. Champion, P. A. Smith and R. L. Smith-Rose), North-Holland, Amsterdam, 256, 1969.

Arnold, F., J. Kissel, D. Krankowsky, H. Wieder and J. Zahringer, Negative ions in the lower ionosphere: A mass-spectrometric measurement, J. Atmos. Terres. Phys., 33, 1169, 1971.

Arnold, F., K. H. Marien and D. Krankowsky, New aspects in lower ionosphere positive cluster ion composition: Results from an improved mass spectrometer probe experiment, Abstract in Methods of Measurements and Results of Lower Ionosphere Structure (Ed. K. Rawer), Akademie-Verlag, Berlin, 239, 1974.

Arnold, F. and D. Krankowsky, Measurements of $H_2O_2^+$ in the D-region and implications for mesospheric H_2O_2, Geophys. Res. Lett., 1, 243, 1974.

Bakker, J. M. B., The time-focusing principle: A double-focusing design for time-of-flight mass spectrometers, Int. J. Mass Spectrom. Ion Phys., 6, 291, 1971.

Bakker, J. M. B., A beam modulated time-of-flight mass spectrometer. Part I: Theoretical considerations, J. Phys. E, 6, 785, 1973.

Barnes, E. E., Electronics for the operation of a rocket borne wedge time of flight mass spectrometer, PSU-IRL-SCI-379(E), The Pennsylvania State University, University Park, Pennsylvania, 1971.

Bennett, W. H., Radiofrequency mass spectrometry, J. Appl. Phys., 21, 143, 1950.

Bolander, R. W., L. B. Allen and J. L. Kassner, Jr., A molecular theory for the nucleation of water vapor, Proceedings 7th International Conference on Condensation and Ice Nuclei, Prague and Vienna, 64, 1969.

Bourdeau, R. E., E. C. Whipple, Jr. and J. F. Clark, Analytic and experimental conductivity between the stratosphere and the ionosphere, J. Geophys. Res., 64, 1363, 1959.

Bowen, P. J., R. L. F. Boyd, W. J. Raitt and A. P. Willmore, Ion composition of the upper F-region, Proc. R. Sco. (London), A281, 504, 1964.

Boyd, R. L. F. and D. Morris, A radiofrequency probe for the mass-spectrometric analysis of ion concentrations, Proc. Phys. Soc., A68, 1, 1955.

Boyd, R. L. F., Some techniques of physical measurement, Proc. R. Soc. (London), A253, 513, 1959.

Boyd, R. L. F., Space science, Nature, 186, 749, 1960.

Boyd, R. L. F., E. B. Dorling, K. Norman and L. J. C. Woolliscroft, Ion mass spectrometry of the lower ionosphere, 1 May 1967 - 15 February 1974, Final Scientific Report AFCRL-TR-74-0503, European Office of Aerospace Research Contract F 61052-67-C-0078, 1974.

Brinton, H. C., L. C. Scott, M. W. Pharo, III and J. T. Coulson, The Bennett ion-mass spectrometer on Atmosphere Explorer-C and -E, Radio Science, 8, 323, 1973.

Brubaker, W. M., Private communication, 1975.

Cameron, A. E. and D. F. Eggers, An ion 'velocitron', Rev. Sci. Instrum., 19, 605, 1948.

Carrico, J. P., Inhomogeneous oscillatory electric field time-of-flight mass spectrometer, Dynamic Mass Spectrometry (ed. P. Price), 2, Heyden and Son, Ltd., London, 161, 1971.

Chapman, S., The absorption and dissociative or ionizing effect of monochromatic radiation in an atmosphere on a rotating earth, Proc. Phys. Soc. (London), 43, 26, 1931a.

Chapman, S., The absorption and dissociative or ionizing effect of monochromatic radiation in an atmosphere on a rotating earth, II. Grazing incidence, Proc. Phys. Soc. (London), 43, 483, 1931b.

Chesworth, E. T. and L. C. Hale, Ice particulates in the mesosphere, Geophys. Res. Lett., 1, 347, 1974.

CIRA 1972, COSPAR International Reference Atmosphere, Akademie-Verlag, Berlin, 1972.

Cuirle, W., Masters thesis in Physics, to be published, 1976.

Dawson, P. H., The acceptance of the quadrople mass filter, Int. J. Mass Spectrom. Ion Phys., 17, 423, 1975.

Diem, H. T., A time-of-flight mass spectrometer suitable for ionospheric composition investigations, PSU-IRL-SCI-309, The Pennsylvania State University, University Park, Pennsylvania, 1967.

Farrokh, H., Design of a simple Gerdien condenser for ionosphere D-region charged particle density and mobility measurements, PSU-IRL-SCI-433, The Pennsylvania State University, University Park, Pennsylvania, 1975.

Ferguson, R. E., K. E. McKulloh and H. M. Rosenstock, Observation of the products of ionic collision processes and ion decomposition in a linear pulsed time-of-flight mass spectrometer, J. Chem. Phys., 42, 100, 1965.

Franklin, J. L., P. M. Hierl and D. H. Whan, Measurement of the translational energy of ions with a time-of-flight mass spectrometer, J. Chem. Phys., 47, 3148, 1967.

Glenn, W. E., Jr., A time-of-flight mass spectrograph, AECD Report No. 3337 (UCRL-1628), 1952.

Goldberg, R. A. and A. C. Aikin, Studies of positive ion composition in the equatorial D-region ionosphere, J. Geophys. Res., 76, 8352, 1971.

Goldberg, R. A. and A. C. Aikin, Comet Enke: Meteor metallic ion identification by mass spectrometer, Science, 180, 294, 1973.

Goldberg, R. A. and L. J. Blumle, Positive ion composition from a rocket borne mass spectrometer, J. Geophys. Res., 75, 133, 1970.

Goldberg, R. A., Silicon ions below 100 km: A case for SiO_2^+, Radio Science, 10, 329, 1975.

Hadley, F. J. and J. L. Franklin, Iterative deconvolution of time-of-flight mass peaks for the determination of translational energy of ions, Int. J. Mass Spectrom. Ion Phys., 18, 249, 1975.

Hazelton, R. B., Pulse circuitry for a flyable time-of-flight mass spectrometer, PSU-IRL-SCI-329(E), The Pennsylvania State University, University Park, Pennsylvania, 1968.

Heaviside, O., Telegraphy. I, Theory, Encycl. Brittanica (10th ed.), 33, 213, 1902.

Hoffman, J. H., Composition measurements of the topside ionosphere, Science, 155, 322, 1967.

Hoffman, J. H., Ion mass spectrometer on Explorer XXXI satellite, Proc. IEEE, 57, 1063, 1969.

Hoffman, J. H., Studies of the composition of the ionosphere with a magnetic deflection mass spectrometer, Int. J. Mass Spectrom. Ion Phys., 4, 315, 1970.

Hoffman, J. H., W. B. Hanson, C. R. Lippincott and E. E. Ferguson, The magnetic ion-mass spectrometer on Atmosphere Explorer, Radio Science, 8, 315, 1973.

Hulbert, E. O., Ionization in the upper atmosphere of the earth, Phys. Rev., 31, 1018, 1928.

Hummel, J. R., A survey of noctilucent cloud phenomenon, PSU-IRL-IR-28, The Pennsylvania State University, University Park, Pennsylvania, 1973.

Hunt, W. W., Jr., Water conglomerates in the D-region, Aeronomy Report No. 32, University of Illinois, Urbana, 311, 1969.

Ionov, N. I. and B. A. Mamyrin, Mass spectrometer with a pulsed ion source, Zh. Tekh. Fiz., 23, 2101, 1953.

Istomin, V. G., Investigation of the ion composition of the earth's atmosphere on geophysical rockets 1957-1959, Planet. Space Sci., 9, 179, 1962.

Istomin, V. G. and A. A. Pokhunkov, Mass-spectrometer measurements of atmospheric composition in the USSR, Space Res. III (Ed. W. Priester), North-Holland, Amsterdam, 117, 1963.

Johannessen A. and D. Krankowsky, Positive-ion composition measurement in the upper mesosphere and lower thermosphere at a high latitude during summer, J. Geophys. Res., 77, 2888, 1972.

Johannessen, A. and D. Krankowsky, Daytime positive ion composition measurement in the altitude range 73-137 km above Sardinia, J. Atmos. Terres. Phys., 36, 1233, 1974.

Johannessen, A., D. Krankowsky, F. Arnold, W. Riedler, M. Friedrich, K. Folkstad, G. Skovli, E. V. Thrane and J. Troim, Detection of water cluster ions at the high latitude summer mesopause, Nature, 235, 215, 1972.

Johnson, C. Y. and J. P. Heppner, Night-time measurement of positive and negative ion composition to 120 km by rocket-borne spectrometer, J. Geophys. Res., 60, 533, 1955.

Johnson, C. Y. and J. P. Heppner, Daytime measurement of positive and negative ion composition to 131 km by rocket-borne spectrometer, J. Geophys. Res., 61, 575, 1956.

Johnson, C. Y. and E. B. Meadows, First investigation of ambient positive-ion composition to 219 km by rocket-borne spectrometer, J. Geophys. Res., 60, 193, 1955.

Karataev, V. I., B. A. Mamyrin and D. V. Shmikk, New method for focusing ion bunches in time-of-flight mass spectrometers, Sov. Phys.-Tech. Phys., 16, 1177, 1972 (translated from Zh. Tekh. Fiz, 41, 1498, 1971).

Katzenstein, H. S. and S. S. Friedland, New time-of-flight mass spectrometer, Rev. Sci. Instrum., 26, 324, 1955.

Keller, R., Spectre de masses obtenu par mesure du temps de vol, Helv. Phys. Acta, 22, 386, 1949.

Kendall, B. R. F., Private communication, 1975.

Kendall, B. R. F. and J. O. Weeks, Transient desorption of water vapor: A potential source of error in upper atmosphere rocket experiments, J. Geophys. Res., 79, 1582, 1974.

Kendall, B. R. F. and R. F. Reiter, Miniature time-of-flight mass spectrometer for ion composition measurements in the lower ionosphere, presented at the 23rd Annual Conference on Mass Spectrometry and Allied Topics, Houston, Texas, May 25-30, 1975.

Kennelly, A. E., On the elevation of the electrically conducting strata of the earth's atmosphere, Elec. World and Eng., 39, 473, 1902.

Krankowsky, D., F. Arnold and H. Wieder, Recent positive and negative ion composition measurements in the lower ionosphere by means of mass spectrometers, in Magnetosphere-Ionosphere Interactions (Ed. K. Folkestad), Oslo University Press, Oslo, Norway, 1972a.

Krankowsky, D., F. Arnold, H. Wieder, J. Kissel and J. Zahringer, Positive ion composition in the lower ionosphere, Radio Science, 7, 93, 1972b.

Krankowsky, D., F. Arnold, H. Wieder and J. Kissel, The elemental and isotopic abundance of metallic ions in the lower E-region as measured by a cryogenically pumped quadrupole mass spectrometer, Int. J. Mass Spectrom. Ion Phys., 8, 379, 1972c.

Liepmann, H. W. and A. Roshko, Elements of Gas Dynamics, Wiley and Sons, New York, 1957.

Lin, Sin-Shong, Detection of large water clusters by a low rf quadrupole mass filter, Rev. Sci. Instrum., 44, 516, 1973.

Lincoln, K. A., A velocity-modulation mass spectrometer, Doctoral dissertation, Stanford University, 1957, University Microfilms, Ann Arbor, Michigan, Publication No. 23204, 88 pp.

Loeb, L. B., On the appearance and mechanisms of formation of Langevin-type ions and related nuclei, Aerosol Science, 2, 133, 1971.

MacKenzie, E. C., The investigation of ionospheric electron density and ion composition using rocket-borne probes, Doctoral dissertation, Electron Physics Department, University of Birmingham, London, 1964.

Marable, N. L. and G. Sanzone, High resolution time-of-flight mass spectrometry, theory of the impulse-focused time-of-flight mass spectrometer, Int. J. Mass Spectrom. Ion Phys., 13, 185, 1974.

Mitra, A. P., D-region in disturbed conditions, including flares and energetic particles, J. Atmos. Terres. Phys., 37, 895, 1975.

Nanevicz, J. E., Results of Titan III flight electrostatic experiments, AFAL-TR-72-325, Lightning and Static Electricity Conference Papers 12-15 December 1972, Las Vegas, Nevada, AFAL AFSC, WPAFB, Ohio, 1972.

Nanevicz, J. E., Flight-test studies of static electrification on a supersonic aircraft, Final Report, Contract F33615-68-C-1359, SRI Project 6091, Stanford Research Institute, Menlo Park, California, 1974.

Narcisi, R. S., Ion composition measurements and related ionospheric processes in the D and lower E-region, Ann. Geophys., 22, 224, 1966.

Narcisi, R. S., Ion composition in the mesosphere, Space Res. VII (Ed. L. Smith-Rose), North-Holland, Amsterdam, 186, 1967.

Narcisi, R. S., On water cluster ions in the ionospheric D region, Planetary Electrodynamics (Ed. S. C. Coroniti and J. Hughes), 2, Gordon and Breach, New York, 447, 1969.

Narcisi, R. S., Shock wave and electric field effects in D-region water cluster ion measurements (abstract), Eos. Trans. AGU, 51, 306, 1970.

Narcisi, R. S., Mass spectrometer measurements in the ionosphere, in Physics and Chemistry of Upper Atmospheres (Ed. B. M. McCormac), D. Reidel, Dordrecht, Holland, 171, 1973.

Narcisi, R. S. and A. D. Bailey, Mass spectrometric measurements of positive ions at altitudes from 64 to 112 kilometers, J. Geophys. Res., 70, 3687, 1965.

Narcisi, R. S., R. A. Langley, H. A. Cohen and J. M. Elwell, Balloon-borne mass spectrometer measurements of the constituents of the atmosphere up to 28 kilometers, AFCRL-66-339, Environmental Research Papers, No. 197, 1966.

Narcisi, R. S., A. D. Bailey and L. Della Lucca, The composition of the lower ionosphere during the 1965 Leonid meteor shower, Space Res. VII (Ed. R L. Smith-Rose), North-Holland, Amsterdam, 446, 19[illegible].

Narcisi, R. S., C. R. Philbrick, A. D. Bailey and L. Della Lucca, Review of daytiime, sunrise and sunset ion composition of the D-region, Aeronomy Report No. 32, University of Illinois, Urbana, 355, 1969a.

Narcisi, R. S., A. D. Bailey and L. Della Lucca, Positive ion composition measurements in the lower ionosphere during the 12 November 1966 solar eclipse, Aeronomy Report No. 32, University of Illinois, Urbana, 450, 1969b.

Narcisi, R. S., A. D. Bailey, L. Della Lucca, C. Sherman and D. M. Thomas, Mass spectrometric measurements of negative ions in the D- and lower E-regions, J. Atmos. Terres. Phys., 33, 1147, 1971.

Narcisi, R. S., C. Sherman, C. R. Philbrick, D. M. Thomas, A. D. Bailey, L. E. Wlodyka, R. A. Wlodyka, D. Baker and G. Federico, Negative ion composition of the D and E regions during a PCA, Proceedings of COSPAR Symposium on Solar Particle Event of November 1969 (Ed. J. C. Ulwick), AFCRL-72-0474, 411, 1972a.

Narcisi, R. S., A. D. Bailey, L. E. Wlodyka and C. R. Philbrick, Ion composition measurements in the lower ionosphere during the November 1966 and March 1970 solar eclipses, J. Atmos. Terres. Phys., 34, 647, 1972b.

Narcisi, R. S., C. R. Philbrick, D. M. Thomas, A. D. Bailey, L. E. Wlodyka, D. Baker, G. Federico, R. Wlodyka and M. E. Gardner, Positive ion composition of the D and E regions during a PCA, Proceedings of COSPAR Symposium on Solar Particle Event of November 1969 (Ed. J. C. Ulwick), AFCRL-72-0474, 421, 1972c.

Narcisi, R. S. and W. Roth, The formation of cluster ions in laboratory sources and in the ionosphere, Advan. Electron. Electron Phys., 29, 79, 1970.

Oran, M. and Y. Paiss, A dynamic mass spectrometer for the study of laser-produced plasmas, Rev. Sci. Instrum., 44, 1293, 1973.

Paul, W. and M. Raether, Das elektrische massenfilter, Z. Physik, 140, 262, 1955.

Pavlenko, V. A., L. N. Ozerov and A. E. Rafal'son, Nonmagnetic time-of-flight mass spectrometers, Sov. Phys.-Tech.-Phys., 13, 431, 1968 (translated from Zh. Tekh. Fiz., 38, 581, 1968).

Pederson, A., Measurement of ion concentration in the D-region of the ionosphere with a Gerdien condenser rocket probe, FOA 3 Report A 607, Research Institute of National Defense, Stockholm, 1963.

Poschenrieder, W. P. and G. H. Oetjen, New directional and energy focusing time-of-flight mass spectrometers for special tasks in vacuum and surface physics, J. Vac. Sci. Tech., 9, 212, 1972.

Powell, H. M., The structure of molecular compounds. IV. Clathrate compounds, J. Chem. Soc. (London), 61, 1948.

Powell, W., Private communication, 1976.

Raitt, W. J., S. Laflin and R. L. F. Boyd, A synoptic view of ionic constitution above the F-layer maximum, Space Res. V (Ed. D. G. King-Hele, P. Muller and G. Righini), North-Holland, Amsterdam, 629, 1965.

Raitt, W. J., J. Blades, T. S. Bowling and A. P. Willmore, A satellite-borne positive ion mass spectrometer, J. Phys. E: Sci. Instrum., 6, 443, 1973.

Rarick, J. P., Deconvolution of physical data, PSU-IRL-SCI-344, The Pennsylvania State University, University Park, Pennsylvania, 1969.

Reiter, R. F. and B. R. F. Kendall, Miniature time-of-flight mass spectrometer with hemispherical electrodes, presented at the 22nd Annual Conference on Mass Spectrometry and Allied Topics, Philadelphia, Pennsylvania, May 19-24, 1974.

Reiter, R. F., Ph.D. Thesis, The Pennsylvania State University, August 1976.

Rogers, A. J. and R. L. F. Boyd, A radiofrequency ion mass spectrometer of very small path length, J. Sci. Instrum., 43, 791, 1966.

Rose, G. and H. U. Widdel, Results of concentration and mobility measurements for positively and negatively charged particles taken between 85 km and 22 km in sounding rocket experiments, Radio Science, 7, 81, 1972.

Sanzone, G., Energy resolution of the conventional time-of-flight mass spectrometer, Rev. Sci. Instrum., 41, 741, 1970.

Sayers, J., Self-contained measuring equipment for electron density and ionic mass spectrum, Proc. R. Soc (London), A253, 522, 1959.

Searcy, J. Q. and J. B. Fenn, Clustering of water on hydrated protons in a supersonic free jet expansion, J. Chem. Phys., 61, 5282, 1974.

Siksna, R., Water clathrates as aerosol particles, UURIE:53:73, Uppsala Universitet, Institutet För Högspänningsforskning, 1973.

Smith, C. R., H. C. Brinton, M. W. Phara, III and H. A. Taylor, Jr., Lower E-region ion concentrations measured at a time of declining solar activity, J. Geophys. Res., 72, 2357, 1967.

Stein, R., The limits of time-of-flight mass spectrometry: General time-focusing relations and an analysis of cylindrical and spherical geometries, Doctoral dissertation, The Pennsylvania State University, University Park, Pennsylvania, 1974.

Stephens, W. E., A pulsed mass spectrometer with time dispersion, Phys. Rev., 69, 691, 1946.

Studier, M. H., Continuous ion source for a time-of-flight mass spectrometer, Rev. Sci. Instrum., 34, 1367, 1963.

Takekoshi, H., K. Tsurocka and S. Shimizer, Bull. Inst. Chem. Res., Kyoto University, 27, 52, 1951, as cited in Zabielski, M. F., Time-of-flight mass spectrometry for ionospheric measurements: Theory and experiments, PSU-IRL-SCI-353, The Pennsylvania State University, University Park, Pennsylvania, 1970.

Taylor, H. A., Jr. and H. C. Brinton, Atmospheric ion composition measured above Wallops Island, Virginia, J. Geophys. Res., 66, 2588, 1961.

Taylor, H. A., Jr., H. C. Brinton and C. R. Smith, Positive ion composition in the magnetoionosphere obtained from the OGO-A satellite, J. Geophys. Res., 70, 5769, 1965.

Taylor, H. A., Jr., H. C. Brinton, M. W. Pharo, III and N. K. Rahman, Thermal ions in the exosphere. Evidence of solar and geomagnetic control, J. Geophys. Res., 73, 5521, 1968.

Townsend, J. W., Jr., Radiofrequency mass spectrometer for upper air research, Rev. Sci. Instrum., 23, 538, 1952.

Wager, J. H., Electronic equipment for in-flight processing of rocket-borne mass spectrometer data, J. Electron. Control, 8, 227, 1960.

Watson-Watt, R. A., Weather and wireless, Q. J. Roy. Meteorol. Soc., 55, 273, 1929.

Widdell, H. U., G. Rose and R. Borchers, Results of concentration and mobility measurements of positively and negatively charged particles taken by a rocket-borne parachuted aspiration (Gerdien) probe in the height region from 72 to 39 km, Pure and Applied Geophysics (PAGEOPH), 84, 154, 1971.

Wiley, W. C. and I. H. McLaren, Time-of-flight mass spectrometer with improved resolution, Rev. Sci. Instrum., 26, 1150, 1955.

Wolff, M. M. and W. E. Stephens, A pulsed mass spectrometer with time dispersion, Rev. Sci. Instrum., 24, 616, 1953.

Young, J. M., C. Y. Johnson and J. C. Holmes, Positive ion composition of a temperate latitude sporadic-E layer as observed during a rocket flight, J. Geophys. Res., 72, 1473, 1967.

Zabielski, M. F., Enhancing effective instrument resolution by an analog method, PSU-IRL-SCI-280, The Pennsylvania State University, University Park, Pennsylvania, 1966.

Zabielski, M. F., Time-of-flight mass spectrometry for ionospheric measurements: Theory and experiments, PSU-IRL-SCI-353, The Pennsylvania State University, University Park, Pennsylvania, 1970.

Zabielski, M. F., H. T. Diem and B. R. F. Kendall, Theoretical analysis of a cylindrical time-of-flight mass spectrometer with radial ion paths, Int. J. Mass Spectrom. Ion Phys., 5, 349, 1970.

Zabielski, M. F., R. Stein and B. R. F. Kendall, Theoretical analysis of a time-of-flight mass spectrometer with spherical electrodes and radial ion paths, Int. J. Mass Spectrom. Ion Phys., 10, 109, 1972/1973.

Zbinden, P. A., M. A. Hidalgo, P. Eberhardt and J. Geiss, Mass spectrometer measurements of the positive ion composition in the D- and E-regions of the ionosphere, Planet. Space Sci., 23, 1621, 1975.

Zhlood'ko, A. D., V. N. Lebedinets and V. B. Shushkova, Meteor ions in the polar ionosphere: Rocket mass-spectrometric measurements and theoretical calculations, Space Res. XIV (Ed. M. J. Rycroft and R. D. Reasenberg), Akademie-Verlag, Berlin, 1974.

APPENDIX 1

INSENSITIVITY OF D-REGION ION MASS SPECTROMETERS TO HEAVY CHARGED PARTICLES

B. R. F. Kendall

ABSTRACT

The types of ion mass spectrometers which have been used in the D-region of the ionosphere are known to discriminate against heavy ions for various reasons. These include ion fragmentation during sampling and mass-dependent transmission through the analyzer. This paper draws attention to an additional source of discrimination against heavy positive ions which results from the use of particle multiplier detectors in conjunction with relatively low incident ion energies of around 2-3 kev. This causes singly-charged ions of mass greater than about 150 amu to have velocities lower than the critical value of about 6×10^4 m/sec needed for kinetic secondary electron emission to take place. Multiplier gain is therefore greatly reduced at high masses. Modifications to existing instrumentation, or new types of mass analyzers altogether, will be necessary if the part of the positive ion mass spectrum above about 150 amu is to be effectively explored.

INTRODUCTION

Since the pioneering work of Narcisi and Bailey (1965), a large number of direct measurements of the ion composition in the D-region of the ionosphere have been made. Examples appear in the work of Goldberg and Blumle (1970), Goldberg and Aikin (1971), Krankowsky et al. (1972), Johannessen et al. (1972), Johannessen and Krankowsky (1974), Zbinden et al. (1975), and Beynon et al. (1976).

The rocket-borne mass spectrometers used for these measurements have typically shared certain features:

1. A draw-in field to attract ions to the entrance of the instrument;
2. An entrance aperture through which the incoming sample of ions and neutral gas is expanded;
3. A mass analyzer of quadrupole or magnetic sector-field type, with a pump to maintain the analyzer well below ambient pressure;
4. A particle multiplier detector to obtain an adequate output signal from the very small ion currents emerging from the analyzer.

Each of these features is associated with its own form of mass discrimination.

MASS DISCRIMINATION PROCESSES

In recent years the breakup of heavy cluster ions, such as $H_3O^+ \cdot (H_2O)_n$, during the draw-in and expansion stages has been generally acknowledged. This biases the observed ion composition in the direction of light masses.

Mass discrimination in the mass analyzer also occurs (Ghosh et al., 1975; Dawson, 1975) and can be substantial for very heavy particles entering off-axis. Again the effect is to discriminate against heavy ions.

Additional mass discrimination results from the use of particle multiplier detectors. It is the purpose of this note to show that this

is an important problem at high masses and that the widespread use of particle multipliers in past experiments may have made them insensitive to the possible presence of positive ions with masses greater than a few hundred amu.

MASS DISCRIMINATION IN PARTICLE MULTIPLIERS

In a particle multiplier used as an ion detector, the incoming ions are accelerated through a potential difference of several kilovolts and strike a conversion dynode. Secondary electrons emitted from this dynode are then accelerated into an electron multiplier structure and, after a suitable number of stages of amplification, an electron output current is produced which is typically $10^4 - 10^6$ times greater than the incoming ion current. In some cases the conversion dynode may be physically and electrically integrated into the remainder of the multiplier structure, but the principle is the same. The conversion dynode is the site of the mass-discriminating effects.

Careful measurements by Pottie et al. (1973) showed that, for the ions of the elements and for most other ions below about 200 amu, the mean number of electrons produced per incident positive ion at a typical conversion dynode is in the range 3-8 at 5 kev energy. The conventional assumption has been that this conversion ratio falls off roughly as the inverse square root of the atomic weight of the ion. This in itself represents a large drop in sensitivity at very high masses. However, Staudenmaier et al. (1976) and Beuhler and Friedman (1977) have recently pointed out that the conversion ratio at high masses eventually falls even more steeply as ion mass is increased at constant energy, reaching very small values for ion velocities below a critical value of about 6×10^4 m/sec. At 2.8 kev, typical of the higher ion input energies used in rocket-borne apparatus,

this critical ion velocity is reached at about 150 amu. Above this mass the only remaining process for ion-electron conversion is a potential (rather than kinetic) process.

The potential process is weak and has not been extensively studied, especially for very heavy ions. The conversion factor is obviously not quite zero for organic ions because these have been recorded by pulse counting techniques up to several thousand amu. At moderate masses, Hagstrum (1956) gives a conversion ratio of around 0.016 for Xe^+ on tungsten at 1000 ev. There is evidence that clustering tends to raise the conversion ratio at a given mass and that the conversion ratio is much higher for negative ions and for ions in excited states. Under other conditions the conversion ratio can apparently be as small as 10^{-3} electrons/ion or less. As Dietz and Hanrahan (1978) put it 'The threshold velocity is an important limitation to ion detection that still is not fully appreciated or fully understood.'

IMPLICATIONS AND CONCLUSIONS

An inevitable result of the various mass discrimination processes discussed above is that conventional types of D-region mass spectrometers are quite insensitive to singly-charged positive ions of greater than about 150 amu and that substantial loss of sensitivity may already have occurred at masses in the 100-150 amu range. In one careful attempt at allowing for mass discrimination, E. Kopp (personal communication, 1978) has reported a sensitivity down by a factor of 5-10 at mass 132 in a rocket-borne magnetic sector-field instrument. G. B. Bunyard (personal communication, 1977) reports the transmission sensitivity alone as being down by a factor of 100 at mass 320 in a commercial quadrupole mass spectrometer, with additional mass discrimination in the multiplier. It appears that all wide-range mass spectrometers, especially those using particle multiplier detectors, would benefit from a careful calibration for mass discrimination with emphasis on the upper mass ranges.

It should be realized that the large sensitivity loss at masses higher than 150 amu is important even though many D-region mass spectrometers are set to scan only up to some lower figure. A high-pass mass filter mode (Bailey and Narcisi, 1966) is used on the quadrupol. mass analyzers employed in most experiments. It involves suppression of the DC voltage applied to the mass filter electrodes. Its purpose is to check for the presence of ion currents at masses above the top of the scan range. Absence of substantial detector output currents in this mode has in the past often been taken as proof of the absence of the corresponding ions. It is now clear that this conclusion has not been justified. Re-examination of existing data obtained in this high-pass mode is desirable. Very small detector output currents may indicate the presence of substantial positive heavy-ion input currents. It is interesting to note that signs of negative heavy ion clusters (for which the multiplier discrimination is likely to be much less) have already been reported (Narcisi et al., 1972).

It appears that the arguments of Rose and Widdell (1972) and Chesworth and Hale (1974) in favor of the presence in the D-region of very heavy ions cannot fairly be dismissed on the basis of existing mass spectrometer data.

Certain laboratory experiments might also yield interesting conclusions if their results could be corrected for mass discrimination. For instance, Lin (1973) observed water vapor clusters containing up to 180 water molecules with a quadrupole mass spectrometer specially modified for use at high masses. The heaviest molecules gave multiplier output currents only 10^{-5} times as great as the current produced by the H_3O^+ ions. Corrections for transmission and multiplier discrimination would probably modify this distribution considerably.

It is important that mass spectrometers with greatly extended upper mass ranges should be flown, in both the stratosphere and the D-region. Useful progress has recently been made in reducing mass discrimination in the sampling process and a constant-sensitivity mode of operation has been developed for quadrupole mass analyzers. Extension of the sampling and analyzer mass ranges in these ways must be accompanied by extension of the ion detector mass range, for instance by using very large post-analyzer accelerating voltages. Alternatively, consideration might be given to large-area mass analyzers which operate at ambient pressure and do not need particle multipliers. Examples are the designs suggested by Rogers and Boyd (1966) and Zabielski et al. (1970), although both of these suffer from a modest resolving power and limited abundance sensitivity. It is interesting to note that two flights with the latter apparatus have each yielded indications of a substantial content of heavy positive charged particles in the D-region. Since the second of these flights showed a normal E-region composition at apogee, there can be reasonable confidence that it was operating correctly. Details will be published elsewhere.

REFERENCES

Bailey, A. D., and R. S. Narcisi, Miniature mass spectrometers for upper atmosphere composition measurements, AFCRL-66-148, Air Force Cambridge Res. Lab., Bedford, Massachusetts, 1966.

Beuhler, R. J., and L. Friedman, Low-noise, high-voltage secondary emission ion detector for heavy ions, Int. Jour. Mass Spectrometry and Ion Physics 23. 81, 1977.

Beynon, W. J. G., E. R. Williams, F. Arnold, D. Krankowsky, W. C. Bain and P. H. G. Dickinson, D-region rocket measurements in winter anomaly absorption conditions, Nature 261, 118, 1976.

Chesworth, E. T., and L. C. Hale, Ice particulates in the lower mesosphere, Geophys. Res. Lett. 1, 347, 1974.

Dawson, P. H., The acceptance of the quadrupole mass filter, Int. Jour. Mass Spectrometry and Ion Physics 17, 423, 1975.

Dietz, L. A., and L. R. Hanrahan, Electron multiplier-scintillator detector for pulse counting positive or negative ions, Rev. Sci. Instrum. 49, 1250, 1978.

Ghosh, P. K., Abha Jain and R. Nagarajan, Effect of ion entry phase, radial velocity and position on quadrupole mass filter operation, Int. Jour. Mass Spectrometry and Ion Physics 18, 1, 1975.

Goldberg, R. A., and A. C. Aikin, Studies of positive ion composition in the equatorial D-region ionosphere, J. Geophys. Res. 76, 8352, 1971.

Goldberg, R. A., and L. J. Blumle, Positive ion composition from a rocket-borne mass spectrometer, J. Geophys. Res. 75, 133, 1970.

Hagstrum, H. D., Auger ejection of electrons from tungsten by noble gas ions, Phys. Rev. 104, 317, 1956.

Johannessen, A., and D. Krankowsky, Daytime positive ion composition measurement in the altitude range 73-137 km above Sardinia, J. Atm. Terr. Phys. 36, 1233, 1974.

Johannessen, A., D. Krankowsky, F. Arnold, W. Riedler, M. Friedrich, K. Folkestad, G. Skovli, E. V. Thrane, and J. Tröim, Detection of water cluster ions at the high-latitude summer mesopause, Nature 235, 215, 1972.

Krankowsky, D., F. Arnold, H. Wieder, J. Kissel, and J. Zähringer, Positive-ion composition in the lower ionosphere, Radio Science 7, 93, 1972.

Lin, S. S., Detection of large water clusters by a low r.f. quadrupole mass filter, Rev. Sci. Instrum. 44, 516, 1973.

Narcisi, R. S., and A. D. Bailey, Mass spectrometric measurements of positive ions at altitudes from 64 to 112 kilometers, J. Geophys. Res. 70, 3687, 1965.

Narcisi, R. S., A. D. Bailey, L. E. Wlodyka, and C. R. Philbrick, Ion composition measurements in the lower ionosphere during the November 1966 and March 1970 solar eclipses, Jour. Atm. Terr. Phys. 34, 647, 1972.

Pottie, R. F., D. L. Cocke, and K. A. Gingerich, Discrimination in electron multipliers for atomic ions II. Comparison of yields for 61 atoms, Int. Jour. Mass Spectrometry and Ion Physics 11, 41, 1973.

Rogers, A. J., and R. L. F. Boyd, A radio frequency ion mass spectrometer of very small path length, Jour. Sci. Instrum. 43, 791, 1966.

Rose, G., and H. U. Widdell, Results of concentration and mobility measurements of positively and negatively charged particles taken between 85 and 22 kilometers in sounding rocket experiments, Radio Science 7, 81, 1972.

Staudenmaier, G., W. O. Hofer, and H. Liebl, Cluster-induced secondary electron emission, Int. Jour. Mass Spectrometry and Ion Physics 21, 103, 1976.

Zabielski, M. F., H. T. Diem, and B. R. F. Kendall, Theoretical analysis of a cylindrical time-of-flight mass spectrometer with radial ion paths, Int. Jour. Mass Spectrometry and Ion Physics 5, 349, 1970.

Zbinden, P. A., M. A. Hidalgo, P. Eberhardt, and J. Geiss, Mass spectrometer measurements of the positive ion composition in the D- and E-regions of the ionosphere, Plan. Space Sci. 23, 1621, 1975.

APPENDIX 2

THE EIBER-LOEB TRANSVERSE MASS FILTER

F. Schwab

This filter relates ion mass to the slope of the output transmission curve. Work was begun in September 1978 by B. Lightfoot and continued through mid-1980.

The major breakthroughs occurring during this time were the operation of the filter with a dual-component (K^+ - Cs^+) ion source to exhibit its differentiating ability, and the functioning of the instrument at background pressures as high as 40 millitorr. Refinements to the device and the techniques needed to operate it have produced consistent data for the dual-ion beam at high pressures.

Two major difficulties were encountered and have been solved satisfactorily. The first concerned a section of tungsten mesh run at dull-red heat and used as an ionization filament. It was found that a partial pressure of oxygen as little as 5×10^{-6} Torr surrounding the filament would produce a stray ion current of approximately 10^{-9} A, masking the known beam. By reducing contaminations in the flowing inert gas system and running the ionizing filament at as low a temperature as possible, this problem was minimized. Secondly, the transmission curves of the heavier Cs^+ ions at high pressures showed a pronounced "sag" or faster fall-off than anticipated, an effect not seen for K^+. Recent calculations of the differing mean-free paths for these ions at 40 milli-torr background pressure indicates that the sag is caused by the greater scattering probability for the Cs^+ ions as they traverse the distance between the ion

source and the mass analyzer.

For the latest experiments, an X - Y recorder was used to display the output transmission curves of the filter in real time. It also appears feasible to interface the filter with a computer (digital or analog), which would be necessary for interpreting many-component data.

References

H. Eiber, Z. Angew. Phys. 15, 461 (1953).

L. B. Loeb, Phys. Rev. 48, 684 (1935).

L. B. Loeb, "Basic Processes of Gaseous Electronics, (Univ. California Press, 1960), p. 22.

APPENDIX 3

PUBLISHED PAPERS BASED ON WORK SUPPORTED
WHOLLY OR IN PART BY
NASA GRANT NGL 39-009-032

1. B. R. F. Kendall and M. F. Zabielski, "High Temperature Insulating Adhesives for Vacuum Applications," J. Vac. Sci. Technol. 3, 114-119 (1966).

2. B. R. F. Kendall and H. M. Luther, "Apparatus for Teaching and Research in Electron Physics," Am. J. Phys. 34, 580-585 (1966).

3. B. R. F. Kendall and H. M. Luther, "Woven Electron Emitters for High Reliability," Electron. Lett. 2, 329-330 (1966).

4. B. R. F. Kendall, "Thermo-Electrically Cooled Baffles for Reducing Rotary Pump Backstreaming," Vacuum 18, 275-276 (1968).

5. B. R. F. Kendall and R. E. Pulfrey, "Theory of Pulsed Molecular-Flow Networks," J. Vac. Sci. Technol. 6, 326-332 (1969).

6. B. R. F. Kendall, H. M. Luther, and D. R. David, "Apparatus for Studying the Principles of Electron Physics," Am. J. Phys. 37, 855-857 (1969), invited paper.

7. B. R. F. Kendall and Gladys Englehart, "New Type of Molecular Mass Gauge for Use with Small Gas Samples," Rev. Sci. Instrum. 41, 1623-1628 (1970).

8. B. R. F. Kendall and M. F. Zabielski, "Compensated Resistors for High Frequency Electrometer Applications," Electron. Lett. 6, 776-778 (1970).

9. M. F. Zabielski, H. T. Diem, and B. R. F. Kendall, "Theoretical Analysis of a Cylindrical Time-of-Flight Mass Spectrometer with Radial Ion Paths," Int. J. Mass Spectrometry and Ion Phys. [illegible], 349-360 (1970).

10. B. R. F. Kendall, "Analogies between Electrical Circuits and Molecular-Flow Networks," J. Vac. Sci. Technol. 9, [illegible] (1972) (Summary of Invited Paper).

11. M. F. Zabielski, Ronald Stein, and B. R. F. Kendall, "Theoretical Analysis of a Time-of-Flight Mass Spectrometer with Spherical Electrodes and Radial Ion Paths," Int. J. Mass Spectrometry and Ion Phys. 10, 109-122 (1972).

12. Robert Pulfrey and B. R. F. Kendall, "Analysis of Gas Mixtures Using Data from Pulsed Vacuum Networks," J. Vac. Sci. Technol. 10, 1150-1152 (1973).

13. B. R. F. Kendall and J. O. Weeks, "Transient Desorption of Water Vapor: A Potential Source of Error in Upper Atmosphere Rocket Experiments," J. Geophys. Res. 79, 1582 (1974).

14. B. R. F. Kendall, "Apparatus for Measuring Internal Volumes of Vacuum Systems," J. Vac. Sci. Technol. 11, 610-611 (1974).

15. B. R. F. Kendall and R. F. Reiter, "Three-Terminal Shielded Resistors for Fast Electrometers," Rev. Sci. Instrum. 45, 850-852 (1974).

16. B. R. F. Kendall and J. O. Weeks, "Bonded Electrodes for Use on the External Surfaces of Spacecraft," Rev. Sci. Instrum. 46, 1123-1125 (1975).